

THE UNIVERSITY OF HULL

Novel Chiral Liquid Crystal Organic-Inorganic Hybrid
Nanoparticle Systems.
Design, Synthesis and Investigation

being a Dissertation submitted in partial fulfilment of
the requirements for the Degree of

Ph.D.

in the University of Hull

by

Ionuț Cameliu Ichim, BEng, MSc

July 2013

Ionut Cameliu Ichim

Ph.D. thesis

Abstract

for “Novel chiral liquid crystal organic-inorganic hybrid nanoparticle systems. Design, synthesis and investigation”

A first step is taken towards the validation of organic synthesis techniques. Small molecular organic compounds were prepared as intermediates for the liquid crystal materials which exhibit room temperature cholesteric mesophases. These cholesterol based materials were then attached to silsesquioxanes. Both materials have low melting points and low transition temperatures. Phase diagrams, contact and miscibility experiments were performed in order to explain a more complicated cholesteric phase behaviour. The cholesteric mesogens were chemically attached to gold and iron/platinum nanoparticles. For all end materials exhaustive characterisation methods were applied.

The questions that were tried to be answered were related to the attachment of cholesterol based mesogens to silsesquioxane cores. Furthermore, the organic-silicon hybrid systems were used as a model for the mesogen covered gold and iron/platinum nanoparticles.

Cholesterol based liquid crystals with chiral nematic mesophase at room temperature were obtained. Hybrid systems with very short pitch cholesteric phase and low transition temperatures were also prepared. A new method for preparing gold nanoparticles was implemented. The present results indicate that it is possible to prepare nanoparticles with chiral nematic phase behaviour close to room temperature and iron/platinum nanoparticles with liquid crystal groups attached.

Acknowledgements

I've been told stories about how long it will take to write the PhD thesis in chemistry and how much it will drain you of all your energy; I have never believe them. Boy! Was I wrong!!! I would here like to express my thanks to the people who have been very helpful to me while working and during the time it took me to write this thesis.

I have been very fortunate with my supervisor, Prof. Georg Mehl, with his unique demeanour and way of being a good boss. He has let me control the project and the work in a higher degree than used to, and at the same time, available at any moment of the day for advices and valuable input. Many thanks go to my second supervisor, Dr. Rob Lewis, for refreshing insight and critical questions when the compulsory reports were Viva Voce-ed.

I would also like to thank the examiners from the thesis defence, Dr. Mike Hird and Dr. Xiangbing Zeng, for agreeing to be part of the committee and for their feedback and suggestions.

The work was funded by the EU FP 7, MC-ITN "Dendreamers" project.

The lab work is invariably a trying experience and not necessarily in terms of the synthesis. Elevators break down at the most unbelievable moments (carrying bottles of solvents), filling out COSHH forms, and even checking the emails can be an astounding challenge.

Many thanks go to all my lab and group colleagues I have had over these almost four years, too many to be named. There were many people who gave interesting feedback and valuable suggestions, people at the various conferences I went to.

I wish to thank to my special colleagues for the enjoyable "lunches" at OGM, the Friday pub sessions, the lab music festivals and the lab conversations which were at least multi lingual and multi cultural. It was exactly what I needed during and after long periods of time spent fighting with synthesis and data (or the absence thereof). It is also wholly attributable to them that none of the computers have ever left the building via the window and taste the concrete outside.

I have been fortunate to come across many funny and good friends, without whom life would be bleak. The colleagues from the “Dendreamers” made every project meeting less scientifically and more fun and interesting.

My parents, grandparents and my brother I would like to thank for their support in all its forms, but also my good and old friends from back home.

Finally I must thank a relatively new friend, for the unstinting reminder that equilibrium is everything and that there are more important things in life than a Ph.D. thesis (namely watch online movies, slamming doors and food). Although I have to say that all that snoring and slapping didn't necessarily help.

Ionut Cameliu Ichim

TABLE OF CONTENTS

<u>CHAPTER I.</u> Introduction	1
I.1. Liquid crystals	2
I.1.1. Chiral liquid crystals	7
I.1.2. Liquid crystal dendrimers	9
I.1.2.1. Side-chain liquid crystal dendrimers	10
I.1.2.2. Siloxane dendrimers	11
I.2. Nanoparticles	20
I.2.1. Gold nanoparticles	23
I.2.1.1. Preparation methods for gold nanoparticles	24
I.2.1.2. Liquid crystalline nanoparticles	33
I.2.2. Magnetic nanoparticles	34
I.2.2.1. Synthesis of magnetic nanoparticles	36
I.2.2.2. Functionalisation of magnetic nanoparticles	38
<u>CHAPTER II.</u> Methods. Characterisation	40
II.1. Optical rotation	41
II.2. Circular dichroism	43
II.3. Optical polarising microscopy	46
II.4. Differential scanning calorimetry	48
II.5. Thermal gravimetric analysis	50
II.6. Gel permeation chromatography	52
II.7. X-ray diffraction	53
II.8. UV-Vis spectroscopy	54
II.9. Transmission electron microscopy	56

<u>CHAPTER III.</u> Target. Scientific objectives	59
<u>CHAPTER IV.</u> Synthesis	65
IV.1. Synthesis. Experimental	66
IV.2. Synthesis. Discussion	112
<u>CHAPTER V.</u> Properties. Discussion of properties	132
V.1. Material M1	133
V.2. Material M2	138
V.3. Material C-M1	144
V.4. Material C-M2	148
V.5. Material 4RM	151
V.6. Material 3RM	151
V.7. Binary mixtures	152
V.8. Material M1-SH	156
V.9. M1 covered gold nanoparticles	158
V.10. Material M1-COOH	166
V.11. Oleic acid/oleyl amine covered iron/platinum nanoparticles	167
V.12. M1 covered iron/platinum nanoparticles	170
<u>CHAPTER VI.</u> Conclusions	178
<u>CHAPTER VII.</u> Outlook	183
References	186

CHAPTER I

INTRODUCTION

I.1. LIQUID CRYSTALS

Liquid crystals are currently a vital and indispensable class of materials, but they are only known for about 120 years. The turning point for the industrial applications was the discovery of the cyano-biphenyl liquid crystals, in the early 70's, by George W. Gray at the University of Hull. From this moment on, a revolution in the industry of display devices has started, taking advantage of the liquid crystals' unique properties. Liquid crystals were first used for applications like thin display screens for PCs and other display devices. The interesting characteristic for these devices is that the optical properties change when an external electric field is applied across the cell containing the liquid crystal. The change is in fact a different organisation of the molecules within the material across the liquid crystal film. Hence, the liquid crystal is not behaving as an electronic material but a molecular one [1].

The vast majority of materials in nature exist in three states of matter. These are the crystal, liquid and gas state and have different characteristics as a function of pressure and temperature. But there is also a different state, a fourth state, the liquid crystal state with its own behaviour and characteristics. As it is suggested by its name, the material in this state of matter has characteristics of a crystal and a liquid at the same time. Under stress a liquid crystal behaves like a liquid, it flows, but also keeps some of the crystal properties, like the anisotropy. To identify the liquid crystal phase, usually the macroscopic behaviour is observed. This behaviour is a combination of order and disorder at microscopic level, order in the long-range orientation. This order combined with the disorder, in the same material, gives liquid crystal its unusual properties and makes them interesting and exciting to work with and not the least, a great potential for applications [2].

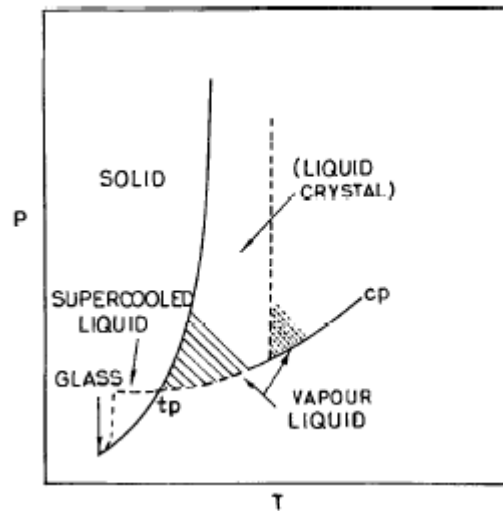


Fig. I.1. Pressure-Temperature phase diagram for a typical system [6]

Liquid crystals are formed by a vast number of materials, if certain conditions of temperature, pressure, concentration and composition are met. Some of these materials that can exhibit a liquid crystalline phase are organic materials, when, on heating, they undergo a transition into a mesophase between the crystal and the liquid phase. These are so called thermotropic liquid crystals. Another class of liquid crystals are the lyotropic liquid crystals. They are formed by amphiphilic molecules, organic materials. The interesting fact about these molecules is that they are composed from two parts, one part is attracted and favours one component of the system, such as a solvent, and the other part does not. The solvent usually used is water. When these amphiphilic molecules are dissolved in water, they aggregate and form micelles. Then, these systems interact to give the mesophase. The liquid crystal phase is mainly controlled by the amphiphile concentration. Most of these molecules are developed and used in the surfactant industry. Liquid crystal phases are also formed by inorganic materials, as clay, in colloidal suspensions and this depends greatly on the particle concentration. Also, a mesophase can be formed by certain polymer solutions where, as the same in the colloid systems, the solvent changes the distance between the polymer chains like the solvent does with the micelles, but their state of aggregation remains almost the same. An example is the Kevlar material which is processed from a nematic polymer solution [2].

The classification of simple liquid crystal forming systems is shown below in Fig. I.2. Thermotropic liquid crystals are classified by molecular shape: polymeric, discotic, chiral and calamitic. The mesophase of each compound is defined according to the degree of order of the phase.

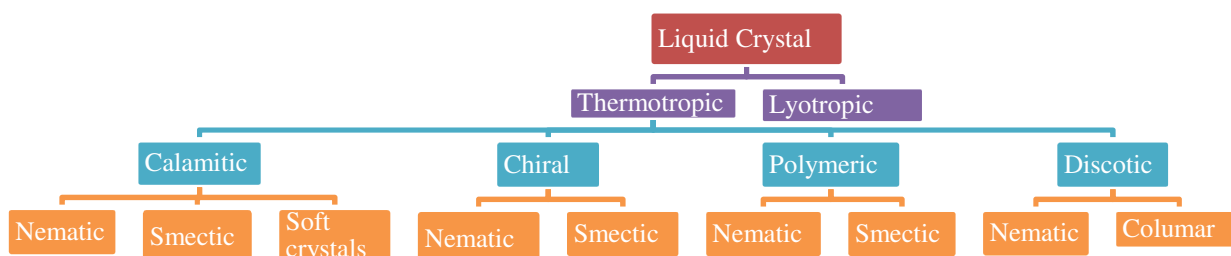


Fig. I.2. A classification of liquid crystals

There are different types of liquid crystals depending on the shape of the mesogenic units. If the molecules are rod-like, the liquid crystals are called “calamitics” (derived from the Greek word *calamos* = rod). If the molecules are disk-like, the liquid crystals are known as “discotics” [4,5]. The lath-like liquid crystals exist when the molecules are intermediate between rod-like and disk-like [6].

The arrangement of liquid crystalline materials is shown below in Fig. I.3. In the crystal state (Cr), all the molecules are arranged in the same direction and fully ordered. Heating a fully ordered crystalline solid causes thermal motion of the molecules within the lattice and this motion increases until the molecules have sufficient energy to break down and lose the long-range orientational and positional order, then a disordered isotropic liquid results (Iso) (T_1). The temperature (T_1) in this process occurs is named melting point. During this process, it takes one step for a compound from being fully ordered to being entirely disordered; however, this is not an universal phenomenon for all compounds. Many compounds are provided with one or more intermediate phases as the temperature increases, these phases are called mesophases and the compounds that have these phases are called liquid crystals.

In crystal state, the molecules are held together by strong intermolecular attraction. At higher temperature, these forces break down, resulting in a lamellar arrangement of molecules when the layers are not perfectly ordered, a smectic phase (T2). T4 represents further heating of the smectic phase; the positional ordering is lost, which produces the nematic phase. T6 describes nematic phase which loses the orientational ordering to give the isotropic liquid. If the compound loses both in-plane and out-of-plane positional order under heating (T3), nematic phase is the only mesophase generated. Conversely, a compound may not exhibit nematic phase, when the smectic liquid crystal is heated, the remaining orientational ordering is lost (T5), which gives the isotropic liquid (Iso) [1].

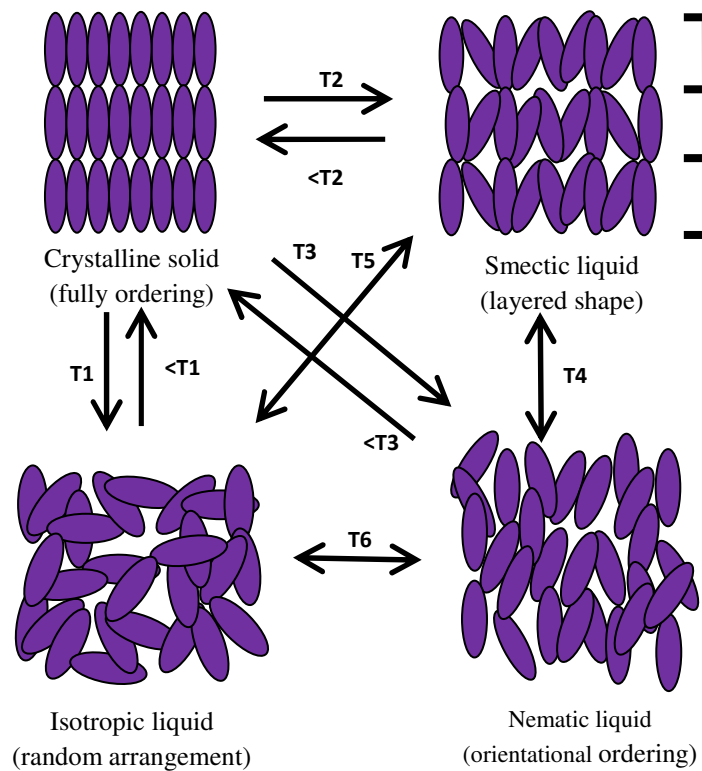


Fig. I.3. Thermal behaviour for a liquid crystalline material

In the nematic phase, the symmetry axes are, as much as possible, parallel to each other and to a certain direction, called the director. With all this, the molecular centres of mass have no long range ordering, it exists only in short range. The nematic phase has a crucial difference from the isotropic phase (Fig.

I.4.) and is the orientational order, which in the nematic phase is long range in opposition to the short range orientational order in isotropic phase. Other parameters may or may not differ from the isotropic phase, such as high fluidity and the magnitude of the anisotropy of the refractive index, the latter being an anisotropic property [2,7].

Mesophases are often identified using a polarising microscope. The optical textures observed under the microscope act like fingerprints, they are unique for each mesophase and different liquid crystals. In Fig. I.4. an example of an optical polarising defect texture is presented, for a mesophase, like the nematic phase. This texture, or what it is seen through the microscope, is created by the anisotropy of the refractive index, or birefringence of the molecules, and a certain distribution of the director through the whole sample. An increase of ordering results in higher ordered mesophases, like the smectic A (SmA) phase. SmA phase has the next level of order meaning that it has an additional translational order in addition to the long range orientational order, but this translational order is in one dimension. Fig. I.4. shows the scheme of the layered structure for a liquid crystal in a smectic A phase.

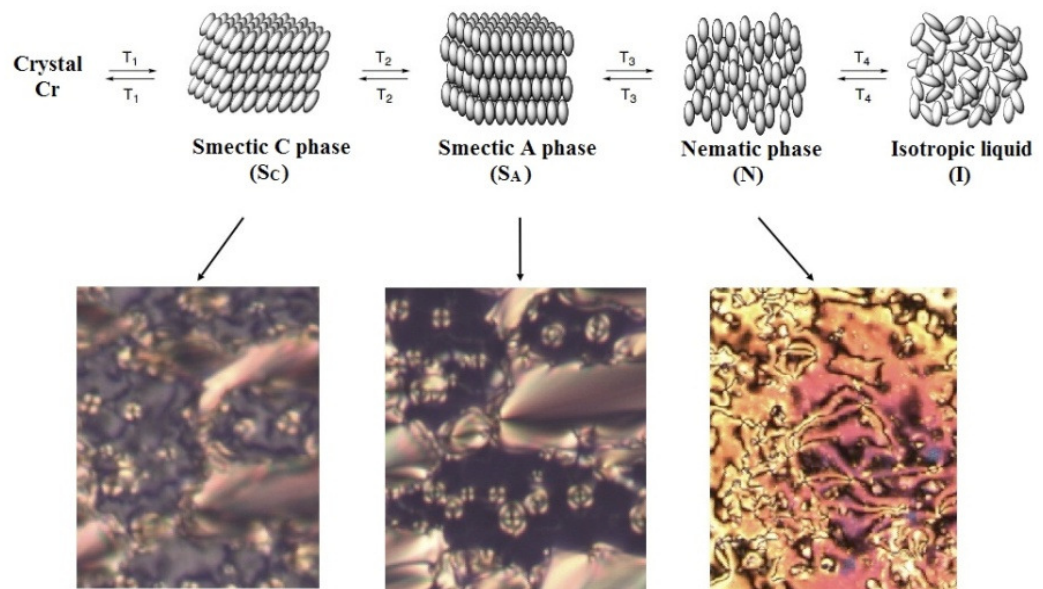


Fig. I.4. Mesophase of liquid crystalline compound

The layer structure of the smectic A phase gives it a much higher viscosity when compared to that for the nematic phase. Looking through the polarising microscope the texture for the smectic A phase is different to that of the nematic phase, as it can be observed from the focal conic fan texture, in Fig. I.4.

A result of an increase of the ordering at a microscopic level in the structure of a smectic A, is the smectic C phase. The crucial difference between the smectic A phase and the smectic C phase is that in SmC the director is tilted with respect to layer normal. The defining parameter for the smectic C phase is the tilt angle, representing the angle between the layer normal and the director [2].

The first thermotropic liquid crystal formed from disk-like molecules was reported in 1977 [2,4]. Since then, numerous mesophases have been discovered and identified. This class of materials that exhibit these mesophases are known as columnar liquid crystals.

The number of compounds that exhibit the columnar phase is large and still growing [2,8]. Perhaps, the most important application for these materials is in electronics, based on the anisotropy of the molecular structure. The central part of these molecules is aromatic and the outer one is aliphatic. Another application for the discotics is in the liquid crystal display industry, where they can improve the optical characteristics for some liquid crystal mixtures [2].

I.1.1. CHIRAL LIQUID CRYSTALS

Molecules may also be chiral in that they are not superimposable on their mirror images; this chirality can result from the tetrahedral arrangement of four different groups around a single carbon atom [2]. Chiral liquid crystals (LCs) continue to fascinate researchers ever since their discovery more than 100 years ago [9]. This is because chiral LC phases formed either by self-assembly or when doped with a host non-chiral LC phase, are intrinsically characterised by an array of unique properties and structures that are promising from both advanced technology and fundamental research points of view [10-12].

A chiral phase has the director twisted into a helix. This is the difference between a mesophase formed from achiral molecules and the chiral phase. The helical chiral structure is characterised by p , the pitch of the helix,

which is the distance needed for the director to make a full rotation (2π) around the helix axis [2]. The pitch is sensitive to temperature, the greater thermal fluctuations of the molecules the smaller pitch length. This behaviour has a potential in thermochromic application of cholesterics (chiral nematic phase), where the wavelength depends on the helical pitch length and so the selective reflection of light [1].

For instance, the frustrated fluid phases such as blue phases (BPs) and the twist grain boundary (TGB) phases [10,11], are of special interest as they arise from antagonistic situations in which the molecules try to organize in a cholesteric-like helical structure, but the molecular interactions may favour the formation of smectic layer structure. Such structures which exhibit both types of structures are impossible to realize and the competition between the two can create frustrated structures, like lattices of screw dislocations. On the other hand, the helical structures of chiral nematic (N^*) or chiral smectic C (SmC^*) have been used in thermochromic and electro-optic devices [3]. The molecular chirality and the nature of the mesogens not only control the properties, but also dictate the preference of one phase over the other. Further, the chiral moieties appear to have a tendency to stabilize the frustrated structures [11,12].

Chiral moieties have been engaged to imbue molecular chirality into the mesogens. They are either synthetic substrates or often chosen from the chiral pool of natural materials, especially steroids [12]. Owing to abundance in nature, steroids, despite their light-sensitive nature, are often used to generate chiral LCs. Not surprisingly, they have been used successfully employed in tuning macroscopic chirality and its associated effects on mesomorphism [14].

Of these materials, *cholesterol* has been incorporated extensively due to its (i) commercial availability as an inexpensive natural product, (ii) rigid structure with eight chiral centres – an attractive feature for realizing chirality in mesophases – and (iii) ease with which the structure can be derivatized [14]. The ability of cholesterol in inducing liquid crystallinity in its various derivatives has been well established; most strikingly, several of them show remarkable properties. This is especially true in the case of nonsymmetric dimers formed by covalently linking a cholesterol moiety to the terminal position of a conventional rod-like mesogens through a flexible spacer [15-18].

A major attraction for these dimers for material scientists is that the cholesterol unit plays multiple roles, such as providing bulkiness, strong chirality, etc., to the system [14]. These materials effectively use the spacer dependence to control the wavelength of selective reflection of light in N* phase. Apart from the strong spacer-parity determined alternation in the transition temperatures and enthalpies, the stabilization and the structure of the layered phase is generally governed by the relative lengths of spacer and terminal tail in these cholesterol-based dimers [14].

I.1.2. LIQUID CRYSTAL DENDRIMERS

Dendrimers were first discovered in the 1970s [19] and since then they have known an impressive rapid pace of development. Nowadays, they found use in many areas of science [20,21]. At microscale, dendrimers have unusual and unique features and these molecular arrangements make them appealing to scientists. Furthermore, the possibility of assembly in new interesting architectures makes dendrimers a challenge for research chemists [22]. The word dendrimer comes from the Greek words *dendros* meaning tree and *meros* meaning part. Dendrimers are a class of monodisperse compounds having a controlled and regular three-dimensional branched morphology [20,21]. As the generation number increases so does the rate of size, in a geometrical manner. Hence, these molecules can possess a large number of functionalities per unit [23]. An interesting and useful fact, when compared to polymers of similar size, is that they have no entanglements and with this lower viscosity and good solubility in most of the organic solvents.

Medicine and materials science are other two of the many areas of applications for these compounds [24]. This is due to the combination of the functionality in the centre of the molecule and at the termini with the large and defined morphology of the superstructures. Other uses, when precisely functionalised, are in biology as drug carrier or gene delivery [25], bio-mimetism [26] because they resemble in shape to some living components, or chemistry due to their catalytic, multiredox, chiroptical properties. Another possible use could be the design of oligomeric materials in which information transfer takes place from

the periphery to the core or vice-versa and expecting synergic phenomena (*i.e.* induction of new properties) and/or cooperative effects (*i.e.* amplification of the existing properties) [27].

I.1.2.1. SIDE-CHAIN LIQUID CRYSTAL DENDRIMERS

The complete structure a side-group liquid crystal dendrimer is composed of a flexible branch-like network with a branching multiplicity N_B , starting from the core as the multipoint initiator, with a connectivity N_C , and mesogenic moieties attached terminally (end-on) or laterally (side-on) at the end part of the branches (Fig. I.5).

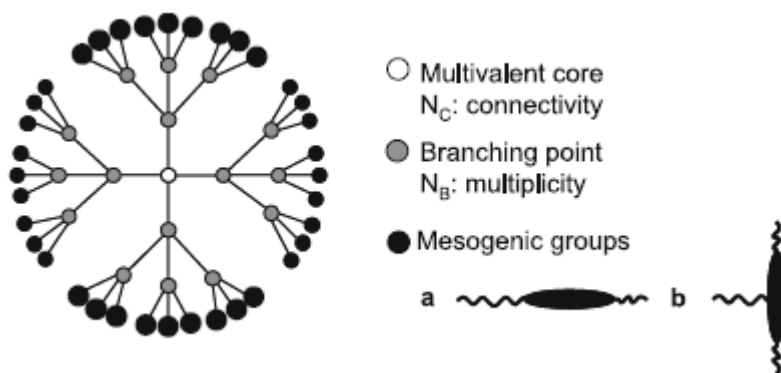


Fig. I.5. Schematic representation of an end-group LC dendrimer, second generation. The mesogenic group is attached terminally (a) or laterally (b) [31]

Step by step synthesis of new supermolecular structures gives materials which are highly monodisperse and with high molecular symmetry. These complex architectures can be prepared or grown by increasing the number of generations of the building blocks, small sub-molecular groups. Through this process usually hyper branched systems are obtained and are characterised by highly complex chemical structures, unusual physical and chemical properties and high levels of symmetry. The morphology for the whole mega structure is modified as the generation number increases and the density of the building blocks in that generation. Hence, the molecule tends to become spherical or globular in shape [28].

I.1.2.2. SILOXANE DENDRIMERS

Only a small number of dendrimer classes have been made and build around a siloxane central core. Fig. 6 shows an example of such siloxane dendrimer composed of methylsesquioxane matrix and six cholesteryl groups attached at the termini using undecylene spacers [29]. This material has a smectic A phase with a broad temperature range. At microscale, in the smectic phase, in one single layer, the complete overlap of the cholesteryl groups is observed and these mesogens are separated by siloxane layers.

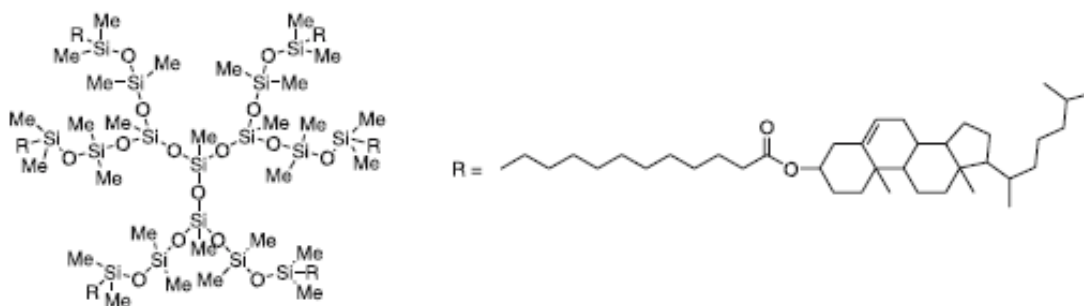


Fig. I.6. Chemical structure of the dendritic methylsesquioxane matrix [31]

A different class of dendrimers are the silsesquioxanes. There are two types of these nanostructures: ladder- and cage-like. For example, the 3D organisation like the organosilicon cage, have great potential in the area of material composites. They can be functionalised in the corners with suitable groups and then combined with organic moieties to form organic-inorganic hybrid systems. One example of such materials that can be obtained in this way is copolymers and they exhibit new and exciting properties [30]. Two major topics were the focus when using these polyhedral organosilicon cages as central core and they are: the development of new synthetic paths and increase the efficiency of already known ones; and to improve the separation techniques [28]. To use the silsesquioxanes cages as central core is very useful as they have several potential branches to be derivatized and so the packing limit can be reached in just a few generations [31].

A silsesquioxane based liquid crystal is composed of the following: a silsesquioxane core; a linking group connecting the inorganic core to the hydrocarbon chain, and it could be a silicon-organic group; the spacer, a hydrocarbon chain situated in between the silicon based core and the mesogenic group; and a last component, the mesogen [28].

So far, in literature has been reported the convergent path as the only route for synthesizing the polyhedral organo-silicon based liquid crystals. Although as concept, it is not restricted to this, this method means that the silsesquioxane core and the mesogenic side-chain are prepared separately and connected in the last step [28].

To synthesize the silsesquioxane core there are two pathways which are used more often. One is the controlled hydrolysis of functionalized trichlorosilanes. A variety of structures can be obtained by controlling the reaction conditions and the follow-up procedures. A second method is the controlled condensation of silicic acid followed by functionalization. From all the cores that can be prepared through one of these two methods, the cubic octasilsesquioxanes are the most used.

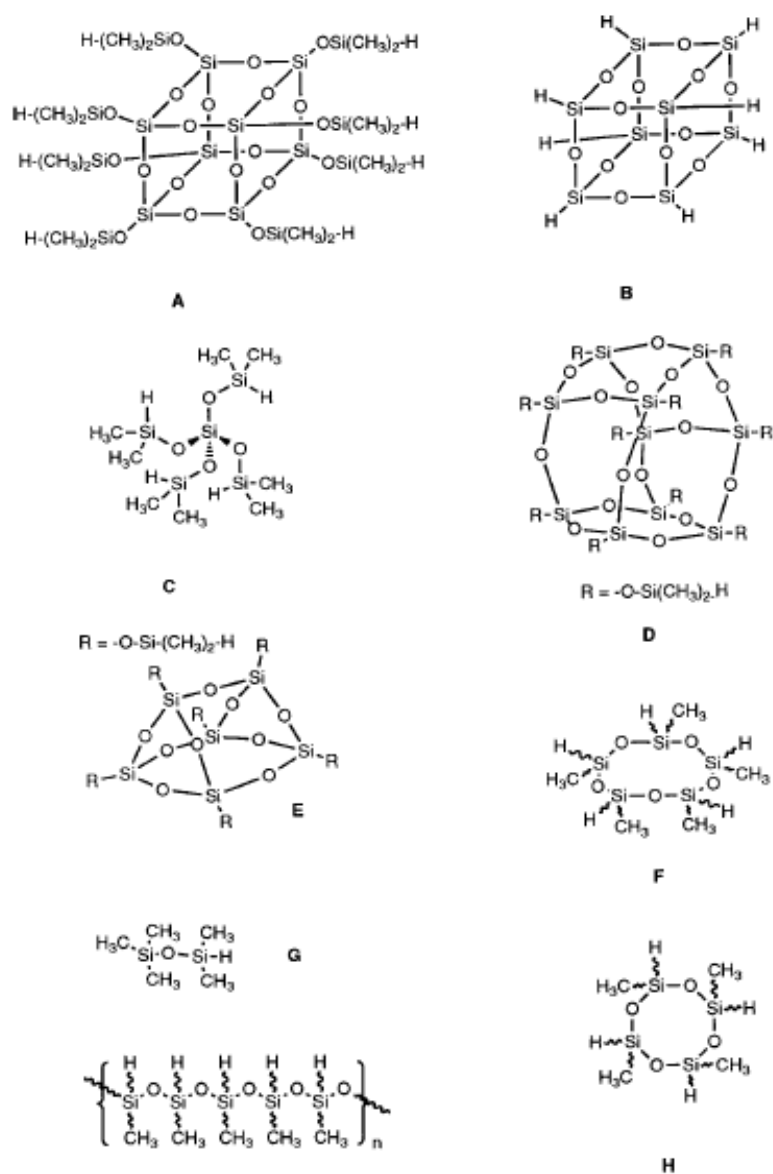


Fig. I.7. Structures of the silicon-containing cores [28]

The reaction of suitable organic groups in combination with well defined inorganic silsesquioxane cores leads to covalently hybrid materials, which exhibit nematic and smectic C phase behaviour close to room temperature.

A limited number of examples of monomeric LC polyhedral silsesquioxane materials have been reported [32-34]. Two approaches have been followed to produce nematic silsesquioxanes; i) the first silsesquioxane nematogen reported was created through the lateral attachment of mesogens to the silsesquioxane core and ii) a completely different approach that utilizes partial substitution of the cubic core.

Octasilsesquioxanes provide a useful central core system due to its high potential to be derivatized. It has eight points where mesogenic units can be attached to and so it can double or even triple the number of mesogens [35]. Earlier in literature, eight cyanobiphenyl groups were attached to the octasilsesquioxane cubic core using flexible aliphatic chains [32]. If flexible hydrocarbon spacers with different lengths are used, the resulting organic-inorganic super hybrids exhibit lamellar smectic A phases. To explain the formation of such liquid crystal phase, the mesogens must associate with one another, and therefore changing the spherical shape of the supermolecule into a rod-like one. Using X-ray diffraction it could be shown that the rod-like molecules pack in disordered layers.

By doubling or tripling the number of mesogens a competition was expected to exist between the need for the supermolecule to remain globular because of packing hindrance and ability for the whole hybrid system to be deformed and fit within the mesomorphic environment. With a high density of mesogens it was thought that mesophase will transform from lamellar to columnar or even cubic phases. The first generation of the dendrimer (Fig. I.8.) exhibits smectic A and C phases. The effect of the dendritic structure is the lowering of the clearing point [36]. These dendrimers have a completely different thermal behaviour compared to conventional liquid crystal polymers.

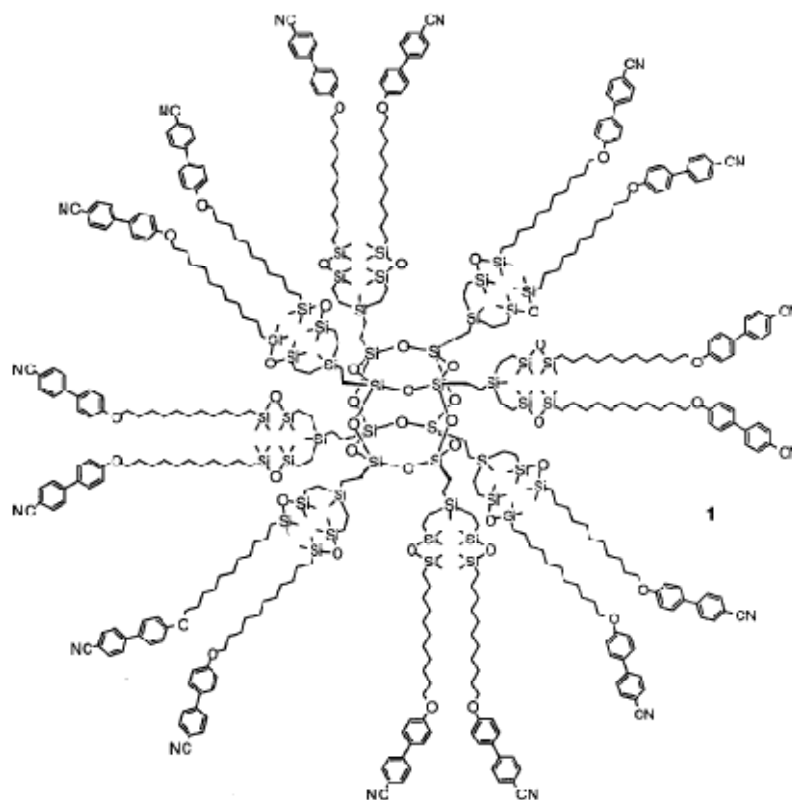


Fig. I.8. Structure of octasilsesquioxane-based dendrimer [36]

The two smectic phases, A and C, were identified through the textures observed using POM, on cooling from the isotropic liquid. The smectic A phase gives a focal conic texture characterized by hyperbolic and elliptical lines of optical discontinuity. Along with the focal conic texture a homeotropic texture was formed. Both these textures and defects were a proof that it was a smectic A phase [37].

If the smectic A phase is cooled a second order phase transition takes place, from the smectic A phase to smectic C phase. After the phase characterisation for smectic C it was revealed that the dendrimer must have a rod-like shape so its packing is in layers. Nevertheless, the layers are diffuse and the molecules within the layers disordered. This dendritic liquid crystal has a quasi-bilayer structure in respect to the mesogen and a monolayer structure in respect to the silsesquioxane cubic core, meaning that it is a microphase separated system. On cooling, either the mesogens tilt or the whole molecule tilts over to form the

smectic C phase. The first scenario is the most likely to be happening. (Fig. I.9.) [36].

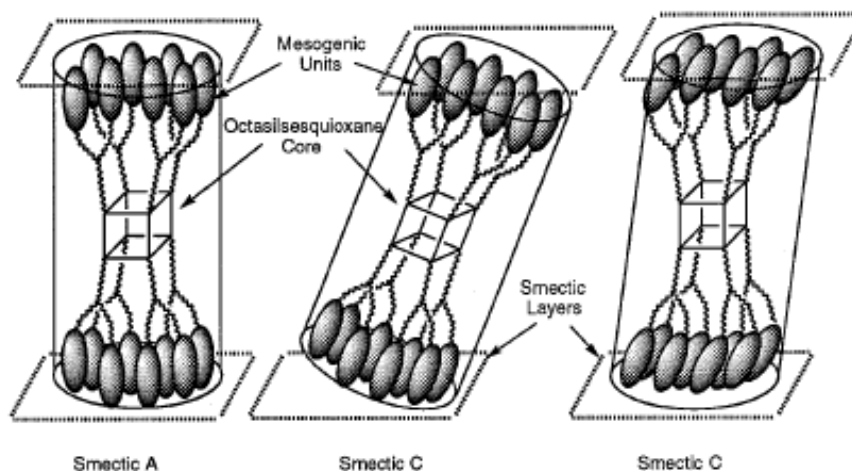


Fig. I.9. Possible molecular topologies enforced by the liquid crystalline environment [36]

Preparing this dendrimer which exhibits smectic C phase makes it easier for the chiral systems to be synthesized and they will exhibit non-linear and anisotropic properties such as piezoelectricity, pyroelectricity and ferroelectricity [36].

The introduction of chirality into spherical dendritic systems provides an opportunity to examine the potential for materials to have molecular defects based on the chirality of the system in a similar way to how, on the mesoscopic scale, boojums are found in chiral nematic phases [38].

From the point of view of how the mesophases are formed, the presence of columnar mesophases suggests that the octasilsesquioxane dendrimer has a disk-like gross molecular shape. The inter-columnar distance, however, is far too small for the long axes of the mesogens to be arranged in the planes of the dendritic discs, that is, like spokes in a wheel. An alternative model could be one in which the long axes of the mesogenic units are perpendicular or near perpendicular to the disc [38].

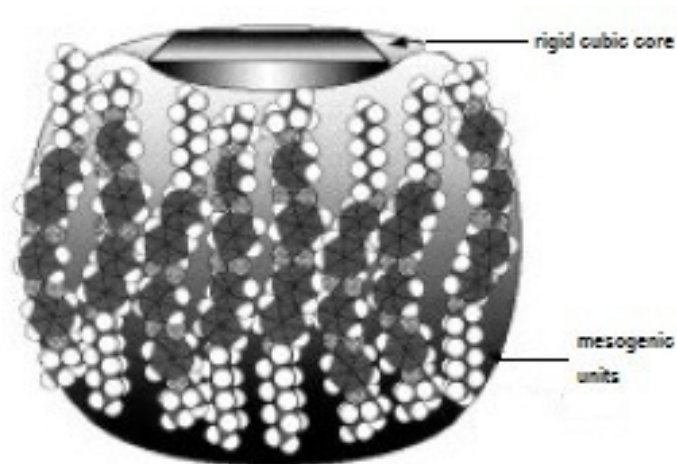


Fig. I.10. Schematic representation of the conformational structure of the dendritic disc [38]

The long axes for the mesogens are considered to be parallel or with a slight tilt with respect to the rotational axis. Considering the rotational axis as a cylinder, the mesogens are packed side-by-side on the exterior of the cylinder. The situation is not that clear regarding the chiral nematic phase. Two possibilities arise, one in which the dendritic molecules might assume more of a rod-shape, thereby self-organizing to give a chiral calamitic nematic phase (Fig. I.11.), or alternatively, the dendritic molecules assume the cotton-reel structure and thus self-organize to give a chiral nematic discotic phase (Fig. I.12.). [38].

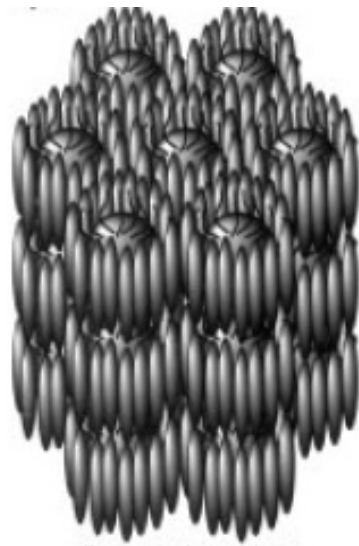


Fig. I.11. A schematic representation of the structure of the disordered hexagonal columnar phase. The octasilsesquioxane core is shown as the top of a ball with the mesogenic units forming a “cloud” around it [38]



Fig. I.12. A proposed model for the chiral nematic discotic phase [38]

The chiral nematic octasilsesquioxane dendrimer is relevant to the field of liquid crystal displays based on light scattering since the use of dendrimers in scattering electro-optical switches has also been reported [39].

In order to assure the formation of liquid crystalline phases above ambient temperature, aromatic core structures of the mesogenic units were selected containing three or four aromatic rings, linked by C-C single bonds or ester groups. In order to assure a suitable stability range of the liquid crystalline phase, terminal alkyl chains of eight or eleven methylene groups were selected. The liquid crystal phase behaviour is governed mainly by microphase separation of the organic and siloxane groups [40].

A different class of mesogens are the metallomesogens. Generally speaking, they are quite difficult to synthesize them and problematic to work with; this is due to the existence of a reactive metallic centre in the side-chain. In order to functionalize the cage, the specific method must be tolerant to the cage, the functional groups in the mesogenic units, but also the functionalisation must avoid any potential interference of the metallic centre. From most cases, the hydrosilylation reaction is sensitive to this interference. The reaction is a metal catalyzed reaction in the presence of another metal. A crucial step is to choose the right catalyst and to avoid side reactions, thus the reaction conditions must be as mild as possible [28].

The use of metallomesogens in the lateral chain creates a wide range of potential interesting materials which are mostly inorganic in structure. Why choose to include metals in mesogenic units? The combination of different properties for each part, organic or inorganic, and their synergetic behaviour make them appealing materials. Amongst the properties expected from the metallic core magnetism and/or conductivity can be noted. And to these the liquid crystalline behaviour is added. The liquid crystal research proved its versatility with the inclusion of metals in the liquid crystal side chains which deals with the soft matter state of the liquid crystal hybrids [28].

If to the silsesquioxane core more than one type of mesogens is attached and if there are still some Si-H groups unconverted, it is possible that the properties of the LCs can be tailored by the selection the appropriate mesogen. For example, if only two rigid mesogens are attached, the phase transition

temperatures tend to depend mostly on the core structure and also the liquid crystals with more aromatic cores in the side-chain have higher transition temperatures [28].

For side-chain liquid crystal polymers it is established that for a given lateral chain the phase transition temperatures increase with the number of repeating units in the polymer, and after a certain value in the degree of polymerisation a plateau is reached and the phase transition temperatures are constant [41]. In case of oligomeric systems, if the number of side-chains is modified from four to eight, the phase transition temperature is not affected to a large degree, but materials having silsesquioxane as the central core tend to have a higher glass transition temperature (T_g). If the glass transition temperature is decreased by an increase of the spacer length, this is possibly due to the plastifying effect of the alkyl groups. The silsesquioxane based materials having longer spacer groups exhibit, at lower temperatures, a crystalline polymorphism that is not yet fully explored and explained. [28].

I.2. NANOPARTICLES

Nanotechnology is currently one of the most important new areas in science. Emerging new applications from nanoscience in the past decade gave a boost to nanomaterials research in terms of financial support, grants, investments in related technologies and areas of applications.

Nanotechnology is the science of materials in the 1-100 nm size range and studies structures, materials and devices and their manipulation. At this scale, the materials acquire unique properties which are most of the times different from the same materials at micro- and macro scale, this is why we can consider them as new chemical compounds.

There is a huge amount of excitement regarding the future of nanotechnology in terms of innovation as it is able to create many new devices and materials with a wide range of applications, such as engineering [42], electronics [43,44], medicine [45,46], optics [47,48], lasers [49] and catalysis [46,50].

At the heart of the nanoscience is the nanoparticle (NP). Even though they have a long history, only in recent years their use reached their potential and the understanding why and what gives nanoparticles their structural properties and unusual functional features. But this was only possible with the development of new instruments for particle characterisation, hence a new disciplinary arose.

We can differentiate two major groups of NPs: organic NPs (micelles, polymer based NPs, carbon nanotubes (CNT)) and inorganic NPs (quantum dots, magnetic NPs, gold NPs).

The applications for nanoparticles are a result of two major factors: organisation and size. As different size of nanoparticles give different properties is hugely exciting in terms of the challenges met by researchers around the world to explain and overcome these obstacles. The polydispersity and purity of these materials are crucial but very difficult to control. These drawbacks are insignificant comparing to the NPs' final applications. As NP's size is decreased, the number of free electrons is reduced and their properties are governed mainly by the quantum effects [51,52]. Also, smaller than 3 nm, gold or silver nanoparticles are no longer considered noble metals, their chemical reactivity is increased significantly and they have high potential to be used in catalysis. Overall, the properties of small nanoparticles differ from the ones in bulk materials, this is why the size-controlled synthesis of these nanoparticles is so important and an ongoing challenge. The formation of ordered systems is crucial when it comes to devices and high-tech applications, molecular machines small in the order of molecules and atoms, ready to perform tasks required and predetermined.

Connected to the size, another important factor is the shape of nanoparticles. This parameter as well can be controlled and the properties can vary function of the packing complexity. For example, one-dimensional (1-D) structures such as nanoribbons, nanotubes or nanowires have a wide range of potential applications from science to engineering. Especially, the nanoribbons through their planar structure can help to understand the transport phenomena in dimensionally confined spaces [53], as only one direction is available for charge transport, the other two are considered negligible. The 3-D nanostructures offer a myriad of potential applications as the final nanostructure is a result of a

synergetic effect of the size, shape and anisotropy of the NPs plus their functionality, brought by the layer(s) that covers the nanoparticles.

Currently, there are two major approaches of forming these nanoparticles, *i.e.* “bottom-up” and “top-down”, with a wide variety of methods used and under continuing development. Through the “bottom-up” approach, small components, like atoms and molecules, are assembled in a controlled process [54]. The “top-down” methods require starting from an assembly, a bulk material and through different techniques, such as lithographic techniques, the formation of smaller moieties with determined and different properties. But these methods lack the necessary resolution and the ability for fine-tuning for the formation of truly three-dimensional structures with precise properties. Therefore, the “bottom-up” molecular self-assembly is the method of choice for preparing most of nanostructures, due to its versatility.

NPs can be synthesised using classical methods and techniques, such as using micro emulsions, reverse micelle formation, electro deposition, lithography, sonication techniques, etc. Also, it worth to note that these NPs can be placed on different surfaces, like Au, Ag, silica, glass, polymers, etc by chemical or physical means; the result is the formation of regularly ordered structures with predictable properties.

In the majority of synthetic procedures of these NPs, organic compounds are involved in the reaction with the role of protecting the NPs, controlling their size, add to their functionality and chemical reactivity, and to modify their physical properties as well. Coordinative ligands, micelles and polymers were used to stabilize the NPs. To further improve their applicability, there is also the possibility of ligand exchange after the nanoparticles are prepared in the right shape and size, using an appropriate compound, in terms of shape, size and functionality.

For NPs which are not made of noble metals, there is always the problem of oxidation, when it is required metal atoms, not oxides or other. So, the organic layer protects against the environment. For example, iron NPs can oxidize quickly unless they are protected. Another way to achieve this is through the “core-shell” method and it is based on encapsulating a nanoparticle inside a bigger one. Therefore, there is a layer of densely packed atoms or molecules covering a smaller nanoparticle. By having this configuration, the complex nanoparticle can

exhibit a synergy of properties; for example, the inner particle can be magnetic and the outer one could give optical behaviour. This example it is not the only one, a vast number of nanoparticles are prepared to have this core-shell structure [55,56].

An important category of materials based on nanoparticles, are liquid crystalline (LC) materials. The liquid crystal nanoparticles' (LCNPs) degree of organisation is based on the fluidity and order that they exhibit. They provide the opportunity for a large number of complex architectures to be created, and with it, unique properties and increased processability.

These properties are given by both the nanoparticle's metallic core and the organic layer(s). Therefore, the properties of LCNPs can be programmed as they are influenced by external stimuli, such as magnetic fields, electric currents, surface effects (mechanical work, chemical interactions).

Two major types of inorganic NPs used extensively in the past few years are: gold nanoparticles (Au NPs) and iron based nanoparticles, like iron platinum nanoparticles (Fe/Pt NPs); the firsts for their optical properties [57] and more, and the latter for their intrinsic magnetic properties [58]. Considering these NPs covered with liquid crystal phase inducing molecules, their properties, processability and potential applications can be increased and/or improved.

I.2.1. GOLD NANOPARTICLES (AuNPs)

Researchers have been focused extensively on AuNPs in the past decades and it is very likely that this trend will continue for the foreseen future. All this interest is due to the vast range of applications for these NPs, and especially due to their optical properties. Nowadays, the AuNPs can be prepared quite easy with relative control of size and shape. As size and shape dictate the properties, and therefore the applications, it has become necessary that the synthesis can be specifically controlled and it is assumed that the final nanomaterials have the programmed shape and low polydispersity.

AuNPs can be prepared in a wide range of shapes, from spherical to triangular to belts and ribbons, in a very well designed and controlled synthesis.

When it comes to properties, first of all, gold nanomaterials exhibit special optical properties due to its surface plasmon resonance. It has been reported extensively that anisotropic gold particles exhibit two surface plasmon resonance absorption peaks corresponding to the light absorption and scattering along the short axes and the same for the long axes of the systems; and, one single absorption band at 520 nm for the spherical gold nanoparticles. Sometimes, there are observed additional peaks in nonspherical nanoparticles. So, UV-Vis spectroscopy is an important tool for characterisation of the gold nanoparticles; even more so, when it comes to applications due to their optical properties.

In terms of optical properties, in the case of spherical gold NPs when suspended in a transparent media, based on their sized the reflected light has different colour. Larger AuNPs, around 100 nm, appear red or purple and for diameters less than 3 nm, the colour shifts to brown.

1.2.1.1. PREPARATION METHODS FOR AuNPs

In the following, the currently most successfully techniques for the preparation of AuNPs with their advantages and disadvantages will be discussed.

Preparing stable dispersions of gold nanoparticles in water is very important for some applications [59]. Although important, the water based synthesis of such nanoparticles has a number of drawbacks such as the difficulty of removing the residue of stabilizers used, ionic interactions, low gold nanoparticle content of the reactions and limited surface derivatisation. Preparing these gold nanoparticles in an organic solvent eliminates the inherent problems when using water. Moreover, AuNPs can be prepared in high concentrations with controlled size and shape and improved monodispersity.

A general way for preparing the AuNPs is the chemical reduction of gold salts. For this method typically four components are used: solvent, metal salt, reducing agent and the stabilizing agent.

For many years two methods for preparing AuNPs: the citrate method [60,61] and the two-phase method [62,63] were extensively used.

In one of them the metal salt is reduced in water, in air at room temperature with a strong reducing agent, such as sodium borohydride, to obtain

small AuNPs in the range of 3-5 nm. Now, this solution can be used as the seed solution to form bigger and anisotropic nanomaterials. The seed particles can be capped with a number of surface groups (surfactants, citrate, polymers, etc). To form different anisotropic structures, a second solution is necessary. This growth solution contains more metal salt, a mild reducing agent and a structure-directing agent. As the weak reducing agent ascorbic acid (vitamin C) is used; by itself and at room temperature it is not strong enough to solely reduce the metal salts to the elemental metal. This is why when the seed solution is added, the growth is resumed at the particle's surface and it assumed to be autocatalytic producing larger particles. At this stage the presence of the structure-directing agent is mandatory to obtain nanorods and not large nanospheres. Cetyltrimethylammonium bromide (CTAB) is used as structure-directing agent, for preparing nanorods. In opposition, using the chloride only spheres are obtained and in the case of using iodide, different mixtures of anisotropic shapes are given. Starting from small spherical nanoparticles, the final nanorods can grow up to 600 nm in length and 20-30 nm in width, but not larger [64].

The growth mechanism for nanorods and other anisotropic shapes was initially discussed controversially. The reason was the understanding how and why from a spherical small NP, the growth seems to prefer just one direction. First, a single crystalline seed particle is formed, and then the surface binding groups (surface-directing agents, surfactants, and capping agents) preferentially bind to only certain faces of the crystal seed or growing nanorods. One difficult question is, when initially there is a spherical seed particle, how the tips of the nanorods are formed. It is not completely explained, but it could be that because of internal twinning and faulty stacking, it is enough to create an anisotropic electric field in the seed and therefore a preferential direction for the nanorods to grow. The second question is how the nanorods grow from the initial spherical seed particle with a preferential tip formed? The answer is the use of structure-directing agent and this works by blocking the long axis sides of the crystal and doing so, it is promoting the growth only on the faces in short axis of the crystal. Considering this model mechanism, even the OH group can be a structure-directing agent and so any small ions can play the role of structure-directing group to form anisotropic shapes.

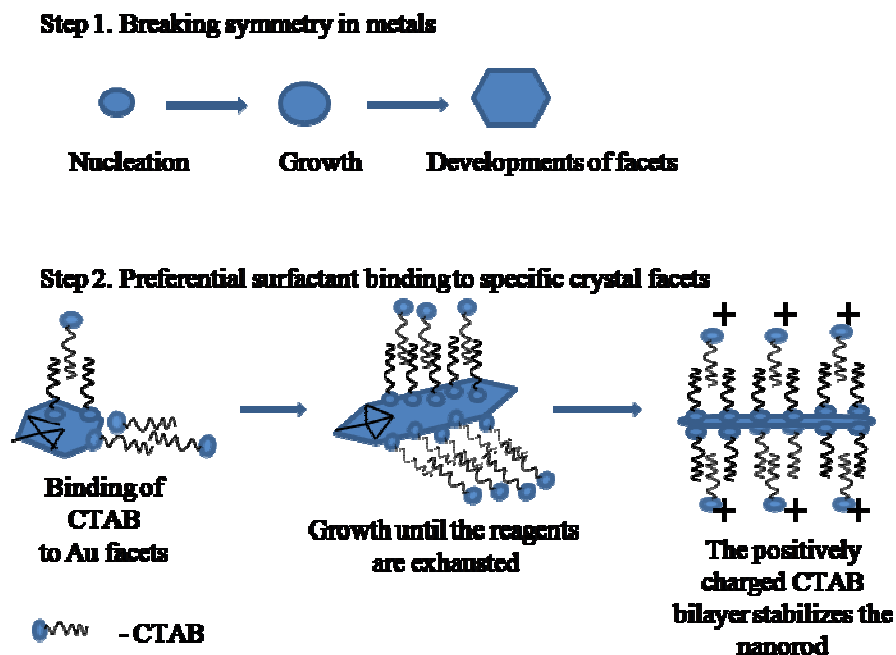


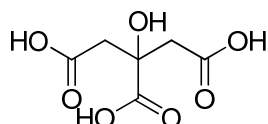
Fig. I.13. Proposed mechanism for metal nanorods growth

Another typical method for preparing GNPs is the reduction of gold chloride with sodium citrate and sodium borohydride [65]. The nanoparticles are formed typically in the range of 2 – 100 nm. Unfortunately, this method has a few drawbacks starting with the fact that it can only produce good quality nanoparticles with size up to 50 nm. For sizes bigger than that the nanoparticles are polydispersed and nonspherical [66]. One way to improve this method is to reduce the gold into small seed particles, but a secondary smaller nanoparticles population is formed and this is in addition to the already prepared nanoparticles. Fortunately, there is a way to overcome this issue and it involves selective reduction of gold at the surface of nanoparticles with a mild reducing agent, such as hydroquinone (HQ) [67]. The way this method works is that hydroquinone which is a weak reducing agent, weak enough not to reduce isolated Au^1 to Au^0 , but only in the presence of metal clusters [68]. Also, gold chloride can be reduced by UV light, so the solution of gold chloride may contain some elemental gold (A^0) clusters. It was observed that a low concentration of citrate gives an improved overall quality of the nanoparticles batch. In summary, using HQ as a mild reducing agent has improved the monodispersity and overall quality in terms

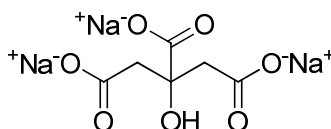
of shape of NPs when it comes to nanoparticles bigger than 50 nm and up to 200 nm.



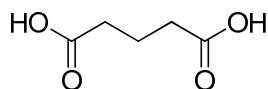
Scheme I.1. Reduction of gold precursor with citric acid



Scheme I.2. Citric acid



Scheme I.3. Trisodium citrate



Scheme I.4. Glutaric acid

When using sodium citrate as reducing agent, the gold salt solution was initially yellow, and after the addition of the prepared sodium citrate solution, the sodium citrate turned into citric acid. At this stage, the yellow solution became colourless and transparent. Afterwards, the solution turned to a black and later to a red colour. Throughout all these stages the solution was kept under stirring. The size of monodispersed particles is controlled by the initial reagent concentration.

Another method for preparing gold nanoparticles is based on the use of sugar (D-glucose) and the reactions are occurring in sonolysis [69]. The major chemical steps are:



From the reaction of D-glucose with radicals from the hydrolysis of water molecules, hydroxyl and hydrogen radicals are formed (Eq. 1), and from the decomposition of D-glucose (Eq. 2) two types of reducing radicals very effective for the reduction of gold chloride ions (Eq. 3) are formed, followed by the growth of the gold particles (Eq. 4).

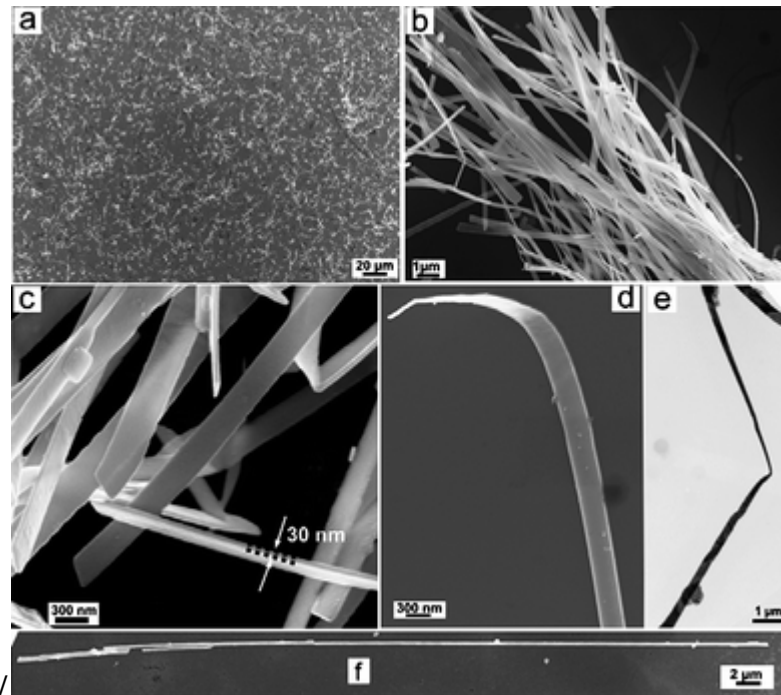


Fig. I.14. TEM images of gold nanobelts.

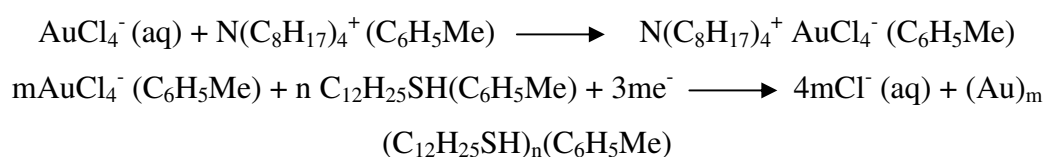
A further method for gold nanoparticles synthesis is based on the reducing and stabilizing effect of block copolymers [70]. There are three main steps that lead to the formation of GNPs from gold chloride: the reduction of AuCl_4^- ions by the copolymers in solution and the formation of Au nanoclusters, followed by the absorption of block copolymers on the gold clusters' surface and

the reduction of gold chloride on the surface and the growth of nanoparticles and the final step, the stabilization of NPs by block copolymers [71].

This particular synthesis and subsequently the nanoparticle formation are enhanced by the increase in molecular weight and the length of the blocks of copolymers, and also by the increase of temperature and concentration. These copolymers play different roles based on a number of variables, such as molecular weight, block length, temperature and polymer concentration. Among the roles played are: size of NPs, shape, yield, formation rate and stability. However, this method has a few limitations and the most important is the low yield of the NP synthesis. Also, the nanoparticle concentration does not increase with the gold salt concentration.

A further method for the synthesis of gold NPs is the so-called Brust-Schiffrin method. This method is based on the growth of metallic nanoclusters simultaneously with the attachment of the thiol self-assembled monolayers (SAMs) on the growing NPs. Since its development, variations of this method are used extensively.

For this to happen, the surface reaction of the thiol moiety during the metal nucleation and growth, a two-phase system is used. In this method AuCl_4^- is transferred from the aqueous solution to toluene using tetraoctylammonium bromide, as phase transfer reagent. Then, it is reduced with a solution of sodium borohydride in the presence of dodecanethiol ($\text{C}_{12}\text{H}_{25}\text{SH}$). The organic phase changes colour on the addition of the reducing agent, from orange to dark brown, in a very short period of time.



*the source of electrons is the BH_4^-

Scheme I.5. Reactions for preparing coated AuNPs

The ratio thiol to gold is determined by the reaction conditions.

The NPs prepared using this method are highly monodisperse. The HRTEM photographs reveal the size of the NPs within 1-3 nm range.

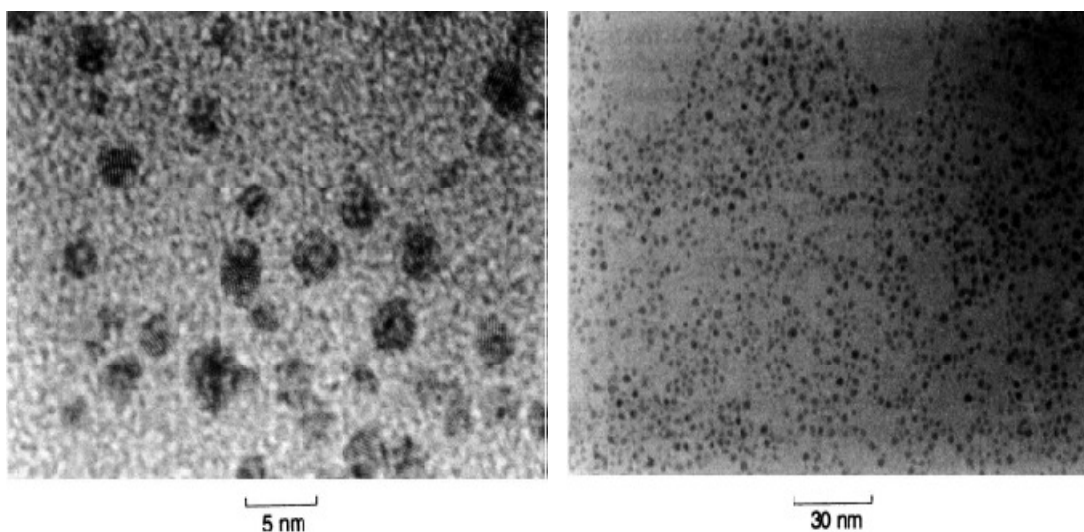
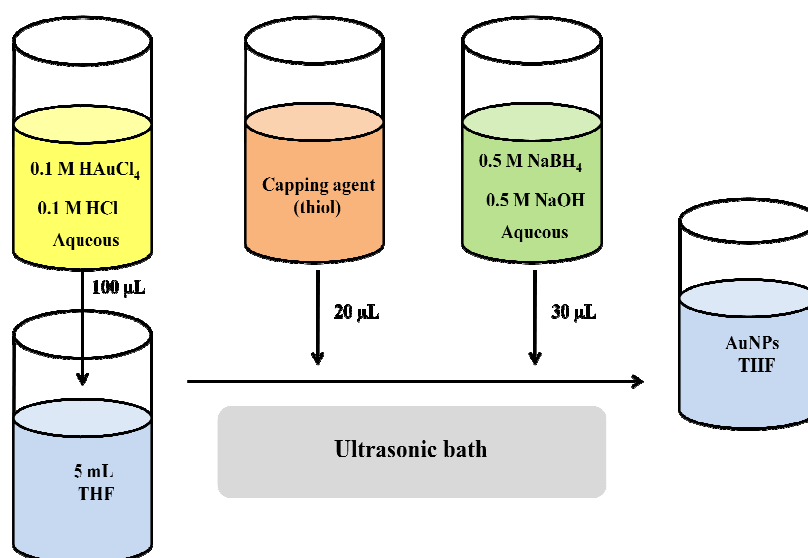


Fig. I.15. TEM images of NPs prepared using Brust method

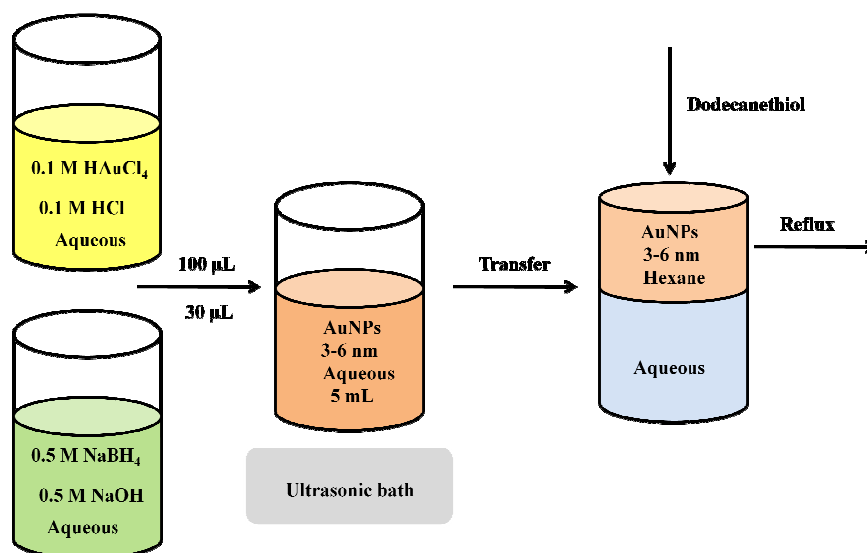
Some of the most important advantages that this method brings are: first, it is a simple way to a direct preparation of surface-functionalized gold NPs; the size of NPs can be controlled simply by the reaction conditions, as the NPs' growth kinetics is determined by the surface coverage; it can be considered that these NPs behave like small and simple chemical compounds, they can be precipitated, redissolved and characterised with no changes in properties.

A different method, based in a way on the Brust method, has been developed by C.-H. Yu. It is a simpler method, the NPs synthesis is carried out in a one-phase system and it requires only the metal precursor, the reducing agent and the functional organic capping agent (thiol). This method removes the necessity of the ligand exchange step, which is used when Brust method is chosen.

This method gives highly monodisperse NPs, good quality and shape, and they can be processed many times without them aggregating and losing their properties. Their size can be controlled though the procedure conditions and NPs with the desired ratio of gold to ligand can be prepared with reproducible results.

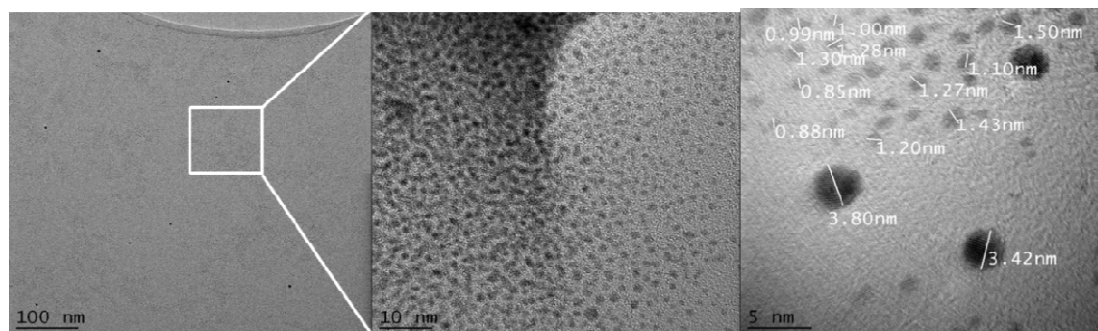


Scheme I.6. Preparation scheme for < 2 nm coated AuNPs



Scheme I.7. Preparation scheme for 3 - 6 nm coated AuNPs

a)



b)

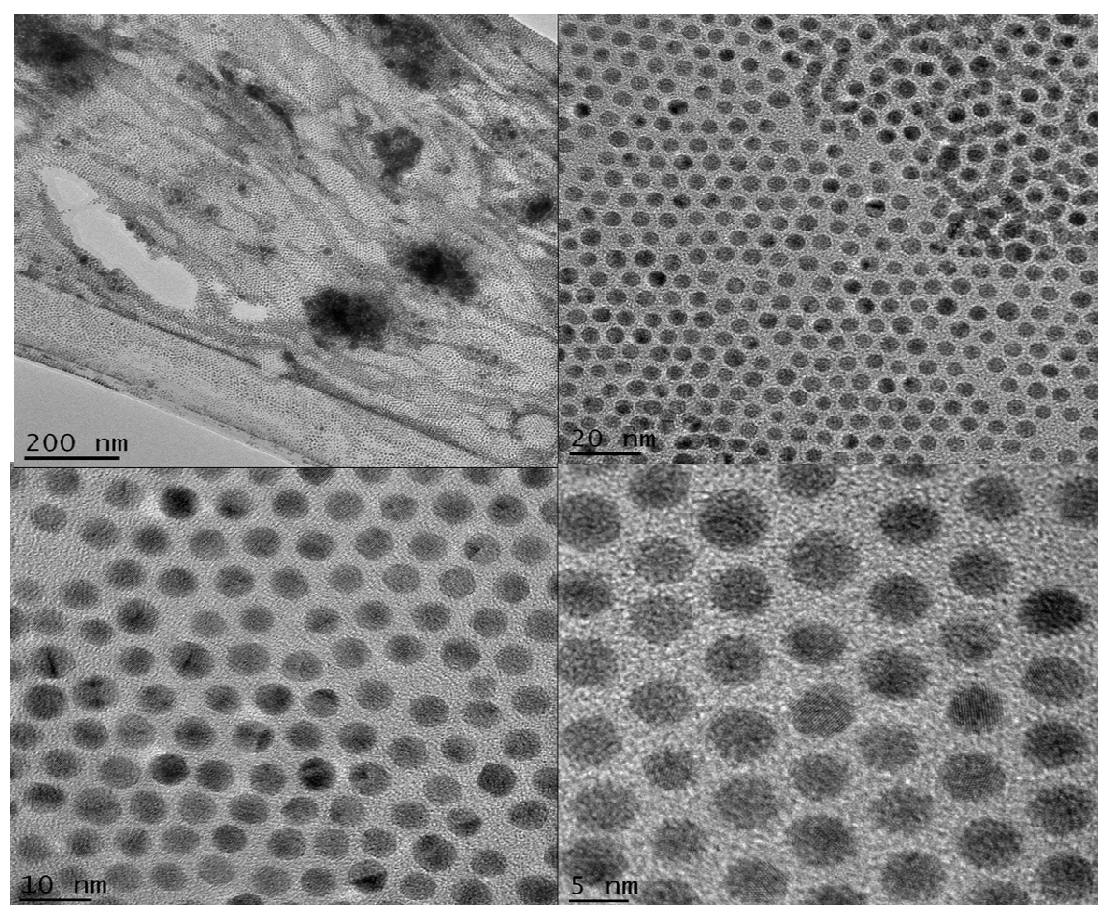


Fig. I.16. TEM images for thiol coated AuNPs: a) < 2 nm
and b) 3 - 6 nm

I.2.1.2. LIQUID CRYSTALLINE NANOPARTICLES (LCNPs)

Liquid crystalline metallic nanoparticle hybrids are of an enormous interest due to their potential applications and very interesting properties. The reason for this is the presence of the two distinct parts, each of them giving different properties. The synergetic effect of the two groups determines a set of properties different from those given by the separate groups.

It is possible to prepare metallic cores of different shapes and sizes covered with one or more layers of organic or hybrid ligands. At present, a wide range of methods to synthesize the metallic NPs with desired shape and size with reproducible results have been reported. The mesogenic organic layer(s) is attached typically directly or through a ligand exchange reaction to the metallic core. Although, the preparation of these hybrid NPs looks fairly easy, to obtain LCNPs is much more difficult. The reason for this is that the LC state depends on a number of parameters. First of all, the anisotropy of the system must be achieved, either from the shape of the metallic core or the molecules that form the outer layer can arrange themselves in such a way that have a certain degree of ordering, but still can maintain the NPs in a fluid state. This is quite difficult to achieve by design, even more so if one aims to design hybrid NPs with specific mesophases and a certain temperature range.

The most common shape for LCNPs is the sphere-like polyhedral. In addition, research has been focused as well on plate-like [72] and rod-like shapes [73,74]. As the last two are anisotropic shapes, the LC behaviour depends less on the chemical structure and arrangement of the ligand. For NPs with spherical polyhedral metallic core the organic layer has an important role in creating the mesogenic behaviour. Hence, the chemical structure, number of ligands, type of attachment are crucial.

To obtain LCNPs, the relationship between the metallic core's shape and size and the organic ligand must be carefully controlled. Therefore, the size of the core is very important. If the core is too large then the organic mesophases-inducing ligands cannot impart any fluidity as well as arrange themselves in an ordered manner for the NPs to be LC. In other words, if the volume fraction of the

molecular corona is too small the solid state properties are determined predominantly by the metallic component.

Overall, the synthetic path to prepare the organic ligand is relatively clear and flexible, this is very helpful in designing the surface chemistry of NP, the anchoring groups and the functional groups.

Depending on the attachment type, side-on or end-on, the mesophases behaviour can be radically changed, therefore, every little change in the chemical structure of the ligand can have a significant influence on the self-assembly behaviour of the LCNPs, and subsequently the LC phase.

There is a synergetic enhancement in these LCNP systems. The self-assembly process of NPs is influenced by the organic layer, the metallic core and the interactions between them.

I.2.2. MAGNETIC NANOPARTICLES

For the past decade the study on magnetization processes has intensified on nanometre length scales. Studies on NPs with different metallic core compositions were undertaken. The most extensively used transition metal in the composition of the metallic core of NPs is iron (Fe), in iron oxides (Fe_3O_4 , $\alpha\text{-Fe}_2\text{O}_3$, $\gamma\text{-Fe}_2\text{O}_3$) and iron alloys (FePt).

Due to its 4 unpaired electrons on the d orbitals, iron has a strong magnetic moment. There are many different magnetic states which can appear when a crystal is formed. In the paramagnetic state, the atomic magnetic moments are not aligned with respect to each other and the crystal has no net magnetic moment. If an external magnetic field is applied, the crystal exhibits a small magnetic moment because some of its numerous individual magnetic moments will align in the same direction. In a ferromagnetic state all the magnetic moments are aligned, even in the absence of an external magnetic field, so overall the crystal has a strong magnetic moment. On the other hand, the ferrimagnetic state is due to magnetic moments of different strengths of two types of atoms, the moments being arranged in an antiparallel fashion. In this case, the net magnetic moment of the crystal is smaller. A different magnetic state is when the magnetic

moments are antiparallel and of equal strengths, the state is antiferromagnetism and has no net magnetic moment.

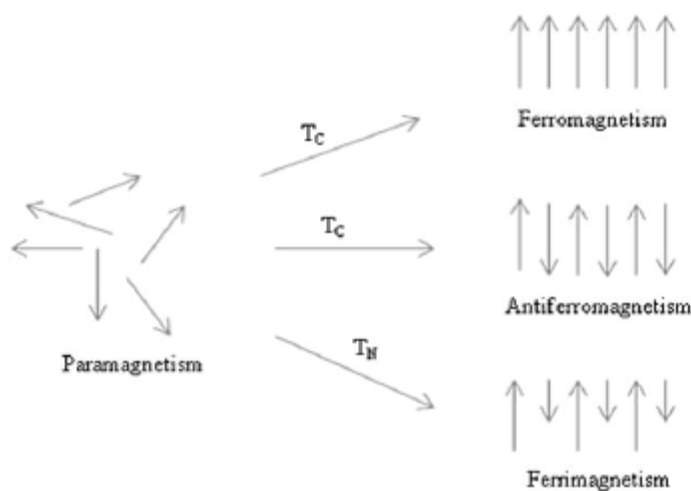


Fig. I.17. Magnetic state and alignment of individual magnetic moments [75]

In a bulk material or a large crystal there are domains with their individual magnetic moments oriented in different directions, so overall the magnetisation of the materials is decreased. But, as the size of the crystal is getting smaller, so the number of domains decreases until there is only a single domain with a magnetic moment not influenced by the magnetisation state of other domains but only by the individual magnetic moments within the single crystal.

If a magnetic field is applied to a ferromagnet, the magnetization curve shows an increase with the external magnetic field strength until a saturation is reached. Overall, the magnetisation curve exhibits a hysteresis loop as not all the domains return to their initial orientation at the same time, as the genetic field is reduced. Hence, when the magnetic field is zero there is still a magnetisation present in the material and can only be removed by applying a coercive field in the opposite direction to the original external magnetic field.

A material with a single domain displays no hysteresis loop and is said to be superparamagnetic. So it is expected that small NPs in the range of a few nanometres to exhibit a superparamagnetic behaviour at room temperature. This property alone is exceptional in terms of applications. But coupled with the LC

properties of NPs those two large application ranges merge giving a huge potential for the LC magnetic NPs.

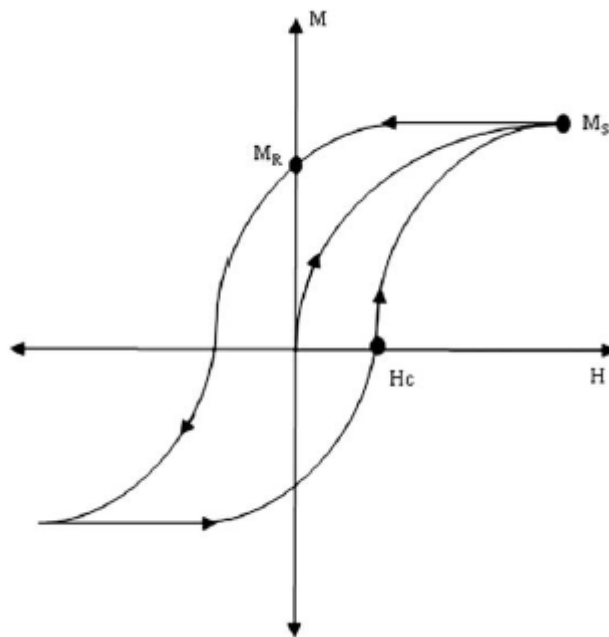


Fig. I.18. The magnetisation curve with hysteresis [75]

I.2.2.1. SYNTHESIS OF MAGNETIC NPs

In the past years, much of the scientific research was focused on synthesis of magnetic nanoparticles. The NPs were prepared in different phases and compositions, including pure single element NPs, oxides and alloys. Like in the whole domain of NPs the synthesis must produce monodisperse, highly stable and shape-controlled magnetic NPs. So the research has focused on developing new and efficient routes on preparing such NPs. Some of the most popular and important synthetic methods are: co-precipitation, thermal reduction and/or decomposition, microemulsion.

Through the **co-precipitation** method high quality iron oxides based NPs are prepared. It is a facile synthesis and reproducible results and materials. This method is based on the addition of a base to an aqueous salts solution of $\text{Fe}^{2+}/\text{Fe}^{3+}$, under inert conditions, starting from room temperature to elevated ones. The composition, shape and size of these magnetic NPs depend on the type of salt

used (nitrate, sulphate, chloride), pH, ratio of $\text{Fe}^{2+}/\text{Fe}^{3+}$ and reaction temperature. By controlling all of these factors the properties of the NPs are reproducible. However, magnetite (Fe_3O_4) NPs are not stable in ambient conditions as they readily undergo an oxidation to maghemite ($\gamma\text{-Fe}_2\text{O}_3$) NPs or dissolved in an acidic medium. Considering that maghemite is a ferrimagnet, oxidation is, most of the time, actually wanted so it is not a problem. Even so, if this transfer occurs, there is still the challenge to control the size of maghemite NPs, as a narrow particle size distribution because the magnetic properties depend directly on the size of the NP. Recently, for a better control of the monodispersity of NPs and also different sizes, organic additives as stabilisation and reducing agents (PVA, trisodium salt of citric acid, oleic acid) are added.

A **microemulsion** is a stable mixture of two immiscible liquids where the interface is stabilized by a film of surfactant molecules. In water-in-oil emulsions the aqueous phase forms droplets of different sizes ranging from 1 nm to 50 nm, stabilized by a monolayer of surfactant. The size of the formed micelle depends on the molar ratio between water and surfactant [76]. If two identical water-in-oil microemulsions are mixed, the droplets will continuously collide and break again and eventually a precipitate inside the droplets is formed. By adding a solvent (ethanol, acetone) the precipitate can be extracted and separated by centrifugation or filtration. Using this method of microemulsion a large number of magnetic metallic single element and alloys are prepared. The most important metals and alloys used for this method are: metallic cobalt, Co/Pt, gold coated Co/Pt, iron oxide alloys with Mn, Co, Zn, Mg, Ni, Cu, Cd. The size of the resulting magnetic NPs is determined by the volume ratio of water and the organic (oil) phase. However, the polydispersity can be rather high. Through the microemulsion technique NPs with a wide range of shapes can be obtained, from spherical to tubes. Although some advantages are obvious, there are serious drawbacks of this method, such as: low yield, narrow working window, large amounts of solvent. Hence, the microemulsion method is not as efficient as others and difficult to scale-up.

Magnetic NPs with smaller size and monodisperse can be synthesized through **thermal decomposition** of organometallic compounds in the presence of stabilizing surfactants in high-boiling point organic solvents [77,78]. As metallic precursors this method uses metal acetylacetonates $[\text{M}(\text{acac})_n]$, where $\text{M} = \text{Fe}, \text{Ni}$,

Co, Mn, Cr, Pt; acac = acetylacetonate; $n = 2$ or 3 as well as carbonyls [79]. As surfactants oleic acid, fatty acids and oleyl- and hexadecylamine are used. To efficiently control the size and shape of the magnetic NPs some parameters are crucial, such as: the ratio of the starting compounds (organometallic reagent and the surfactant) and the solvent, the reaction temperature and the reaction time. If the metal in the organometallic reagent is zerovalent, as in carbonyls, the thermal decomposition initially leads to the formation of the elemental metal and in the second step it can be oxidized to metal oxide NPs. For instance, if the iron carbonyl is decomposed in the first step in the presence of oleic acid and oleyl amine in octyl ether as solvent at 100°C , it can be then oxidized at higher temperatures. Alternatively, after the first low temperature decomposition of the iron carbonyl a platinum reagent (Pt acetylacetonate) is added, Fe/Pt alloy magnetic NPs are obtained. The process is so-called polyol process, because the reducing agent is a polyol or a diol, in this case is hexadecanediol. The Pt precursor is Pt acetylacetonate, the Fe precursor is Fe pentacarbonyl. Adding the capping agents (OA, OA), they are all mixed in a high boiling solvent like octyl ether, around 300°C and reacted for 1h until the solution turns black. Then the NPs are washed with ethanol and precipitated using a centrifuge [80]. It is crucially important to have air stable magnetic NPs, if not for the easy handling, then for the application areas.

1.2.2.2. FUNCTIONALIZATION OF MAGNETIC NPs

The protective layer(s) that covers and surrounds the magnetic NPs is not only to serve as protection barrier against degradations, but also a mean to functionalize it further, giving NPs a widened application range.

The research for developing viable magnetic NPs started with making the synthesis simpler, controlling the size and shape, looking for excellent monodispersity of these NPs and not the least, good stability. After these parameters and criteria are met, it was a logical step to look for improvement, in terms of new applications. And the way to do that is to modify or add new properties by altering the outer protective layer of NPs. The surface

functionalization opened a new range of applications, such as: catalysis, biotechnology, medicine, electronics and engineering.

By having two distinct moieties with different properties, *i.e.* the metallic magnetic core and the organic outer shell, the application potential was improved dramatically. On one hand, these hybrid systems can be controlled with an external magnetic field and on the other hand, the organic functionalized layer can give new and numerous properties by itself or by attaching new active centres.

A new type of hybrid system is the liquid crystal magnetic NPs. It was not achieved yet with applicable results, but promising research is making its way through. However, what it was done, was mixtures between liquid crystals and magnetic NPs [81]. The magnetic NPs were doped with nematic and smectic liquid crystals. It was clear that the two types of materials influence each other, but the scale and the results depend on a large number of parameters. Combining the two different materials with their own properties into one material with exceptional properties, it is worth to overcome the synthetic problems.

CHAPTER II

METHODS. CHARACTERISATION

All the compounds investigated in this research project which needed characterisation were characterised with one or more of these methods:

- Optical rotation
- Circular dichroism
- Optical polarising microscopy
- Differential scanning calorimetry
- Thermal gravimetric analysis
- Gel permeation chromatography
- X-ray diffraction
- UV-Vis spectroscopy
- Transmission electron microscopy

In the following pages, all these methods are presented, in terms of the exact equipment used, name and specifications, basic principles, advantages and drawbacks and some application areas are described.

II.1. Optical rotation

The measurements for the optical rotation were performed on a *polAAr 3001* Automatic polarimeter, with a cell length of 0.25 dm. All the samples were dissolved in chloroform.

Optical rotation is defined as the turning of the plane of the linearly polarised light as it passes through certain compounds. These materials can be solutions of chiral molecules or solids with the ability to rotate the plane of polarised light, such as quartz. This method can be used successfully to characterise chiral materials in solution, in optics to help manipulating the polarisation, in mineralogy to identify minerals, in industry to measure syrup concentrations and furthermore, in diabetic people for measuring the blood sugar levels.

For a pure material in solution, if the path length, the wavelength of the light and the specific rotation are known, then the optical rotation can be used to calculate its concentration.

Optical rotation measurements are performed on a polarimeter. There is a linear dependence between the optical rotation and the concentration of the optically active species in solution and a nonlinear relationship between the optical rotation and the wavelength of the polarised light used.

The specific rotation of a chiral compound $[\alpha]$ is defined as the angle of rotation α of linearly polarized light when it passes through a sample with a path length of 1 decimetre and a concentration of 1 gram per 1 millilitre solution. The specific rotation is the main feature to quantify the chirality of a chemical compounds.

For a given wavelength of light and temperature, the specific rotation is a characteristic property of that certain material.

A positive value of the specific rotation means dextrorotation that is the plane of polarised light is rotated clockwise as the light passes through the sample towards the observer; and a negative value means a levorotation, an anticlockwise rotation of the plane of polarised light.

For chiral compounds in solutions, the following equation is used:

$$[\alpha]_{\lambda}^T = \frac{\alpha}{l \times c}$$

where, l is the path length (in decimetres), c is the concentration (in g/mL), for a sample at a temperature T (given in degrees Celsius) and wavelength λ (in nanometres).

When expressing the specific rotation, if the wavelength of the polarised light used is 589 nm (sodium D line), the symbol “D” is used. Furthermore, the sign of rotation, positive or negative, is always written; the concentration of the sample in solution is given in brackets and no units, as it is considered to be g/100mL. Temperature values at which the measurements were performed, as well as the solvent used for dissolution, must be provided. If the temperature is not specified then it is assumed to be room temperature.

The formal unit for specific rotation is $\text{deg dm}^{-1}\text{cm}^3 \text{g}^{-1}$. For example:

$$[\alpha]_{\text{D}}^{25} = -34^{\circ} (c 25.0, \text{dioxane}) \text{ for cholesterol.}$$

II.2. Circular dichroism (CD)

The CD experiments were carried out using a Jasco J-810 CD spectrometer. The samples were cast from THF solutions as thin films on Quartz substrate. The sample size was about 1cm x 1cm. At Diamond beamline B23 a vertical source of size 0.5mm x 0.5 mm was used, so that the samples prepared on small quartz discs (6.5mm diameter) can be mounted on top of a Linkam heating cell for temperature control. The preparation procedure of the thin film was exactly the same.

Chiral molecules are characterised by not having superimposable mirror images. This lack of symmetry has an impact on a number of physical properties; one of them is the interaction with polarised light. This interaction is molecule specific (Fig. II.1.) and has thus found to be of a great importance for characterising small molecules but also large superstructures [82].

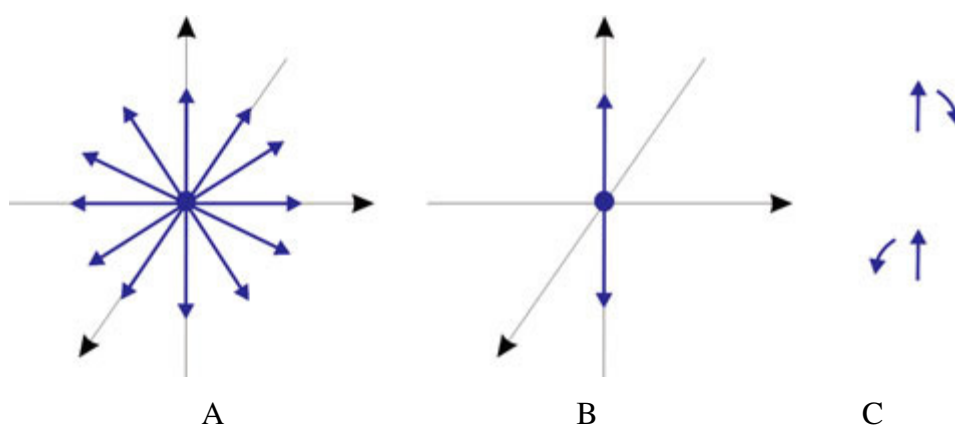


Fig. II.1. Schemes of the electric field components of unpolarized light (A), linearly polarized light (B) and circularly polarized light (C)

Dichroism can be defined as the property of a material which absorbs light differently depending on the type of the polarisation of the incident beam. Circular dichroism occurs when the absorption of right-handed circularly polarised light is different to that of the absorption of left-handed circularly polarised light. Hence, it can be said that the material exhibits circular dichroism (Fig. II.1.) [83,84,85-87].

When circularly polarised light is used, a secondary absorbance component can be calculated from circular dichroism. This secondary absorbance can be measured by switching between right and left circularly polarised light and quantify the difference in absorbance [84,85].

These differences are quite small but readily detectable. CD measurements give detailed information about the enantiomeric mixtures and the structure of liquid crystals, carbohydrates, proteins, pharmaceuticals, among others [82]. Furthermore, CD spectroscopy can give information on the conformational changes in the structure of molecules. The shape of the CD curve and the positive and the negative maxima can give more specific information on the molecule investigated.

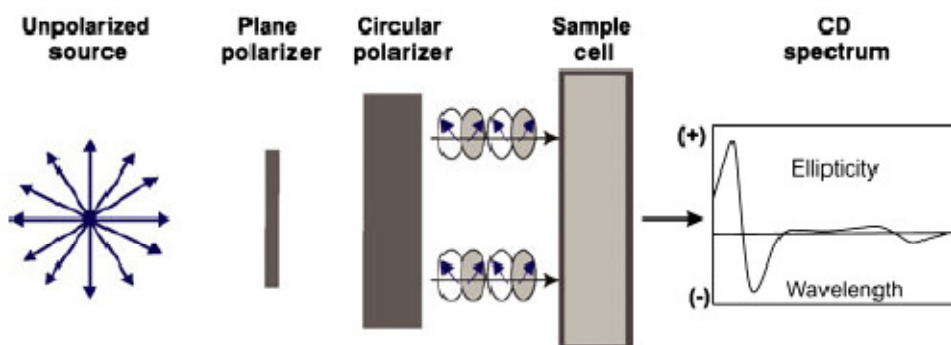


Fig. II.2. Scheme of the CD spectrometer

The common measuring unit for the CD is “ellipticity” which can be defined as the tangent of the ratio of the minor to major elliptical axis. Hence, circular dichroism is the appearance of ellipticity [83]. In the literature, typically, the CD spectra of a material, are reported using mean residue ellipticity (degree $\text{cm}^2 \text{dmol}^{-1}$) and molar circular dichroism (or delta epsilon- $\Delta\epsilon$) ($\text{L mol}^{-1} \text{cm}^{-1}$).

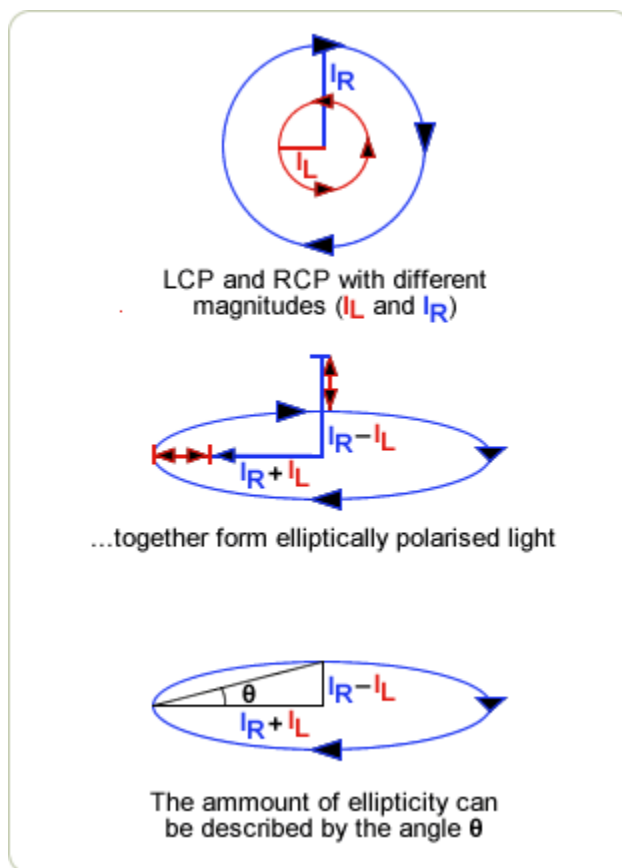


Fig. II.3. Depiction of the calculation of ellipticity

where, LCP is the left circularly polarised light and RCP the right circularly polarised light.

$$\tan \theta = \frac{I_R - I_L}{I_R + I_L}$$

Linear polarised light has the ellipticity (θ) of 0 degrees and fully LCP or RCP have + or - 45 degrees, respectively. Using ellipticity as a measurement unit is more advantageous that is more easily related to optical rotation measurements and polarimetry. Both optical rotation and ellipticity are measurements of changes in polarisation state of a linear polarised light. Furthermore, they both have the same units and similar amplitudes for a given sample.

In the past decades, a number of variations of CD were developed in order to improve the analysis on the structure of a wide range of molecules, asymmetric but also symmetric ones. The most used CD methods are

conventional CD: electronic circular dichroism (ECD), vibrational circular dichroism (VCD, FTIR-VCD), magnetic circular dichroism (MCD, magnetic vibrational circular dichroism (MVCD), XMCD), near-infrared circular dichroism (NIR-CD), fluorescence detected circular dichroism (FDCD), HPLC-circular dichroism and synchrotron radiation circular dichroism (SRCD).

Based on these, recent developments in calculating the optical rotation and CD spectra of molecules, these methods are used in areas of drugs research, microfluidics, pharmacology and biology is in place.

CD is used for assessing the thermal stability of compounds by observing changes in the CD spectrum as a function of temperature [88]. Or alternatively, a single or a narrow wavelength interval is chosen and the focus on the variation of the spectrum with changing temperature. This can give information on some specific features of the molecular structure.

The circular dichroism is influenced by the ground and excited states of the molecule, both of these depend on a number of external parameters and the molecular structure.

An important optical phenomenon is the Cotton effect and it represents the change in optical rotation or circular dichroism with wavelength in the vicinity of an absorption band. The Cotton effect may be either positive or negative.

II.3. Optical polarised microscopy (OPM)

Optical polarised microscopy (OPM) was performed on an Olympus BX51TF microscope equipped with an Olympus InfinityX camera. Hot stage microscopy was performed with a Linkam LTS350 hot stage and a Linkam LNP temperature controller or a Mettler Toledo FP82 hot stage and Mettler Toledo FP90 Central Processor control unit. For materials which needed to be melted for an easier manipulation or a controlled melt, a Leica VMHB was used. Solid and powdered materials were placed between a microscopy slide and a cover glass slip and heated to the desired temperature.

An optical polarising microscope uses polarised light in order to investigate optical properties of materials. As application areas for this instrument it can be enumerate liquid crystals, biology, and medicinal chemistry.

There are two types of optical polarising microscopes: ones that use transmitted light to observe the optical properties of the sample and ones with incident light.

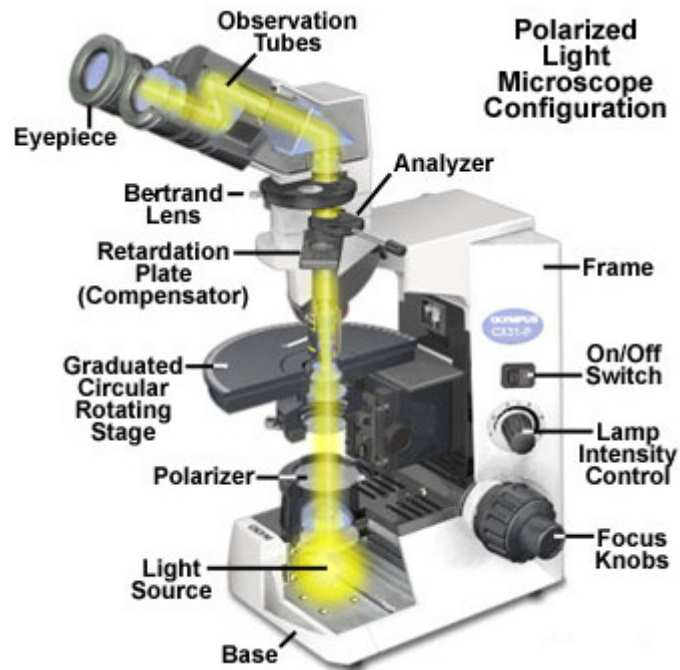


Fig. II.4. A schematic construction of a transmitted light polarizing microscope [89]

As depicted in Fig. II.4., the optical polarising microscope compared to a typical optical microscope, has a different and more complex construction with some additional components such as: a polarizing condenser with a polarizer, a rotating stage, an objective for polarized light, a central revolving piece that allows optical axis adjustment for the objective, an analyzer, a Bertrand lens, a compensator and an eyepiece.

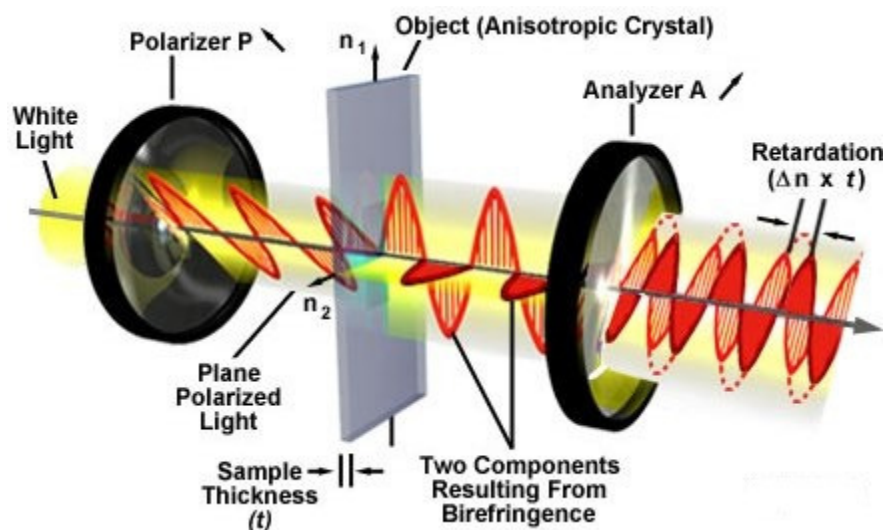


Fig. II.5. Depiction of how OPMs work [90]

II.4. Differential scanning calorimetry (DSC)

DSC measurements were performed on a Mettler Toledo DSC822 with a Mettler Toledo TSO801RO Sample Robot and a Haake EK90/MT cooling unit. For samples which needed a much lower cooling temperature, the DSC measurements were performed on a Perkin Elmer DSC7 with a Perkin Elmer P-E TAC7/3 Instrument controller. All the transition values and enthalpy calculations were taken from the second or third of three heating and cooling cycles, so that each sample had the same thermal history.

DSC measures temperatures and heat flows for physical and chemical transformations that take place in a material, as a function of time and temperature. The measurements are carried out in a controlled atmosphere.

For the DSC analysis to work the sample and the reference material are kept at the same temperature throughout the whole experiment. In most cases, the DSC measurement is designed in such a way that the sample's temperature is increased linearly with time. The reference material must have a well known and defined heat capacity over the temperature range the experiment is done.

These experiments can give qualitative and quantitative information on chemical and physical changes which take place in a material during or after exothermic or endothermic processes.

The DSC analysis can provide information on: melting and boiling points, glass transitions, crystallization time and temperature, specific heat, oxidative/thermal stability, reaction kinetics, heats of fusion and reactions, rate and degree of cure, percent crystallinity and purity.

The basic principle for the DSC technique consists in the following: when a material experiences a chemical or a physical change like a phase transition, more or less heat needs to flow through the sample, so both the reference and the sample be maintained at the same temperature. The difference in heat which passes through the sample depends whether the process is exothermic or endothermic.

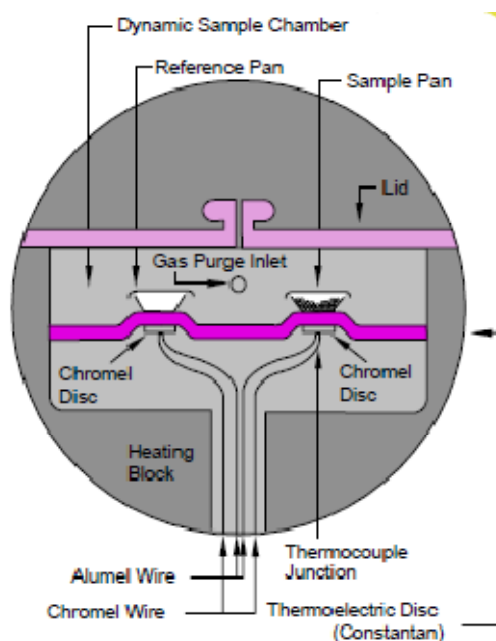


Fig. II.6. A schematic representation of a DSC analysis chamber

For example, when a solid melts to a liquid, the sample requires more heat so the temperature of both the sample and the reference increase at the same rate. The explanation is that the sample goes through an endothermic process, so it absorbs heat as it transforms from a solid to a liquid. This applies also to

exothermic processes and on cooling, such as a crystallisation, when less heat is required to increase the sample's temperature.

DSC instruments are able to measure the amounts of heat released or absorbed during chemical or physical transition. It can be performed by measuring the heat flow difference between the sample and reference. Furthermore, DSC methods can quantify more subtle transitions such as glass transitions. DSC spectrometers are used in industry on large scale for quality control due to its ability to evaluate and measure the purity of materials by evaluating the reproducibility of melting points and the width of melting ranges and also for studying polymer curing.

DSC experiments give typically a curve of the heat flow as a function of temperature or time. Depending on the method used, exothermic processes can be shown in the DSC spectra as a positive or a negative peak. Based on the DSC curve, transition enthalpies can also be calculated by integrating the peak for the desired transition.

One of the important applications of the DSC method is the study and characterisation of liquid crystals. Most of materials transit directly from the solid state to an isotropic liquid, but there are some compounds going through a third state, an anisotropic liquid, named the liquid crystalline phase, which exhibits the characteristics for both the solid and the liquid. The DSC is capable of observing and measuring the small enthalpy changes when a solid goes to the liquid crystal state and from a liquid crystal to an isotropic liquid.

II.5. Thermo-gravimetric analysis (TGA)

Thermal Gravimetric Analysis (TGA) was performed on a Mettler Toledo TGA/DSC1 controlled with a GC100 gas controller. Samples were run in air and nitrogen. Alumina crucibles of 17 μ L were used. The data was treated with STAR software, version 11.

The TGA can be used as a stand-alone instrument, but also as a complementary instrument to a DSC and it measures the changes of the sample's mass versus temperature or versus time. Similar to the DSC, the TGA measurements can be carried out in different atmospheres. For example, if the

DSC can establish that the process is exothermic or endothermic, then the TGA can determine whether it was a chemical or physical change. A chemical process is accompanied by a change in mass and if it is a physical process no mass change occurs. An example of a chemical process is the iron rusting in air and for a physical change it would be the melting of a solid to a liquid.

TGA spectroscopy is generally used to determine specific properties and features of materials which experience a gain or loss in mass due to loss of volatile compounds (such as moisture), decomposition and/or oxidation. Some common applications of the TGA are: moisture and volatiles content of materials, composition of multicomponent systems, oxidative stability of materials, thermal stability of materials, decomposition kinetics of materials, estimated lifetime of a product.

For a TGA to be successful and give the maximum information, it must have high precision in measuring a change in mass, change in temperature and the temperature itself. So, the basic requirements in terms of instrumentation for the TGA are a high precision balance and a reliable and programmable furnace. The operational programs for the furnace can set it for a constant heating rate or for registering a constant loss of mass as a function of time.

The basic principle for a TGA consists in a continuously weighing of the sample whilst heated up to 2000°C, depending on the analysis program and the type of the instrument. As the furnace temperature increases, different components from the sample material evaporate or decompose and their mass loss can be measured and calculated in weight percentage. The results are plotted in a graph with the temperature on the X-axis and the mass loss on the Y-axis. Furthermore, the data can be processed through curve smoothing and first derivatives to determine inflection points to help with further interpretation.

The TGA is used for the characterisation and verifying the purity of materials. It is also used in NPs research in the characterisation of their coatings. The most common mass losses in TGA are due to oxidative processes.

II.6. Gel permeation chromatography (GPC)

The GPC analysis was performed on a Viscotek system composed of VE1122 Solvent Delivery System, VE7510 GPC Degasser, VE5111 Injektor Valve Bracket and VE3500 RI Detector. As the internal reference toluene was used. The samples were dissolved in high purity HPLC grade tetrahydrofuran.

GPC analysis is used for the separation of mixtures of molecules based on their size, or in other words, as they are in solution, their hydrodynamic volume, so molecules or particles of different sizes will elute (filter) through the column at different speeds. It uses a column, a tube filled with small porous polymeric beads as stationary phase and an organic solvent flowing through it playing the role of the mobile phase. The polymeric beads have pores of different sizes; smaller particles enter the pore whilst larger ones do not, traversing the column faster, eluting first.

GPC is actually measuring the molecular volume and shape as a function of intrinsic viscosity.

Some of the advantages of the GPC method are: it is a rapid and routinely used method, molecular weights can be identified, it can analyse polydisperse mixtures, high mass compounds can be identified even in low concentrations, and the method can find molecules of similar sizes but with different shapes.

In the GPC analysis standards and internal references are needed.

GPC is used for a number of applications mostly in the analysis of synthetic or natural polymers, large molecular weight compounds and mixtures of them. GPC analysis can give information on properties or features such as molecular weight, polydispersity index, viscosity, conformation, molecular size, the purity of polymer mixtures or copolymer compositions.

II.7. X-ray diffraction (XRD)

X-rays were generated using a copper tube (Cu K α radiation, graphite monochromator, $\lambda = 1.54 \text{ \AA}$) and detected on a 2-D image plate MAR345 detector with the plate diameter 345 mm, distance from detector 300 mm and the samples were heated in the presence of a magnetic field using a home-built capillary furnace. The data was analysed using “Datasqueeze” software and OriginPro 8.6 software package from OriginLab.

The samples for the XRD were prepared by making fibres from the material to be analysed. Fibres were drawn from the liquid crystalline melting of the material with a spatula then the fibres were cooled quickly in air. An interesting property of these materials was their ability to form fibres, even though they do not consist of long polymer chains. It is known that fibres are associated with polymers because it occurs when there are a large number of interactions between molecular neighbours. These interactions are caused by covalent bonds over many atoms that hold the material together and forming fibres. Typically, low molecular weight compounds are held together by weak intermolecular interactions such as Van der Waals forces and so the materials cannot form fibres as they cannot withstand the tensile force when drawn or if they are crystalline, the crystals simply break.

XRD is the main method for the characterisation of atomic and molecular structure of materials, new materials or materials which appear similar after using other methods. The basic principle of the method is the following: the sample is mounted on a goniometer and gradually rotated whilst irradiated by X-rays; when the X-ray is hitting the internal structure of atoms and planes, it diffracts in many directions, producing a diffraction pattern of regularly spaced spots known as *reflections*. These directions are specific for certain atomic and molecular internal arrangement.

Bragg equation helps by measuring the intensity of scattered waves as a function of scattering angle:

$$2d\sin\theta = n\lambda$$

where, d is the spacing between diffracting planes, θ is the incident angle, n is any integer, and λ is the wavelength of the incident beam.

Additionally, other types of information can be obtained using XRD, such as the type of chemical bonds or the atoms disorder within the crystal. If the crystal regions within the material are too small or not uniform enough, poor resolution or errors can result.

X-rays are used for producing the diffraction patterns because their wavelength λ have the same order of magnitude (0.1–10 nm) as the d spacing between planes.

II.8. UV-Vis spectroscopy

The optical properties were examined with a Varian Cary 50 BIO UV/VIS spectrophotometer equipped with a Varian Cary single cell peltier accessory (for temperature controlled measurements) and a Thermo Oriel Illuminator with Xenon and/or Mercury lamps and Oriel Instruments power supply and controller. The wavelength of the spectrometer is in the range of 200 – 900 nm.

The basic parts of a UV-Vis spectrophotometer are the following: a light source, a holder for the quartz cell containing the sample, a monochromator or a prism to separate the different wavelengths of light and a detector.

Ultraviolet–visible spectroscopy (UV-Vis) refers to absorption or reflectance spectroscopy in the ultraviolet-visible spectral region of electromagnetic radiation. UV-Vis spectrophotometry uses light in the visible part of the spectra and adjacent (near-UV and near-infrared (NIR)) ranges. Absorption spectroscopy measures transitions of electrons from the ground state to the excited state.

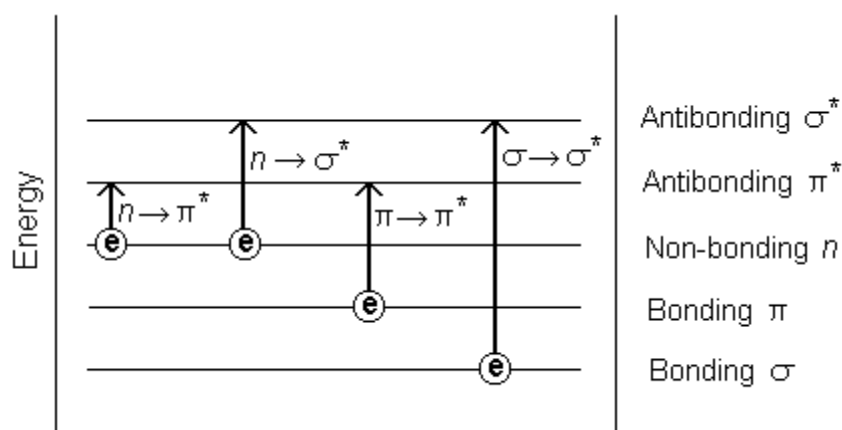
Molecules containing π -electrons or n-electrons (non-bonding electrons) absorb energy in the form of light from the UV or visible part of the spectra and so the electrons are excited to higher energy anti-bonding molecular orbitals. The smaller the energy gap between the highest occupied molecular orbital (HOMO) and lowest unoccupied molecular orbital (LUMO), the more

easily the electrons get excited and the longer the wavelength of the light that they can absorb.

In organic molecules, in order to obtain absorption of ultraviolet or visible light, chemical groups must exist (chromophores) which contain electrons on the valence orbital in a low excitation energy. The UV-Vis absorption spectrum of these molecules is complex because there are two other transitions that take place, such as vibrational and rotational transitions. Thus, the spectrum of a molecule looks like a continuous absorption band.

Different molecules absorb electromagnetic radiation of different wavelengths. An absorption spectrum will exhibit absorption bands corresponding to structural groups within the molecule.

The possible electronic transitions of σ , p and n electrons are:



- σ to σ^* transitions

An electron in a bonding σ orbital is excited to the corresponding anti-bonding orbital σ^* . The energy for this transition is large. For example, methane (which can only undergo σ to σ^* transitions) shows an absorbance maximum at 125 nm. Absorptions due to σ to σ^* transitions are not seen in a UV-Vis spectrum, the wavelength is too short.

- n to σ^* transitions

Saturated organic compounds containing atoms with lone pairs (non-bonding electrons) can exhibit of n to σ^* transitions. Light with the wavelength in the 150-250 nm range can initiate them. The number of organic functional groups with n to σ^* peaks in the UV region is quite small. These electronic transitions need less energy than the σ to σ^* transitions.

- n to π^* and π to π^* transitions

Most absorption UV-Vis spectroscopy spectra of organic materials is based on transitions of n or π electrons to the π^* excited state. The reason is that the absorption peaks for these transitions are in the region of the spectrum (200 - 700 nm) used experimentally. These organic materials have an unsaturated group in their molecules to provide the π electrons.

UV-Vis spectroscopy is usually performed for materials in solutions, but it can also be done for solids and gases. The method is used in chemistry for quantitative identification of transition metals, highly conjugated organic materials and biological macromolecules.

Solutions of transition metals ions can have colour, absorbing visible light. The cause for this is the d electrons from the metal which can be excited from one energy state to another. The colour of the metal solutions is affected by other species such as anions or ligands.

The radiation absorption of a solution is proportionally to the concentration of the active materials in the solution and the path length. Hence, if the path length is known and fixed, the UV-Vis spectrometry can be used to determine the concentration of the absorbing compounds in that solution. To find out how quickly the absorbance changes with the concentration, references are used (containing tables with molar extinction coefficients) or a calibration curve.

II.9. Transmission electron microscopy (TEM)

TEM was performed with a JEOL 2010 instrument, running at 200kV with a lanthanum hexaboride (LaB_6) crystal filament. Images were taken with a Gatan Ultrascan 4000, a 64 megapixel digital camera operated using Digital Micrograph.

TEM samples preparation can be complex as the films of the materials to be analysed should not have more than hundreds of nanometres thickness. Some materials are small enough to be electron transparent (nanotubes, powders) and so their preparation is simpler. They are dissolved in a solution and deposited onto the TEM grids or films.

A TEM works on the same basic principle as the optical microscope, with the difference that the TEM uses electrons instead of light. What can be seen through a microscope is limited on the wavelength of the “light” source. Electrons have a very short wavelength (depending on their kinetic energy, λ of electrons is in the order of pm) and this is why, using TEM techniques, it is possible to obtain images with resolutions, thousands of times better than that of an optical microscope.

The electrons emitted at the top of the TEM travel through vacuum inside the column of the microscope. They are focused in a very thin beam of electrons using electromagnetic lenses instead of glass lenses used in the light microscope. Then the electrons interact with the sample travelling through it; some of the electrons are scattered hitting more dense parts of the sample and disappearing from the main beam. The unscattered electrons reach the fluorescent screen at the bottom of the microscope and this interaction gives an image of the shadows of the sample. The image is in black and white with different parts displayed in different shades of grey depending on the density of the part that the electron beam has hit. These images can be visualised directly by the TEM operator and/or photographed with a digital camera.

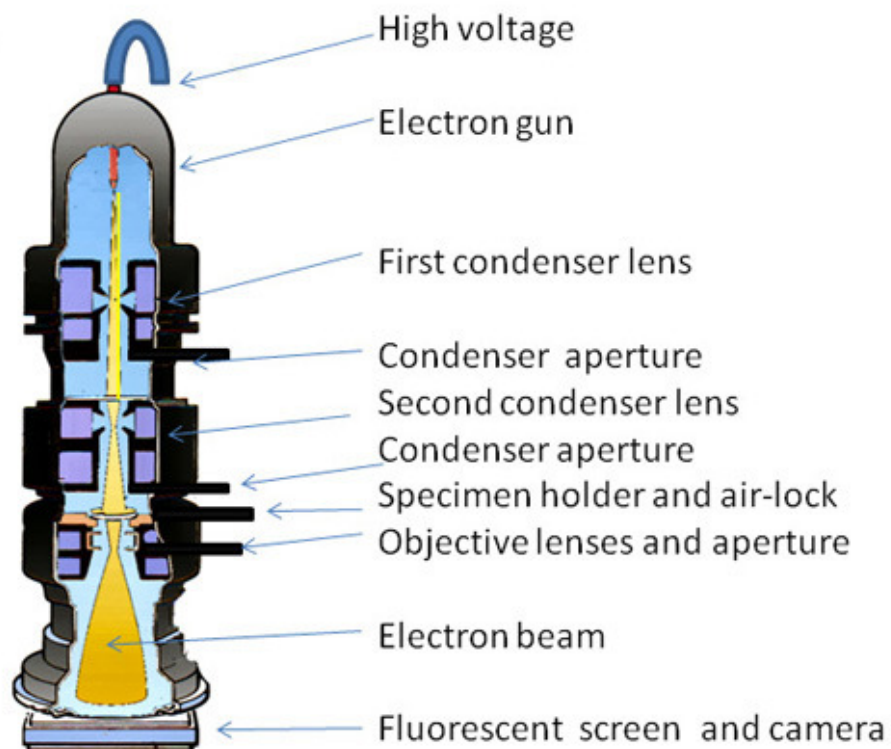


Fig. II.7. A schematic representation of a TEM [91]

Due to the use of electrons in TEM, objects as small as a few Ångstrom (10^{-10} m) can be seen. Details in the biological cells can be identified as many other different materials. The resolution can approach atomic levels. Achieving this high level of magnification, TEM can be used in various areas such as nanotechnology, medical, biological and material research, forensic analysis, gemmology and metallurgy, as well as industry and education.

TEMs provide morphological, topographical, compositional and crystalline information. TEMs can be used in semiconductor analysis and production and the manufacturing of computer and silicon chips. Technology companies use TEMs to identify fractures, flaws and damages to micro-sized objects.

Transmission Electron Microscope is a very sophisticated instrument with a number of advantages such as: it offers the most powerful magnification, over one million times; it has a wide-range of applications and can be utilized in a variety of different scientific, educational and industrial fields; it gives information of surface features, shape and size; it provides information on element and compound structure; images can be high-quality and detailed; it is easy to operate with proper training.

TEM has also a number of disadvantages including: TEMs are large and very expensive; the technique can only be used to analyse samples which are electron transparent; sample preparation can be complex and is prone to artefacts; it requires special training and maintenance (including maintaining the voltage, current to the electromagnetic coils, cooling); images are black and white. Transmission Electron Microscopes are very sensitive instruments to vibrations and electromagnetic fields and must be kept in areas isolated from any possible disturbances and exposures.

High-resolution transmission electron microscopy (HRTEM) is an imaging mode of the transmission electron microscope (TEM) that allows the imaging of the structure of a material at an atomic scale. Because of its very high resolution, it is an important instrument to study nanoscale properties of materials.

CHAPTER III

TARGET. SCIENTIFIC OBJECTIVES

The overall aim of the project is to synthesise nanoparticle systems which form a chiral nematic phase or superstructure. In order to achieve this, new mesogenic systems based on side-on cholesterol moieties are to be synthesised. By preparing these materials controlled transition temperatures and avoidance of smectic phases is expected. In silsesquioxane systems, the liquid crystal phase behaviour is anticipated to be governed mainly by microphase separation of the organic and siloxane groups, nevertheless, optical activity is expected in the final compounds. Additionally, other methods and procedures can be explored in order to explain the behaviour of these structures: contact and miscibility experiments and phase diagrams of binary mixtures between the mesogens and the final compounds and known nematogens. Complete and extensive characterisation is to be performed on final materials and their intermediates.

For NPs, two main categories are to be synthesised: gold NPs and iron/platinum NPs. Subsequently, the NPs are to be covered with a chemically bonded layer of mesogenic groups. Liquid crystal phase behaviour is to be expected with a combination of unique properties due to the synergetic effect of the organic-inorganic moieties. In order to achieve this, NPs have to have a very narrow size distribution and a certain orientation and organization.

In conclusion, the suitable functionalisation must be achieved in order to attach the cholesterol based mesogens onto the NPs. Correlations between the number of organic groups attached and the size of the NP systems and the liquid crystal properties are to be estimated.

Complete and extensive characterisation is to be performed on final NP materials and the functionalised starting materials.

1. Silsesquioxane based systems

The organosilicon cubes are used with great interest in the area of nanocomposites. They are useful model compounds because they are monodisperse; hence they can be used as scaffolds to study the behaviour of mesogens.

Octasilsesquioxanes, as a central core system, it has eight points where it can be potentially derivatised with mesogenic groups. Additionally, the number of mesogenic units attached to the central core can be doubled or tripled by making the cholesterol-based unit part of the dendritic group.

If a mesogen like cyano-biphenyl group with a flexible spacer is attached end-on, it can form SmA phase. On the other hand, if a mesogen like one with 3 benzenic rings and flexible alkyl chains is attached side-on, a discotic columnar phase is formed. Surprisingly, these molecules by themselves form a nematic phase. It was also observed that the transition temperatures increase with the number of mesogenic units attached [28,40]. It can clearly be seen the versatility and potential of these silsesquioxanes as central core.

The mesogens interact between them and changing the overall globular shape of the entire molecule into a rod-like shape, thereby self-organizing to give a chiral calamitic nematic phase. The introduction of chirality into spherical dendritic systems provides an opportunity to examine the potential for materials to have molecular defects based on the chirality of the system.

The liquid crystal phase behaviour is anticipated to be governed mainly by microphase separation of the organic and siloxane groups.

The chemically attachment of these mesogens to the silsesquioxane core is done through a hydrosilylation reaction.

Additionally, other methods and procedures can be explored in order to explain the behaviour of these structures: contact and miscibility experiments and phase diagrams of binary mixtures between the mesogens and the final compounds and known nematogens.

For the exploration and characterisation of properties for these compounds and their intermediates, a number of methods will be employed such as for optical properties (DSC, OPM, UV-Vis, CD, optical rotation), purity (NMR, GPC, EA, MS), TEM, TGA, XRD.

2. Coated nanoparticle hybrid systems

Nanoparticles based on metals represent at the moment one of the most interesting and with great potential research area, scientifically and technologically. The organic layer that covers the nanoparticles has at least two major advantages: increases the processability (such as the solubility) of these hybrid systems and secondly, if the organic groups are suitable, it allows the investigation of novel and synergistic property combinations, ranging from application in the fields of optics, electronics and catalysis to biomedical research [92,93].

In order to possess such interesting properties, nanoparticles must meet three crucial criteria such as a very narrow size distribution, functionalisation with appropriate organic moieties and they have to have a certain organization and orientation.

The investigation of the condensed state properties of nanoparticles had focused mainly on crystalline systems or on the incorporation of nanoparticles into matrices. In the context of liquid crystal, nanoparticles were investigated in terms of properties, being dispersed into low molecular weight liquid crystals. It has been found that the presence of nanoparticles can alter the dielectric behaviour dramatically and this could potentially result in devices with significantly enhanced switching speeds compared to current systems [94]. Viewed in more general terms, the use of the mesomorphic state for the organisation of nanoparticles opens up the utilisation of techniques employed for fabrication of large panel displays, or alternatively if higher ordered LC phases are used, for the controlled bottom-up self organisation in two- or three-dimensional lattices, depending on the type of mesophase. This might be particularly valuable in applications associated with the optical, magnetic or conducting properties of nanoparticles.

Theoretical work has focused on the effects of spherical particles (mainly colloids) dispersed in rod shaped liquid crystals, in other words systems where particles are much larger in diameter than the length of typical liquid crystals [95,96]. Less effort has been concentrated on nanoparticles which exhibit LC behaviour [97,98].

The main obstacle to overcome in the design of these nanoparticles was to merge two vital parameters for liquid crystallinity: the shape of the nanoparticles and the nematic phase organisation. The nematic phase is characterised by long-range orientation in one direction and the absence of positional order [98].

For nanoparticles, liquid crystalline properties have to be introduced through the organic layer covering their surface. If the organic layer has a thickness of a few nanometres (1-3 nm) is difficult to achieve LC properties as only the distortion of the organic layer altering the polyhedral shape can contribute [97]. Shape anisotropy can be achieved using conventional mesogens. Due to surface anchoring effects, nanoparticles should be small enough so that these effects do not play an important role. On the other hand, full coverage of the particle surface with mesogenic groups is likely to reduce mobility, due to crowding of the organic groups, resulting in a loss of LC behaviour. In this context, the comparison with LC dendrimers, where the mesogens are positioned at the surface of the dendrimers, can be helpful. For low generations, the dendritic core is usually deformed, the mesogens dominate the structure of the mesophases, for higher generations the crowding of the dendritic core tend to drive the self-assembly behaviour [31,99,100]. Considering this fact, the difference between nanoparticles and dendrimers is that the dendritic core behaves like a fluid in the mesophase, helping to balance the system in a LC phase.

As the packing behaviour of hard bodies is dependent on geometry and polydispersity, small nanoparticles in the range of 1-2 nm should be used. For particles this small, polydispersity can be easier controlled, having variations in size smaller than the full length of an extended typical mesogen [97,101].

The mesogens are separated by an alkyl spacer from the core and linked *via* a thiol group to the surface to the particles forming monolayers on the surface of the nanoparticles. Low coverage of particles with only mesogens results in systems which are less stable at elevated temperatures [105]. This behaviour is possibly due to the cleavage of Au-S bonds (¹H NMR can detect the signal for terminal methylene group) or to surface reorganisation [102].

These LC nanoparticles can be prepared by attaching hydrocarbon chains and mesogens in a two step process [103,104]. First, gold nanoparticles are covered with a hydrocarbon layer and in a second step an exchange reaction is

involved after which the gold nanoparticles are protected by a cholesterol-based mesogen monolayer. The reaction time allows, within limits, a control of the number of mesogens attached to the nanoparticles [98,103,104].

Particles with shorter hydrocarbon chains than six ethylene groups proves to be difficult to purify and an upper limit of twelve ethylene groups is set in order to avoid an enveloping of the mesogenic groups into the hydrocarbon sheet covering the nanoparticles [105].

The combination of elemental analysis, $^1\text{H-NMR}$ and TEM using an established methodology should allow an estimation of the size of the particles [103,104]. A variation in the particle size and the hydrocarbon chain length modifies the onset and the range of the liquid crystal phase.

The $^1\text{H-NMR}$ spectrum of the gold nanoparticles should show that the hydrocarbon chains and the mesogens are chemically attached to the gold nanoparticles through thiol groups and they are not present as free surfactant thiols.

The synthesis of Au and Fe/Pt NPs was chosen. The challenge is to find the perfect balance between the shape and size of NPs. In order for the NPs to be liquid crystalline they have to be small, the number of mesogens attached to NPs and the size of molecules that compose the outer layer of NPs must be controlled.

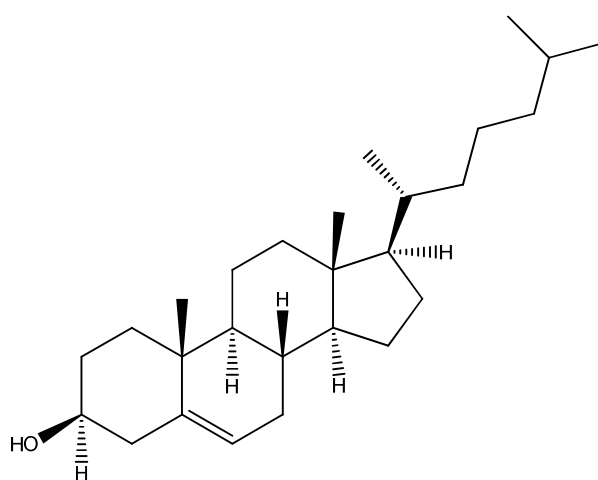
For the exploration and characterisation of properties for these compounds and their intermediates, a number of methods will be employed such as for optical properties (DSC, OPM, UV-Vis, CD, optical rotation), purity (NMR, GPC, EA, MS), TEM, TGA, XRD.

CHAPTER IV

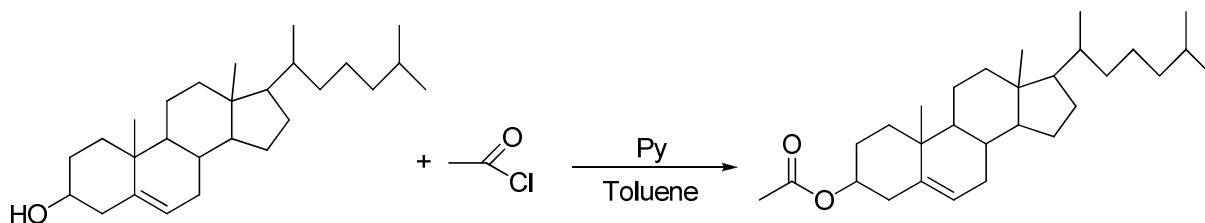
SYNTHESIS

IV.1. SYNTHESIS. EXPERIMENTAL

Considering that cholesterol is a chiral molecule and it is used extensively throughout the thesis, it is important to note the 3D structure of the molecule.



Preparation of 3-acetyl-cholesterol



Cholesterol (50 g, 0.13 mol) and pyridine (12 ml, 0.15 mol) were added in a flask with 500 ml toluene. Small portions of acetyl chloride (11 ml, 0.15 mol) were added to the mixture over a period of 30 min. The solution was left stirring over night. The next day, the solution was heated under reflux for 2 hours to complete the reaction. The mixture was filtered and the product on the filter paper washed with toluene. The filtrate was concentrated and washed 6 times with water. The organic phase was concentrated, then dissolved in DCM (dichloromethane) and dried over MgSO_4 . The solution was filtered and then concentrated. The product was recrystallized in ethanol giving off white crystals.

Yield: 43.3 g, 78%

$^1\text{H-NMR}$ (CDCl_3) δ : 5.37 (t, chol- $\text{CH}=\text{C}$ -), 4.60 (m, chol- CH-O -), 2.31 (dd, chol- $\text{CH}_2\text{-C}=\text{CH}$ -), 2.03 (s, $\text{CH}_3\text{-C}=\text{O}$), 1.90 (dd, chol- $\text{CH}_2\text{-CH-O}$ -), 1.84 (dd, chol- $\text{CH}_2\text{-CH}=\text{C}$ -), 1.05-1.65 (m, chol H), 1.02 (s, chol- $\text{CH}_3\text{-C-C}=\text{CH}$ -), 0.90 (d, chol- $\text{CH}_3\text{-CH}$ -), 0.85 (d, chol- $(\text{CH}_3)_2\text{-CH}$ -), 0.67 (s, chol- $\text{CH}_3\text{-C}$ -)

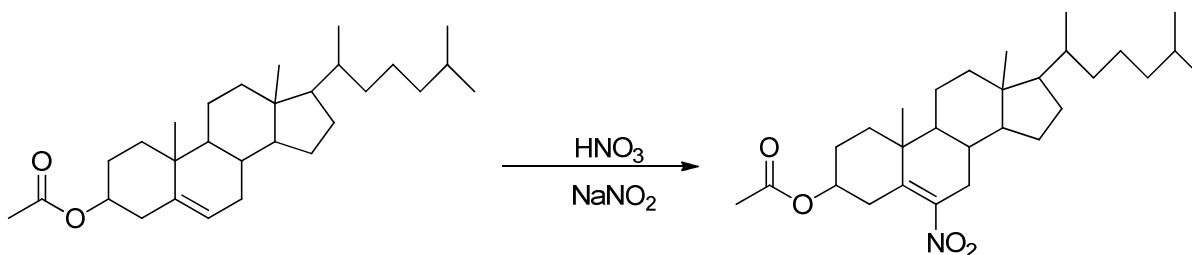
$^{13}\text{C-NMR}$ (CDCl_3) δ : 170.53 (carboxyl), 139.63 (ethylene), 122.64 (ethylene), 73.96 (cyclohexane), 56.65 (cyclopentane), 56.10 (cyclopentane), 50.00 (cyclohexane), 42.20 (cyclopentane), 39.49 (cyclohexane), 39.50 (aliphatic), 36.16 (aliphatic), 35-39 (2C, aliphatic), 35-39 (2C, cyclohexane), 31.85 (cyclohexane), 26-29 (2C, aliphatic), 27.75 (cyclohexane), 18-25 (4C, aliphatic), 18-25 (2C, cyclopentane) 18-25, (3C, cyclohexane), 11.84 (aliphatic)

MS m/z : 450.192 (+ ^{23}Na)

EA: - experimentally: C 81.33%; H 11.54%

- calculated: C 81.25%; H 11.29%

Preparation of 3-acetyl-6-nitrocholesterol



Sodium nitrite (9.5 g, 0.14 mol) was added in small portions, to a stirred solution of nitric acid (300 ml) and cholesteryl acetate (15 g, 0.035 mol), over a period of 20 min. An ice-water mixture (500 ml) was added and the product filtered off and washed with water. The resulting product was purified by recrystallisation in methanol, twice. The purity of the product was confirmed by TLC (DCM).

Yield: 7.5 g, 48%

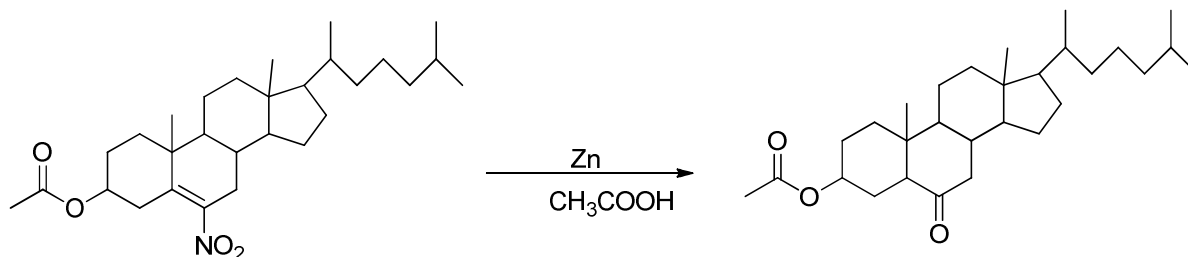
¹H-NMR (CDCl₃) δ : 4.63 (q, chol-CH-O-), 2.75 (dd, chol-CH₂-CH=C-), 2.45 (dd, chol-CH₂-C=CH-), 2.03 (s, CH₃-C=O), 1.96 (dd, chol-CH₂-CH-O-), 1.05-1.65 (m, chol H), 1.02 (s, chol-CH₃-C-C=CH-), 0.90 (d, chol-CH₃-CH-), 0.85 (d, chol-(CH₃)₂-CH-), 0.67 (s, chol-CH₃-C-)

¹³C-NMR (CDCl₃) δ : 170.11 (carboxyl), 146.68 (ethylene), 137.39 (ethylene), 71.93 (cyclohexane), 56.00 (cyclopentane), 55.92 (cyclopentane), 48.87 (cyclohexane), 42.10 (cyclopentane), 39.44 (cyclohexane), 39.25 (aliphatic), 36.16 (aliphatic), 35-39 (2C, aliphatic), 35-39 (2C, cyclohexane), 31.85 (cyclohexane), 26-29 (2C, aliphatic), 27.98 (cyclohexane), 18-25 (4C, aliphatic), 18-25 (2C, cyclopentane) 18-25, (3C, cyclohexane), 11.83 (aliphatic)

MS m/z: 467.228 (+ ²³Na)

EA: - experimentally: C 73.31%; H 10.25%; N 2.86%
- calculated: C 73.53%; H 10.00%; N 2.96%

Preparation of 3-acetyl-6-oxocholestan



Water (20 ml) was added to 3-acetyl-6-nitrocholesterol (11 g, 0.023 mol) which was dissolved in acetic acid (225 ml). Zinc powder (20 g) was added over a period of 30 min. The solution was heated under reflux for 4 hours, after which time the mixture was filtered whilst hot. The Zn powder was washed with acetic acid (2 x 20 ml) and the filtrate was diluted with water (250 ml) to yield a product as white precipitate. The product was purified by recrystallisation in methanol, twice. The purity of the product was confirmed by TLC (DCM).

Yield: 6.3 g, 58%

¹H-NMR (CDCl₃) δ: 4.65 (q, chol-CH-O-), 2.32 (dd, chol-CH₂-CH-O-), 2.25 (dd, chol-CH₂-C=O), 2.02 (s, CH₃-C=O), 1.96 (dd, chol-CH₂-CH-O-), 1.05-1.65 (m, chol H), 0.90 (d, chol-CH₃-CH-), 0.85 (d, chol-(CH₃)₂-CH-), 0.76 (s, chol-CH₃-C-CH-), 0.66 (s, chol-CH₃-C-)

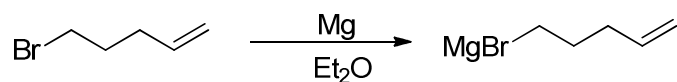
¹³C-NMR (CDCl₃) δ: 210.36 (carbonyl), 170.54 (carboxyl), 72.78 (cyclohexane), 56.62 (cyclopentane), 56.41 (cyclohexane), 56.04 (cyclopentane), 53.95 (cyclohexane), 46.61 (cyclohexane), 42.80 (cyclopentane), 40.90 (cyclohexane), 39.39 (2C, aliphatic), 35-39 (2C, aliphatic), 35-39 (2C, cyclohexane), 26-29 (2C, aliphatic), 27.95 (cyclohexane), 18-25 (3C, aliphatic), 18-25 (2C, cyclopentane) 18-25, (3C, cyclohexane), 12.97 (aliphatic), 11.96 (aliphatic)

MS m/z: 496.240 (+ ^{23}Na)

EA: - experimentally: C 78.50%; H 11.02%

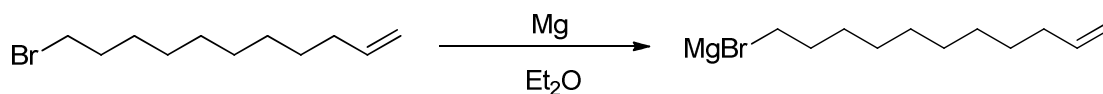
- calculated: C 78.33%; H 10.88%

Preparation of 1-penten-5-yl magnesium bromide



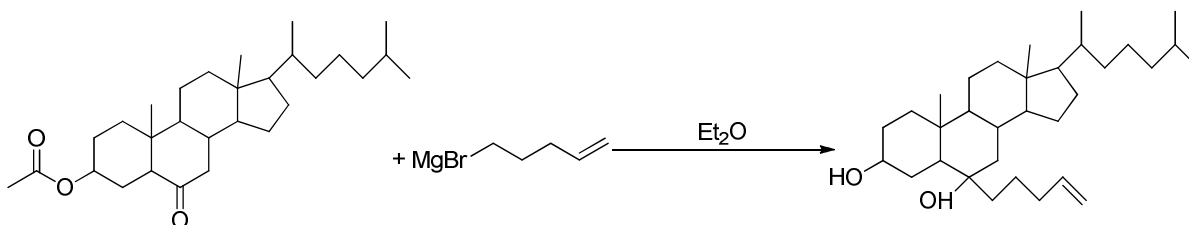
The glassware used for this Grignard reaction was dried in an oven at 120°C for 2 h. Magnesium turnings (2 g, 0.083 mol) were covered with dry diethyl ether (40 ml). Half of the 5-bromo-1-pentene (9.85 ml, 0.083 mol) in ether (60 ml) was added in the reaction flask and the other half was added dropwise. Iodine (2-3 crystals) was added to initiate the reaction which was left until most of the magnesium had dissolved (30-60 min). The resultant product was used without further purification in the next reaction.

Preparation of 1-penten-11-yl magnesium bromide



The work method is the same as discussed for the synthesis of 1-penten-5-yl magnesium bromide.

Preparation of 3,6-dihydroxy-6-pentenylcholestan



3-acetyl-6-oxocholestan (7.1 g, 0.016 mol) was dissolved in ether (80 ml) and slowly added into the 1-penten-5-yl magnesium bromide (previous reaction) over a period of 30 min. The mixture was heated under reflux over night (20 h). Excess Grignard reagent then was decomposed by methanol. The precipitated salts were dissolved with 10% aqueous hydrochloric acid. The solution is washed twice with water and evaporated. The residue is recrystallized twice from DCM. The resulting product is purified by column chromatography (ethyl acetate/hexane = 1/3) to yield the pure product. The purity of the product was confirmed by TLC (DCM).

Yield: 4.5 g, 60%

¹H-NMR (CDCl₃) δ: 5.80 (q, -CH=C), 4.97 (m, CH₂=CH-), 3.57 (q, chol-CH-OH), 2.03 (m, -CH₂-CH=CH₂) 1.05-1.65 (m, chol H), 0.90 (d, chol-CH₃-CH-), 0.85 (d, chol-(CH₃)₂-CH-), 0.68 (s, chol-CH₃-C-)

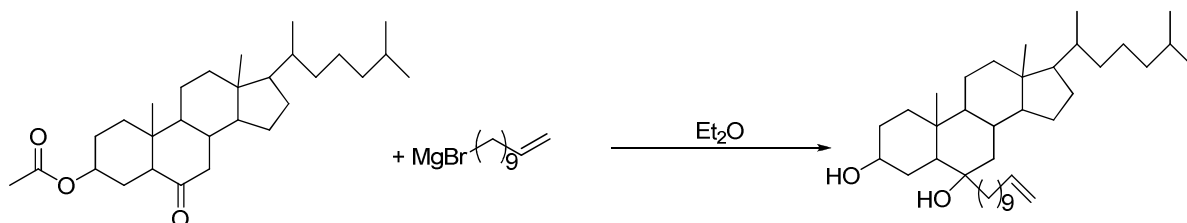
¹³C-NMR (CDCl₃) δ: 138.60 (ethylene), 114.69 (ethylene), 73.68 (cyclohexane), 71.89 (cyclohexane), 56.27 (cyclopentane), 56.17 (cyclohexane), 53.97 (cyclopentane), 48.42 (cyclohexane), 42.56 (cyclopentane), 27-43 (5C, cyclohexane), 27-43 (8C, aliphatic), 18-25 (3C, aliphatic), 18-25 (2C, cyclopentane), 18-25 (3C, cyclohexane), 15.74 (aliphatic), 12.09 (aliphatic)

MS m/z: 495.273 (+ ²³Na)

EA: - experimentally: C 81.08%; H 12.16%

- calculated: C 81.29%; H 11.94%

Preparation of 3,6-dihydroxy-6-undecenylcholestan



The work method is the same as discussed for the synthesis of 3,6-dihydroxy-6-pentenylcholestan.

Yield: 5.3 g, 60%

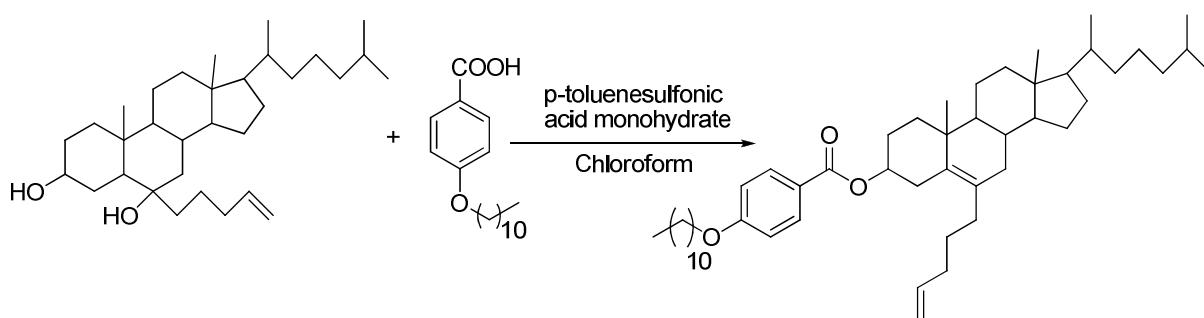
¹H-NMR (CDCl₃) δ: 5.81 (m, -CH=C), 4.97 (dd, CH₂=CH-), 3.58 (q, chol-CH-OH), 2.05 (m, -CH₂-CH=CH₂) 1.05-1.65 (m, chol H), 0.91 (d, chol-CH₃-CH-), 0.85 (d, chol-(CH₃)₂-CH-), 0.61 (s, chol-CH₃-C-)

¹³C-NMR (CDCl₃) δ: 138.60 (ethylene), 114.69 (ethylene), 73.68 (cyclohexane), 71.89 (cyclohexane), 56.28 (cyclopentane), 56.19 (cyclohexane), 53.99 (cyclopentane), 48.29 (cyclohexane), 42.74 (cyclopentane), 42.74 (aliphatic), 27-40 (5C, cyclohexane), 27-40 (10C, aliphatic), 18-25 (6C, aliphatic), 18-25 (2C, cyclopentane), 18-25 (3C, cyclohexane), 15.75 (aliphatic), 12.09 (aliphatic)

EA: - experimentally: C 81.97%; H 12.57%

- calculated: C 81.95%; H 12.31%

Preparation of 4-undecyloxy-6-pentenylcholestanol



3,6-dihydroxy-6-pentenylcholestan (6 g, 12.74 mmol) and 11-undecyloxybenzoic acid (4.38 g, 15 mmol, excess) were dissolved in 100 ml chloroform. 2.85 g (15

mmol) 4-toluenesulfonic acid monohydrate were added. The reaction was left overnight at 60°C. The reaction was checked by TLC. The activated molecular sieves were added starting with the fourth day of reaction when equilibrium was reached. Small portions of activated molecular sieves were added every day until no change was observed (day 6).

Thereafter, the solution was concentrated and dissolved in dichloromethane and put it in a fridge under ice to precipitate the non-converted 11-undecyloxybenzoic acid precipitated. The mixture was filtrated and the filtrate washed twice with saturated solution of NaHCO₃ and dried over Na₂SO₄. After the filtration, the solution was concentrated and the mixture was purified by column chromatography using a dichloromethane/hexane = 1/1 solvent mixture.

Yield: 5.5 g, 60%

¹H-NMR (CDCl₃) δ: 7.98 (d, Ar), 6.90 (d, Ar), 5.80 (m, -CH=C), 4.99 (dd, CH₂=CH-), 4.74 (q, chol-CH-O-), 4.00 (t, -CH₂-O-), 2.89 (dd, -CH₂-C=C-), 1.90 (m, -CH₂-CH=CH₂), 1.05-1.65 (m, chol H), 0.91 (d, chol-CH₃-CH-), 0.86 (d, chol-(CH₃)₂-CH-), 0.68 (s, CH₃-C-)

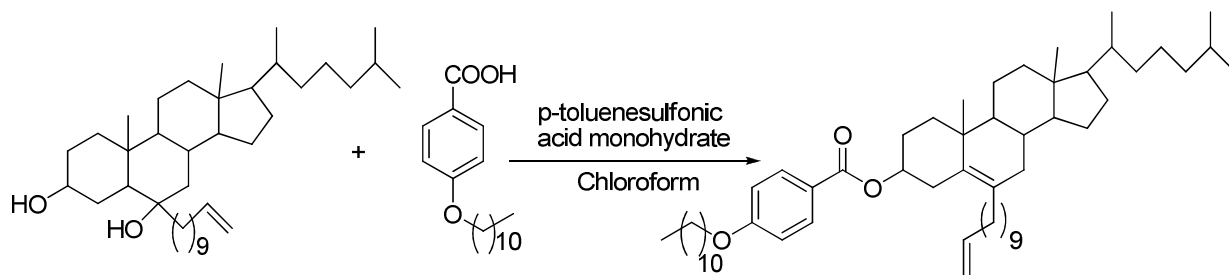
¹³C-NMR (CDCl₃) δ: 165.82 (carboxyl), 162.78 (Ar), 138.98 (ethylene), 132.61 (2C, Ar), 131.50 (Ar), 131.24 (2C, Ar), 123.06 (ethylene), 114.32 (ethylene), 113.94 (ethylene), 74.21 (cyclohexane), 68.18 (cyclohexane), 56.71 (cyclopentane), 56.11 (cyclohexane), 50.12 (2C, cyclohexane), 42.20 (cyclopentane), 18-40 (5C, cyclohexane), 18-40 (22C, aliphatic), 18-40 (3C, cyclopentane), 14.11 (aliphatic), 11.87 (aliphatic)

EA: - experimentally: C 81.34%; H 11.07%

- calculated: C 82.36%; H 11.06%

Phase transition temperatures: Cr 69 N* 92 Iso

Preparation of M2 material



The synthetic method is the same as discussed for the synthesis of 4-undecyloxy-6-pentenylcholestanol.

Yield: 7.2 g, 70%

¹H-NMR (CDCl₃) δ: 7.99 (d, Ar), 6.89 (d, Ar), 5.78 (m, -CH=C), 4.92 (dd, CH₂=CH-), 4.75 (q, chol-CH-O-), 3.99 (t, -CH₂-O-), 2.89 (dd, -CH₂-C=C-), 2.00 (m, -CH₂-CH=CH₂), 1.05-1.65 (m, chol H), 0.91 (d, chol-CH₃-CH-), 0.86 (d, chol-(CH₃)₂-CH-), 0.68 (s, CH₃-C-)

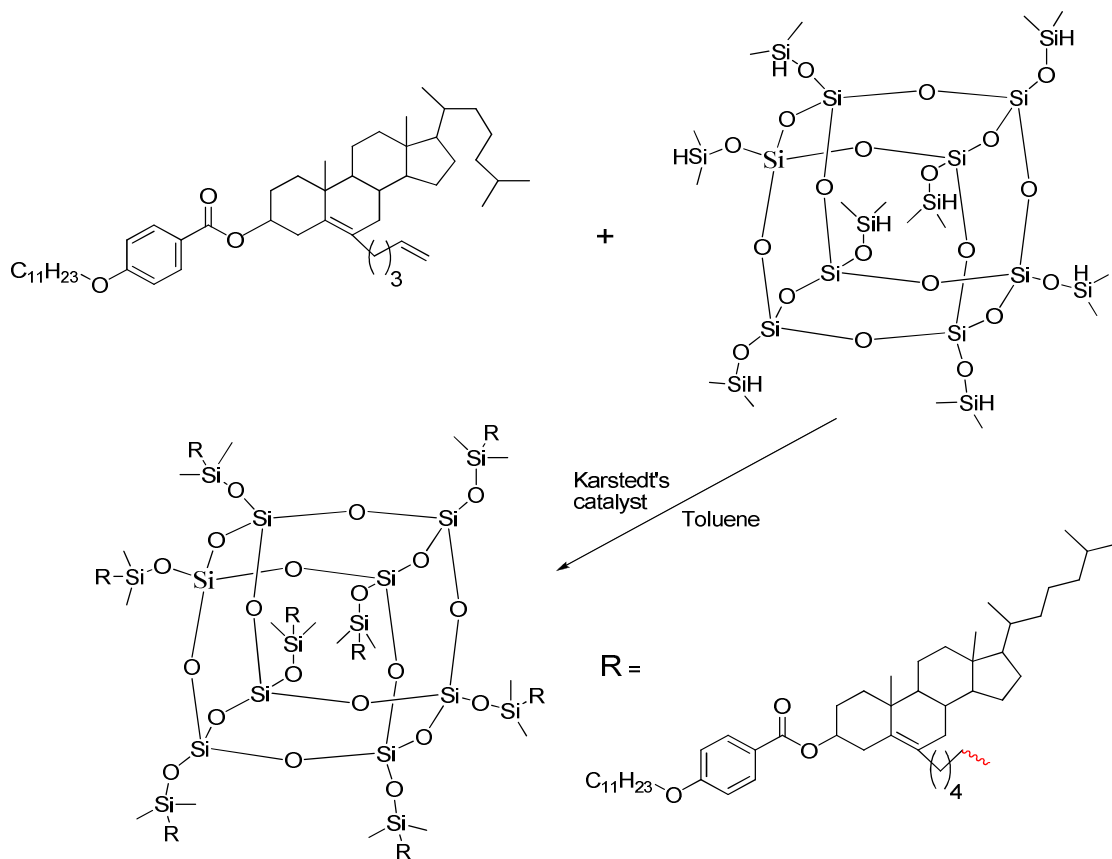
¹³C-NMR (CDCl₃) δ: 165.78 (carboxyl), 162.76 (Ar), 139.27 (ethylene), 132.17 (2C, Ar), 131.64 (Ar), 131.49 (2C, Ar), 123.09 (ethylene), 114.03 (ethylene), 113.93 (ethylene), 74.30 (cyclohexane), 68.17 (cyclohexane), 56.72 (cyclopentane), 56.11 (cyclohexane), 50.15 (2C, cyclohexane), 42.20 (cyclopentane), 18-40 (5C, cyclohexane), 18-40 (28C, aliphatic), 18-40 (3C, cyclopentane), 14.11 (aliphatic), 11.87 (aliphatic)

EA: - experimentally: C 83.00%; H 11.63%

- calculated: C 82.70%; H 11.40%

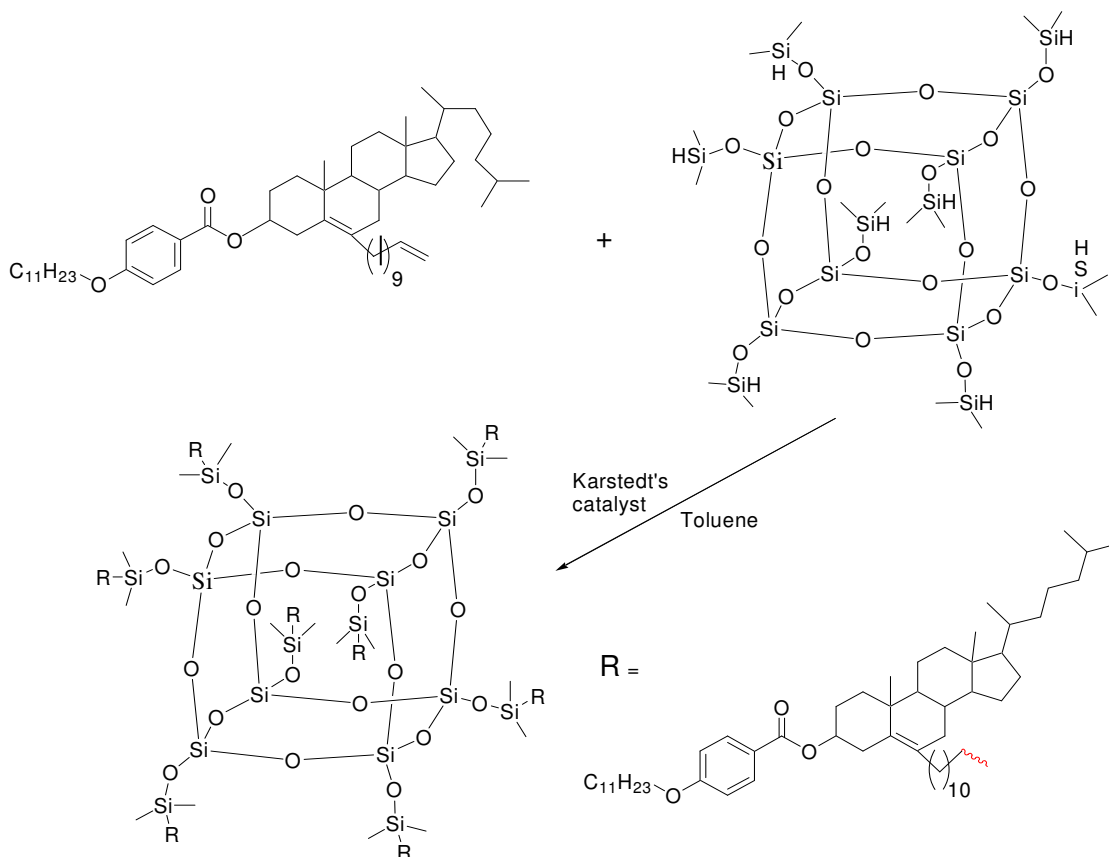
Phase transition temperatures: T_g -22 N* 42 Iso

Preparation of C-M2-X material



A solution of dry toluene (15 ml), monomer (0.38 g; 0.52 mmol) and 6.7 μ l of 2% solution of Karstedt's catalyst dissolved in xylene was gently aerated for 1 min. Then a solution of POSS (polyhedral oligomeric silsesquioxane – $R_4SiO_{1.5}$) (0.033 g; 0.0325 mmol) in dry toluene (5 ml) was added dropwise at room temperatures over a period of 1h. After the addition was complete, the reaction continued for $\frac{1}{2}$ h and a tip full of spatula of triphenylphosphine (Ph_3P) was added to convert the catalyst to less reactive Ph_3P complex and the solution was concentrated under reduced pressure. The material was precipitated in methanol, repeatedly until no monomer could be detected by TLC. At the end, recrystallisation from pentane is required. The purity must be confirmed by GPC. Further purification involves freeze-drying the sample.

Preparation of C-M2 material



The synthetic method is the same as discussed for the synthesis for C-M2-X material.

Yield: 0.1 g, 45%

GPC (+THF): 1 peak at 15.76 ml

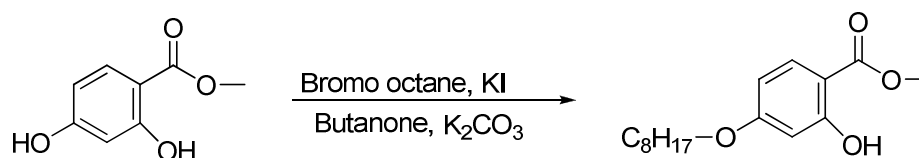
$^1\text{H-NMR}$ (CDCl_3) δ : 7.99 (d, Ar), 6.89 (d, Ar), 4.75 (q, chol- CH-O-), 3.99 (t, - $\text{CH}_2\text{-O-}$), 2.89 (dd, - $\text{CH}_2\text{-C=C-}$), 1.00-2.00 (m, chol H), 1.00-2.00 (m, ...- $\text{CH}_2\text{-CH}_2\text{-Si-}$), 0.91 (d, chol- $\text{CH}_3\text{-CH-}$), 0.86 (d, chol-(CH_3) $_2\text{-CH-}$), 0.68 (s, $\text{CH}_3\text{-C-}$), 0.53 (m, - $\text{CH}_2\text{-Si-}$), 0.19 (s, -(CH_3) $_2\text{-Si-}$)

$^{13}\text{C-NMR}$ (CDCl_3) δ : 165.78 (carboxyl), 162.76 (Ar), 132.17 (2C, Ar), 131.64 (Ar), 131.49 (2C, Ar), 123.09 (ethylene), 113.93 (ethylene), 74.30 (cyclohexane), 68.17 (cyclohexane), 56.72 (cyclopentane), 56.11 (cyclohexane), 50.15 (2C, cyclohexane), 42.20 (cyclopentane), 18-40 (5C, cyclohexane), 18-40 (28C, aliphatic), 18-40 (3C, cyclopentane), 14.11 (aliphatic), 11.87 (aliphatic)

EA: - experimentally: C 71.84%; H 10.42%
- calculated: C 74.06%; H 10.61%

Phase transition temperatures: Tg 10 N* 22 Iso

Preparation of methyl 2-hydroxy-4-octyloxybenzoate



A solution of bromooctane (31.24 ml; 0.18 mol) in dry butanone (100 ml) was added under reflux to a suspension of methyl-2,4-dihydroxy benzoate (25.2 g; 0.15 mol), potassium carbonate anhydrous (103.5 g ; 0.75 mol) in dry butanone (500 ml) over a period of 6 h. The reaction mixture was heated under reflux for three days until the reaction is complete. The mixture was filtrated, the filtrate concentrated and the residue recrystallized from methanol giving white crystals.

Yield: 21 g, 50%

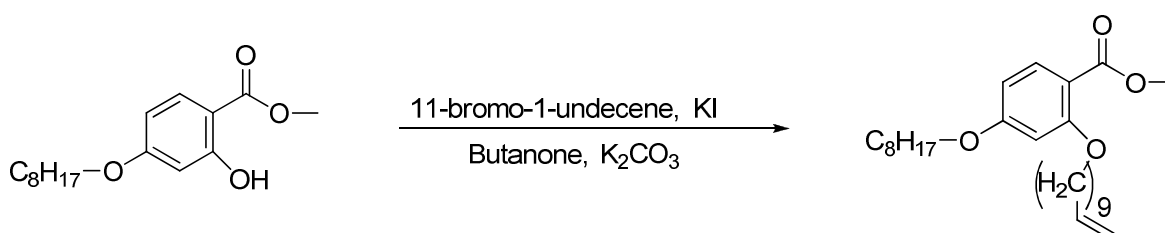
¹H-NMR (CDCl₃) δ: 10.94 (Ar-OH), 7.71 (d, Ar), 6.42 (m, Ar), 3.96 (t, -CH₂-O-Ar), 3.90 (s, CH₃-O-), 1.20-1.80 (m, chol H), 0.88 (s, CH₃-C-)

¹³C-NMR (CDCl₃) δ: 170.42 (carboxyl), 165.20 (Ar), 163.73 (Ar), 131.12 (Ar), 131.50 (Ar), 107.94 (Ar), 105.16 (Ar), 101.09 (Ar), 68.26 (aliphatic), 51.92 (aliphatic), 31.77 (aliphatic), 28-30 (3C, aliphatic), 25.94 (aliphatic), 22.63 (aliphatic), 14.07 (aliphatic)

EA: - experimentally: C 68.71%; H 8.81%

- calculated: C 68.54%; H 8.63%

Preparation of methyl 4-octyloxy-2-(undec-10-en-1-yloxy) benzoate



Bromo-undecene (25.7 ml; 0.117 mol) was added to a suspension of methyl 2-hydroxy-4-octyloxybenzoate (25.2 g; 0.09 mol), K₂CO₃ (136.5 g; 0.99 mol), KI (2.73 g; 0.016) in dry butanone (400 ml) and the mixture was heated under reflux until the reaction was complete (7-8 days). The reaction mixture was filtered and the butanone distilled off. After drying the residue in vacuum a slightly yellow oil was obtained which could be used in the next reaction without further purification.

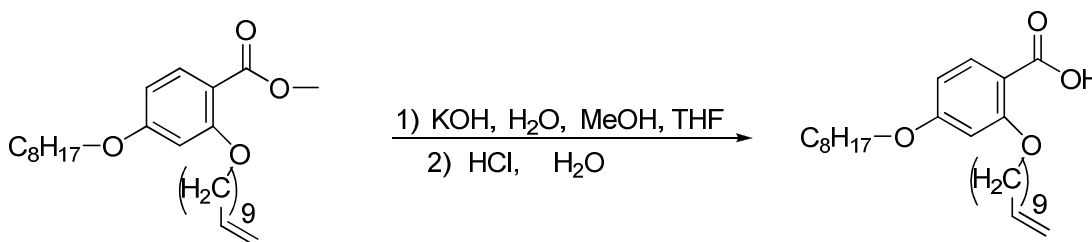
Yield: 36.8 g, 95%

¹H-NMR (CDCl₃) δ: 7.83 (d, Ar), 6.45 (2C, Ar), 5.79 (m, -CH=C), 4.93 (dd, CH₂=CH-), 3.97 (t, -CH₂-O-), 3.84 (s, CH₃-O-), 2.03 (m, -CH₂-CH=CH₂), 1.20-1.90 (m, aliphatic), 0.88 (s, CH₃-C-)

EA: - experimentally: C 71.13%; H 10.99%

- calculated: C 74.96%; H 10.25%

Preparation of 4-octyloxy-2-(undec-10-en-1-yloxy) benzoic acid



Methyl 4-octyloxy-2-(undec-10-en-1-yloxy) benzoate (37.65 g; 0.09 mol) was dissolved in THF (100 ml) and methanol (500 ml). A solution of KOH (28 g; 0.5 mol) in water (80 ml) was added. After stirring for 2 days at room temperature the reaction was completed by heating at reflux for 2 h. The solvents were distilled off and ice/water (300 ml) added. After acidification with conc. HCl (45 ml – 125 ml sol. of 36% HCl) the mixture was extracted with CH₂Cl₂ (6 X 100 ml). After drying the CH₂Cl₂ phase with MgSO₄ the solvent was distilled off. Recrystallisation from hexane yielded off-white crystals.

Yield: 22.6 g, 60%.

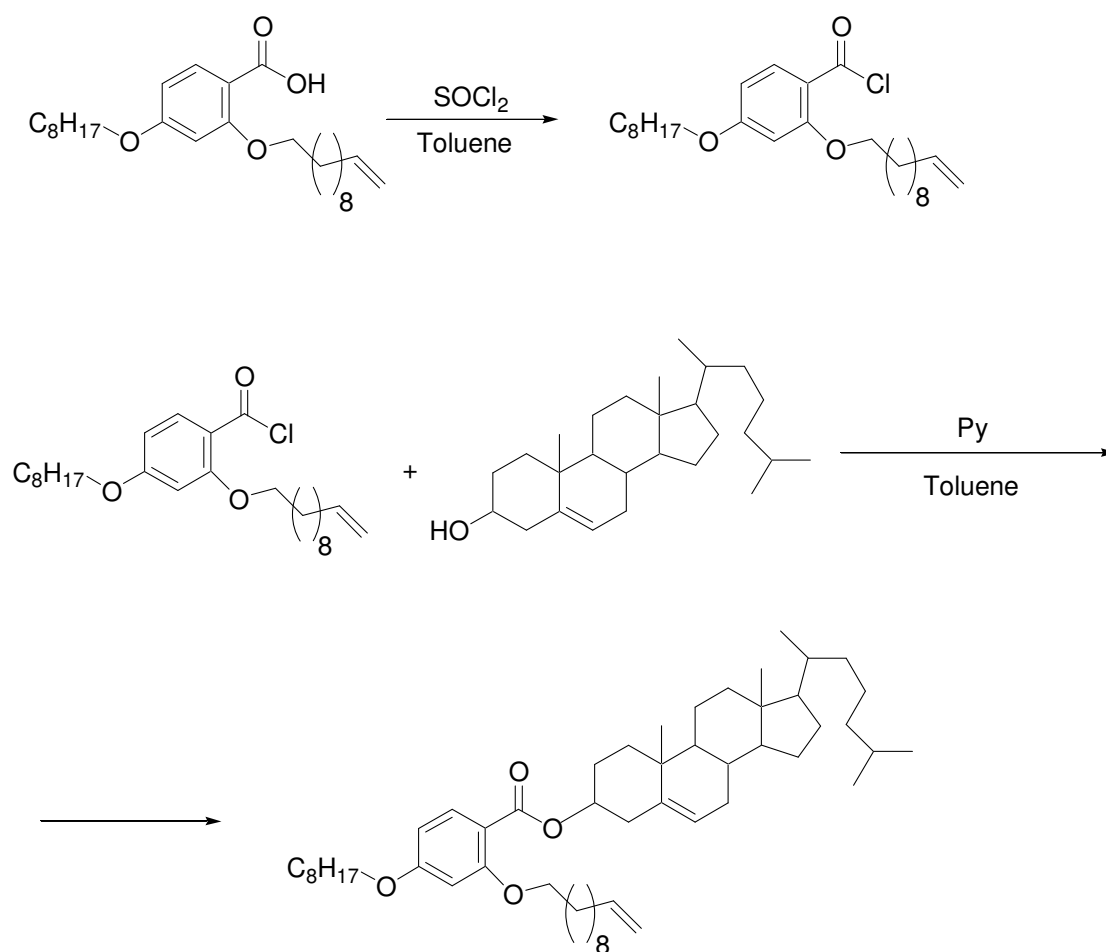
¹H-NMR (CDCl₃) δ: 10.77 (s, -OH), 8.10 (d, Ar), 6.62 (d, Ar), 6.50 (s, Ar), 5.80 (m, -CH=C), 4.97 (dd, CH₂=CH-), 4.18 (t, -CH₂-O-), 3.99 (t, -CH₂-O-), 2.05 (m, -CH₂-CH=CH₂), 1.20-2.00 (m, aliphatic), 0.87 (s, CH₃-C-)

¹³C-NMR (CDCl₃) δ: 165.31 (carboxyl), 164.60 (Ar), 158.92 (Ar), 139.11 (Ar), 135.40 (Ar), 114.13 (Ar), 110.15 (Ar), 107.01 (ethylene), 99.72 (ethylene), 70.12 (aliphatic), 68.53 (aliphatic), 22-34 (14C, aliphatic), 14.06 (aliphatic)

MS m/z: 441.308 (+ ²³Na)

EA: - experimentally: C 74.85%; H 9.84%
- calculated: C 74.60%; H 10.11%

Preparation of M1 material



4-octyloxy-2-(undec-10-en-1-yloxy) benzoic acid (2 g; 4.8 mmol) was dissolved in dry toluene (40 ml). Thionyl chloride (7.5 ml; 103 mmol) was added and the solution heated gradually from r.t. to 80°C for 3 h, the reaction being completed after heating at reflux for 1 h. The thionyl chloride and toluene were distilled off using a vacuum pump. A solution of cholesterol (1.85 g; 4.8 mmol) and pyridine (7.5 ml; 94 mmol) in toluene (10 ml) was added to the residue. The mixture was heated to 80°C overnight and the reaction completed after heated to reflux for 1 h. Ice/water (80 ml) and ether/hexane=1/1 (80 ml) were added. The phases were separated and the aqueous layer was extracted with chloroform (2 X 60 ml). The

combined organic layers were dried with MgSO_4 and the solvents distilled off. The residue was purified by column chromatography ($\text{CH}_2\text{Cl}_2/\text{hexane}=1/1$).

Yield: 3.4 g, 90%

$^1\text{H-NMR}$ (CDCl_3) δ : 7.79 (d, Ar), 6.43 (d, Ar), 6.42 (s, Ar), 5.79 (m, $-\text{CH}=\text{C}$), 5.40 (d, chol- $\text{CH}=\text{C}$ -), 5.00 (dd, $\text{CH}_2=\text{CH}$ -), 4.82 (q, chol- CH-O -), 3.97 (t, $-\text{CH}_2\text{-O}$ -), 2.44 (dd, chol- $\text{CH}_2\text{-C}=\text{C}$ -), 2.00 (m, $-\text{CH}_2\text{-CH}=\text{CH}_2$), 1.00-1.90 (m, chol H), 0.91 (d, chol- $\text{CH}_3\text{-CH}$ -), 0.86 (d, chol- $(\text{CH}_3)_2\text{-CH}$ -), 0.68 (s, $\text{CH}_3\text{-C}$ -)

$^{13}\text{C-NMR}$ (CDCl_3) δ : 165.71 (carboxyl), 163.50 (Ar), 160.61 (Ar), 139.96 (Ar), 139.22 (Ar), 133.66 (Ar), 122.49 (Ar), 114.13 (ethylene), 113.17 (ethylene), 104.96 (ethylene), 100.19 (ethylene), 73.92 (cyclohexane), 68.81 (aliphatic), 68.17 (aliphatic), 56.71 (cyclopentane), 56.15 (cyclohexane), 50.05 (2C, cyclohexane), 42.33 (cyclopentane), 18-40 (6C, cyclohexane), 18-40 (23C, aliphatic), 18-40 (3C, cyclopentane), 14.12 (aliphatic), 11.86 (aliphatic)

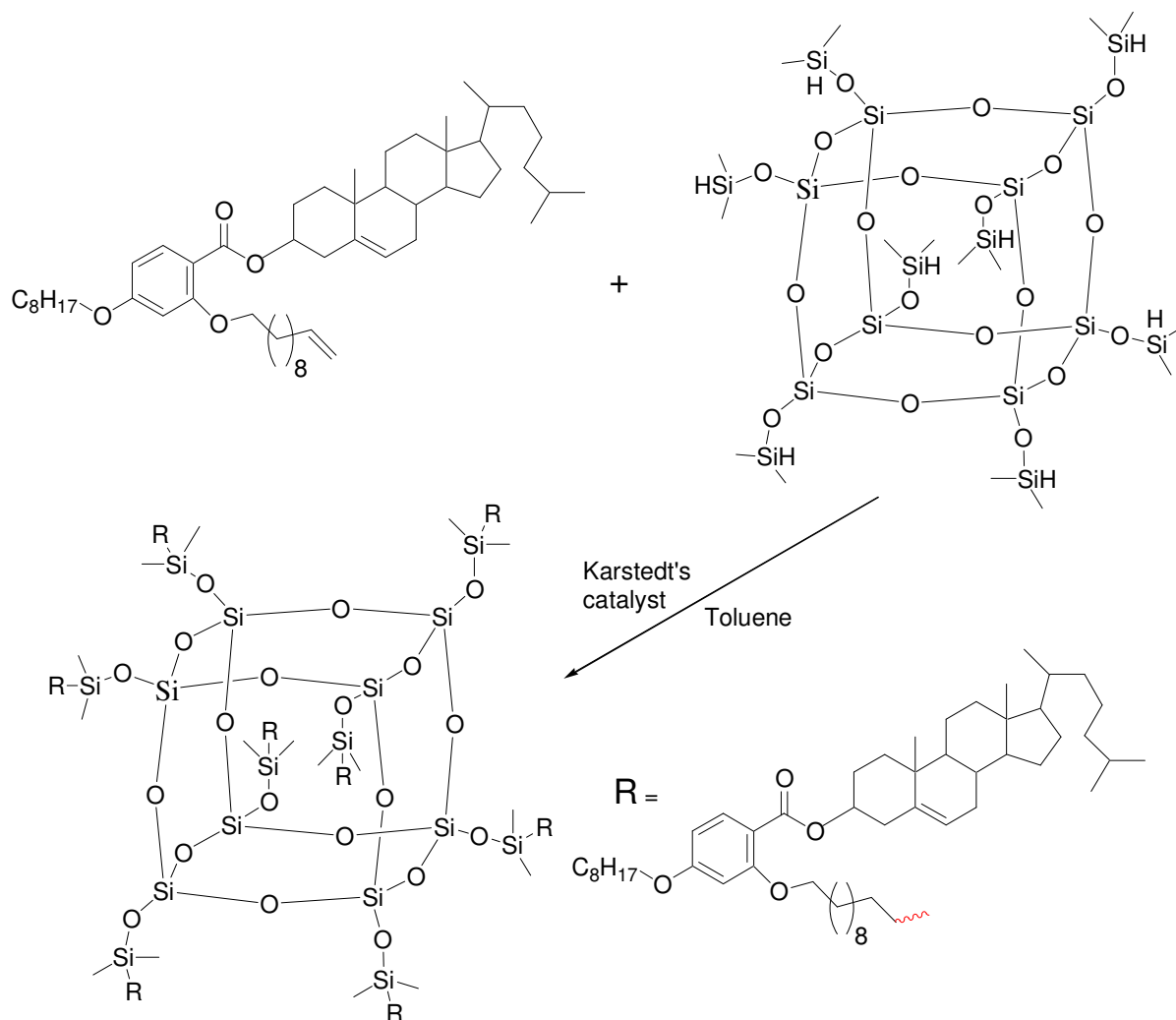
MS m/z : 809.701 (+ ^{23}Na)

EA: - experimentally: C 81.00%; H 11.00%

- calculated: C 80.86%; H 11.01%

Phase transition temperatures: T_g -25 N* 57 Iso

Preparation of C-M1 material



The synthetic procedure is the same as discussed for the synthesis for C-M2-X and C-M2 materials.

Yield: 0.1 g, 40%

GPC (+THF): 1 peak at 15.88 ml

¹H-NMR (CDCl₃) δ: 7.75 (d, Ar), 6.41 (d, Ar), 6.38 (s, Ar), 5.34 (d, chol-CH=C-), 4.77 (q, chol-CH-O-), 3.91 (t, -CH₂-O-), 2.39 (dd, chol-CH₂-C=C-), 0.80-2.00 (m, chol H), 0.80-2.00 (m, -CH₂-CH₂-Si-), 0.63 (s, CH₃-C-), 0.53 (m, -CH₂-Si-), 0.19 (s, -(CH₃)₂-Si-)

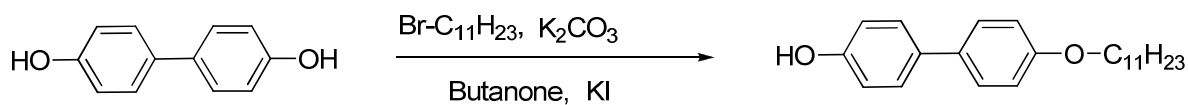
¹³C-NMR (CDCl₃) δ: 165.71 (carboxyl), 163.50 (Ar), 160.61 (Ar), 139.96 (Ar), 139.22 (Ar), 133.66 (Ar), 122.49 (Ar), 114.13 (ethylene), 113.17 (ethylene), 104.96 (ethylene), 100.19 (ethylene), 73.92 (cyclohexane), 68.81 (aliphatic), 68.17 (aliphatic), 56.71 (cyclopentane), 56.15 (cyclohexane), 50.05 (2C, cyclohexane), 42.33 (cyclopentane), 18-40 (6C, cyclohexane), 18-40 (23C, aliphatic), 18-40 (3C, cyclopentane), 14.12 (aliphatic), 11.86 (aliphatic)

EA: - experimentally: C 68.83%; H 10.49%

- calculated: C 72.24%; H 10.25%

Phase transition temperatures: T_g 27 N* 38 Iso

Preparation of 4-hydroxy-4'-undecyloxybiphenyl



Bromoundecane was added dropwise to a suspension of biphenol (26 g; 0.14 mol), potassium carbonate anhydrous (20.7 g; 0.15 mol) in ethanol (200 ml). A catalytic amount of KI is added to the mixture. The reaction mixture is heated at

reflux overnight. Purification is obtained by recrystallisation from THF with ethanol.

Yield: 21.4 g, 45%

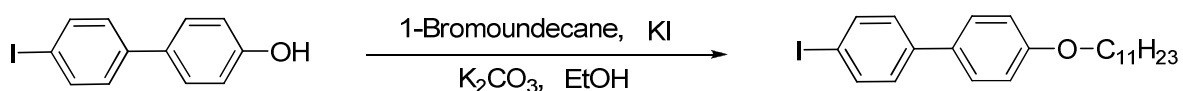
¹H-NMR (CDCl₃) δ: 7.43 (d, Ar), 6.95 (d, Ar), 6.87 (d, Ar), 3.98 (t, -CH₂-O-Ar), 1.78 (q, -CH₂-CH₂-O-), 1.20-1.60 (m, chol H), 0.88 (s, CH₃-C-)

¹³C-NMR (CDCl₃) δ: 127.93 (Ar), 127.65 (Ar), 115.54 (4C, Ar), 114.73 (6C, Ar), 68.00 (aliphatic), 22-32 (9C, aliphatic), 13.50 (aliphatic)

EA: - experimentally: C 80.69%; H 9.91%

- calculated: C 81.13%; H 9.47%

Preparation of 4-iodo-4'-undecyloxybiphenyl



1-Bromoundecane (3.8 ml; 17 mmol) was added to a suspension of 4-iodo-biphenol (5 g; 16.9 mmol), potassium carbonate anhydrous (2.35 g; 17 mmol) in ethanol (40 ml). To this mixture, a catalytic amount of KI was added. The reaction mixture was heated under reflux overnight until the reaction is complete. The mixture was filtrated, the filtrate concentrated and the residue purified by column chromatography (CH₂Cl₂/hexane=1/1).

Yield: 6.8 g, 90%

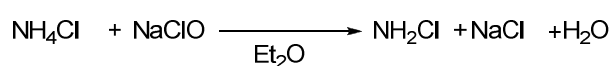
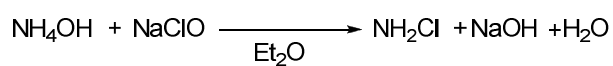
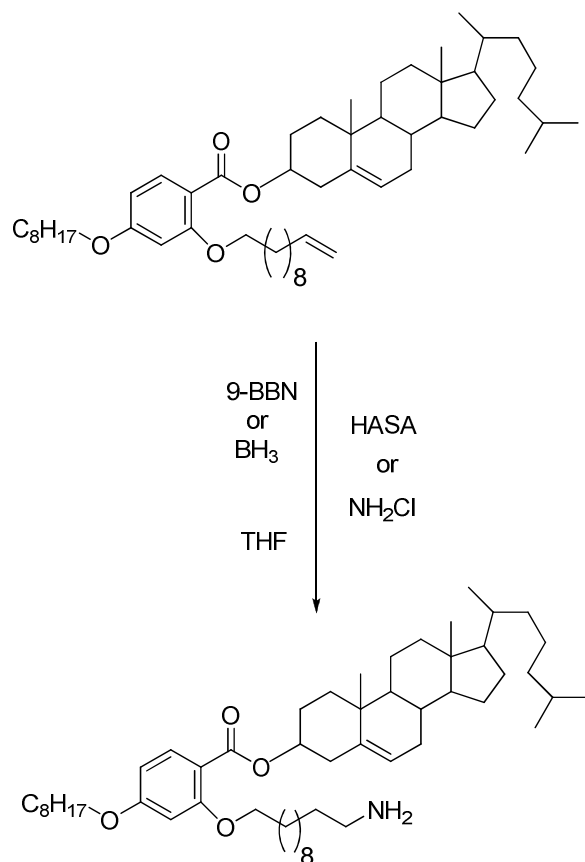
¹H-NMR (CDCl₃) δ: 7.72 (d, Ar), 7.46 (d, Ar), 7.26 (d, Ar), 6.95 (d, Ar), 3.99 (t, -CH₂-O-Ar), 1.79 (q, -CH₂-CH₂-O-), 1.20-1.60 (m, chol H), 0.88 (s, CH₃-C-)

¹³C-NMR (CDCl₃) δ: 159.03 (Ar), 140.37 (Ar), 137.72 (Ar), 132.22 (Ar), 128.53 (Ar), 127.86 (Ar), 114.87 (Ar), 92.03 (Ar), 68.10 (aliphatic), 22-32 (9C, aliphatic), 14.12 (aliphatic)

EA: - experimentally: C 61.44%; H 7.07%

- calculated: C 61.33%; H 6.94%

Preparation of M1- and M2-based amines



Synthesis of chloramine:

1.

The reaction flask was maintained at -11°C. 20 ml of a 2.28 mol/l ammonium chloride solution were introduced into the reactor. A 2.07 mol/l sodium hypochlorite solution was prepared, the sodium hydroxide concentration of which is 0.12 mol/l. 20 ml of the prepared solution, cooled to -15°C, were subsequently introduced drop wise into the reactor.

The ratio of the ammonium chloride concentration to the sodium hypochlorite concentration ($[\text{NH}_4\text{Cl}]/[\text{NaOCl}]$) was equal to 1.1. The addition lasted 15 min and was carried out using a dropping funnel. The temperature of the reaction medium settled at -7°C with stirring. For cooling the ice baths, a mixture of salt and ice was used.

2.

The procedure was the same as above, with the difference that instead of NH_4Cl , aqueous ammonia was used.

Reaction of organoboranes with hydroxylamine-O-sulfonic acid. The alkene was dissolved in THF. After flushing with nitrogen the hydroboration was accomplished by a solution of borane (BH_3) or 9-BBN (9-Borabicyclo(3.3.1)nonane) in THF. To the solution was added solid hydroxylamine-O-sulfonic acid and the reaction mixture was heated under reflux for 3 h.

The work-up can be carried out in two ways:

The reaction mixture was acidified with hydrochloric acid and the acidified solution extracted with ether. The solution was made strongly alkaline with sodium hydroxide and the amine extracted with ether.

The solvent is removed and the residue purified by column chromatography.

Yield: <10%

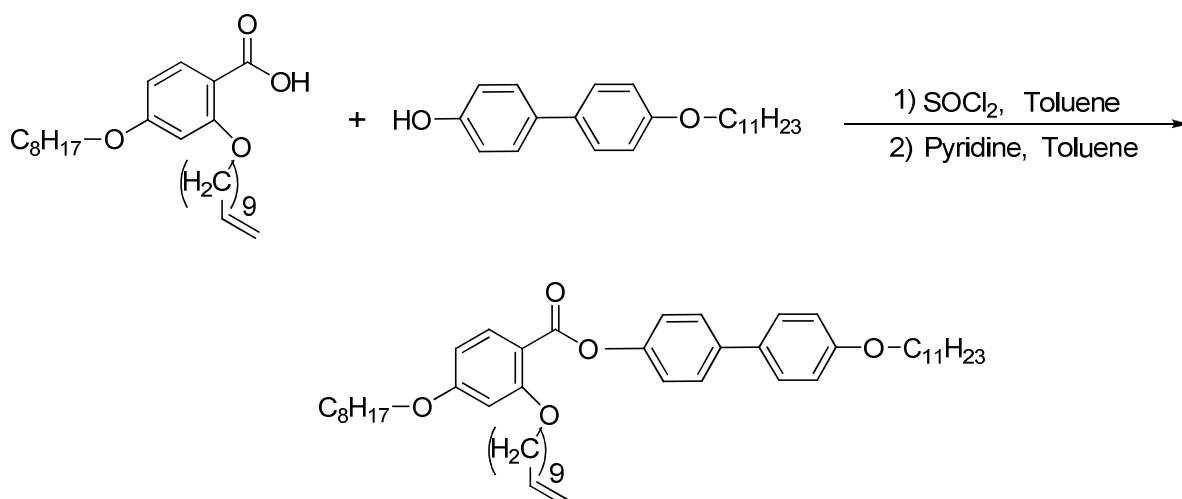
$^1\text{H-NMR}$ (CDCl_3) δ : 7.78 (d, Ar), 6.43 (m, Ar), 5.39 (d, chol- $\text{CH}=\text{C}$ -), 4.80 (q, chol- CH-O -), 3.97 (t, $-\text{CH}_2\text{-O}$ -), 2.90 (t, $-\text{CH}_2\text{-NH}_2$ -), 2.43 (dd, chol- $\text{CH}_2\text{-C}=\text{C}$ -), 0.90-2.00 (m, chol H, $-\text{NH}_2$), 0.86 (d, chol- $(\text{CH}_3)_2\text{-CH}$ -), 0.67 (s, $\text{CH}_3\text{-C}$ -)

$^{13}\text{C-NMR}$ (CDCl_3) δ : 168.82 (carboxyl), 166.60 (Ar), 163.76 (Ar), 143.01 (Ar), 136.73 (Ar), 125.56 (Ar), 116.13 (Ar), 108.03 (ethylene), 103.27 (ethylene), 76.95 (cyclohexane), 71.87 (aliphatic), 71.27 (aliphatic), 59.77 (cyclopentane), 59.21 (cyclohexane), 56.51 (cyclohexane), 53.13 (cyclohexane), 38-46 (cyclopentane), 38-46 (2C, aliphatic), 21-35 (6C, cyclohexane), 21-35 (22C, aliphatic), 21-35 (3C, cyclopentane), 17.19 (aliphatic), 16.80 (aliphatic), 14.95 (aliphatic)

MS m/z: 827.757 (+ ²³Na)

Phase transition temperatures: T_g 5 N* 48 Iso

Preparation of 4'-undecyloxybiphenyl-4-yl-4-octyloxy-2-(undec-10-en-1-yloxy) benzoate (3RM)



4-octyloxy-2-(undec-10-en-1-yloxy) benzoic acid (1 g; 2.4 mmol) was dissolved in dry toluene (20 ml). Thionyl chloride (3.5 ml; 48 mmol) was added and the solution heated gradually from r.t. to 80°C for 3 h, the reaction being completed after heating at reflux for 1 h. The thionyl chloride and toluene were distilled off. A solution of 4-hydroxy-4'-undecyloxybiphenyl (0.82 g; 2.4 mmol) and pyridine (3.9 ml; 48 mmol) in toluene (25 ml) was added to the residue. The mixture was heated to 80°C overnight and the reaction completed after heated to reflux for 1 h. Ice/water (40 ml) and ether/hexane=1/1 (40 ml) were added. The phases were separated and the aqueous layer extracted with chloroform (2 x 30 ml). The

combined organic layers were dried with MgSO_4 and the solvents distilled off. The residue was purified by column chromatography ($\text{CH}_2\text{Cl}_2/\text{hexane}=1/1$).

Yield: 1.6 g, 90%

$^1\text{H-NMR}$ (CDCl_3) δ : 8.03 (d, Ar), 7.55 (d, Ar), 7.49 (d, Ar), 7.24 (d, Ar), 6.96 (d, Ar), 6.51 (m, Ar), 5.78 (m, $-\text{CH}=\text{C}$), 4.95 (dd, $\text{CH}_2=\text{CH}-$), 4.02 (m, $-\text{CH}_2-\text{O}-$), 2.00 (m, $-\text{CH}_2-\text{CH}=\text{CH}_2$), 1.20-1.90 (m, aliphatic), 0.89 (m, $\text{CH}_3-\text{C}-$)

$^{13}\text{C-NMR}$ (CDCl_3) δ : 165.37 (carboxyl), 164.24 (Ar), 161.60 (Ar), 158.65 (Ar), 150.11 (Ar), 139.20 (Ar), 138.24 (Ar), 134.42 (Ar), 132.93 (Ar), 128.05 (2C, Ar), 127.58 (2C, Ar), 122.12 (2C, Ar), 114.74 (2C, Ar), 114.07 (Ar), 111.28 (Ar), 105.23 (ethylene), 100.17 (ethylene), 68.90 (aliphatic), 68.30 (aliphatic), 68.06 (aliphatic), 22-34 (23C, aliphatic), 14.10 (2C, aliphatic)

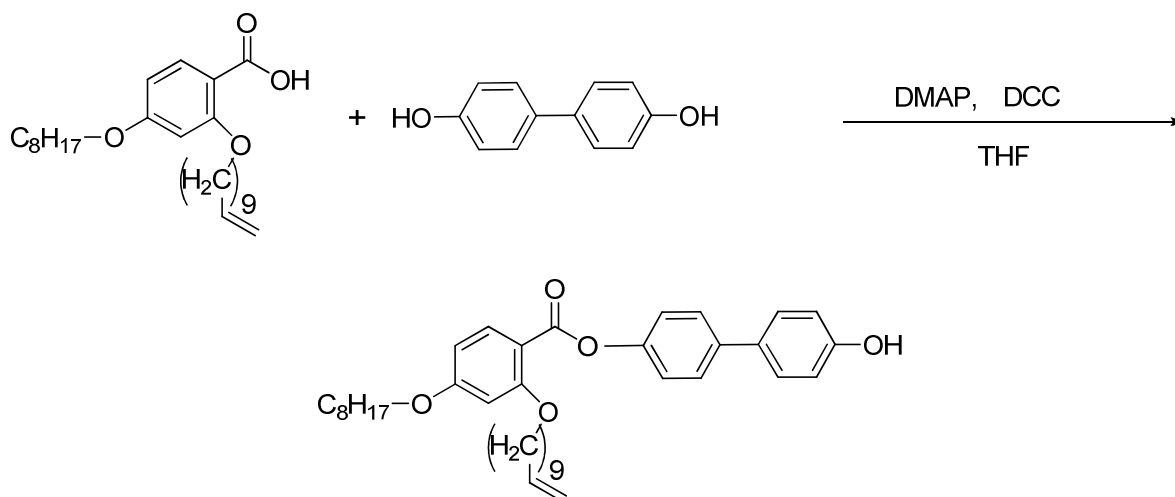
MS m/z : 763.662 (+ ^{23}Na)

EA: - experimentally: C 79.51%; H 9.97%

- calculated: C 79.41%; H 9.79%

Phase transition temperatures: Cr 26 N 62 Iso

Preparation of 4'-hydroxy-4-yl-4-octyloxy-2-(undec-10-en-1-yloxy) benzoate



4-octyloxy-2-(undec-10-en-1-yloxy) benzoic acid (10 g; 24 mmol), 4,4'-biphenol (15 g; 80 mmol) and 4-dimethylaminopyridine (DMAP) (1 g; 8.2 mmol) were added to 200 ml THF. N,N'-dicyclohexylcarbodiimide (DCC) (8.24 g; 40 mmol) was added to the mixture and stirred at r.t. overnight. After filtration, the residue is recrystallised from ethanol.

Yield: 7 g, 50%

¹H-NMR (CDCl₃) δ: 8.05 (d, Ar), 7.48 (d, Ar), 7.33 (d, Ar), 7.21 (d, Ar), 6.77 (d, Ar), 6.51 (m, Ar), 5.78 (m, -CH=C), 4.95 (dd, CH₂=CH-), 4.02 (m, -CH₂-O-), 2.00 (m, -CH₂-CH=CH₂), 1.20-1.90 (m, aliphatic), 0.89 (m, CH₃-C-)

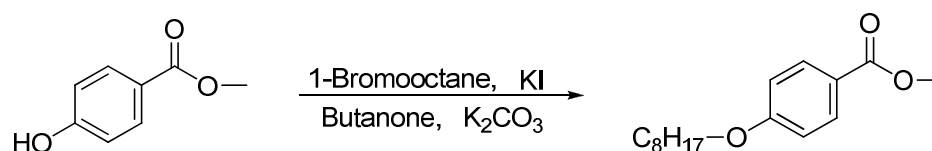
¹³C-NMR (CDCl₃) δ: 164.64 (carboxyl), 164.55 (Ar), 161.77 (Ar), 155.34 (Ar), 150.05 (Ar), 139.21 (Ar), 138.33 (Ar), 134.51 (Ar), 132.91 (Ar), 128.24 (2C, Ar), 127.61 (2C, Ar), 122.17 (2C, Ar), 115.63 (2C, Ar), 114.06 (Ar), 110.99 (Ar), 105.28 (ethylene), 100.15 (ethylene), 68.94 (aliphatic), 68.34 (aliphatic), 22-34 (14C, aliphatic), 14.09 (aliphatic)

MS m/z: 609.331 (+ ^{23}Na)

EA: - experimentally: C 78.00%; H 8.50%

- calculated: C 77.78%; H 8.59%

Preparation of methyl 4-octyloxybenzoate



1-Bromooctane (21.6 ml; 0.125 mol) in 100 ml butanone, was added dropwise, under reflux, to a mixture of methyl 4-hydroxybenzoate (19 g; 0.125 mol), K_2CO_3 anhydrous (86.25 g; 0.625 mol) and catalytic amount of KI in 400 ml of butanone. The reaction mixture is heated to reflux overnight, filtrated and the residue recrystallised from methanol.

Yield: 19.9 g, 60%

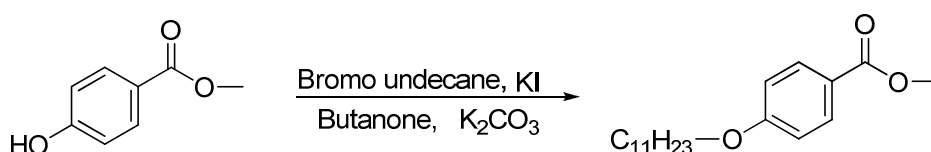
$^1\text{H-NMR}$ (CDCl_3) δ : 7.97 (d, Ar), 6.89 (d, Ar), 3.99 (t, $-\text{CH}_2-\text{O}-\text{Ar}$), 3.87 (s, $\text{CH}_3-\text{O}-$), 1.20-1.90 (m, chol H), 0.88 (s, $\text{CH}_3-\text{C}-$)

$^{13}\text{C-NMR}$ (CDCl_3) δ : 166.90 (carboxyl), 162.93 (Ar), 131.53 (2C, Ar), 122.26 (Ar), 114.02 (2C, Ar), 68.17 (aliphatic), 51.78 (aliphatic), 31.77 (aliphatic), 28-30 (3C, aliphatic), 25.96 (aliphatic), 22.63 (aliphatic), 14.07 (aliphatic)

MS m/z: 288.309 (+ ^{23}Na)

EA: - experimentally: C 71.71%; H 9.69%
- calculated: C 72.69%; H 9.15%

Preparation of methyl 4-undecyloxybenzoate



The synthesis and work up are similar with the method for the preparation of methyl 4-octyloxybenzoate.

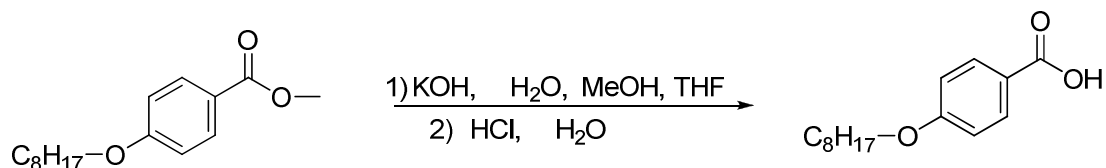
Yield: 23 g, 60%

¹H-NMR (CDCl₃) δ: 7.97 (d, Ar), 6.89 (d, Ar), 3.99 (t, -CH₂-O-Ar), 3.87 (s, CH₃-O-), 1.20-1.90 (m, chol H), 0.88 (s, CH₃-C-)

¹³C-NMR (CDCl₃) δ: 166.91 (carboxyl), 162.94 (Ar), 131.54 (2C, Ar), 122.27 (Ar), 114.03 (2C, Ar), 68.18 (aliphatic), 51.81 (aliphatic), 31.89 (aliphatic), 28-30 (6C, aliphatic), 25.96 (aliphatic), 22.60 (aliphatic), 14.10 (aliphatic)

EA: - experimentally: C 74.76%; H 10.09%
- calculated: C 74.47%; H 9.87%

Preparation of 4-octyloxy benzoic acid



Methyl 4-octyloxybenzoate (18 g; 0.07 mol) was added to a solution of KOH (16.8 g; 0.3 mol) in water (50 ml) and THF (80 ml) and methanol (400 ml). The reaction mixture was stirred at r.t. for two days and the reaction was completed by heated to reflux for 2 h. The solvent was distilled off and ice/water (250 ml) was added and then the solution was acidified with HCl 36% (100 ml). The mixture was extracted with dichloromethane (6 X 100 ml). The organic phase was dried over MgSO_4 , then filtrated and concentrated. The product was purified by recrystallisation in hexane.

Yield: 10.5 g, 60%

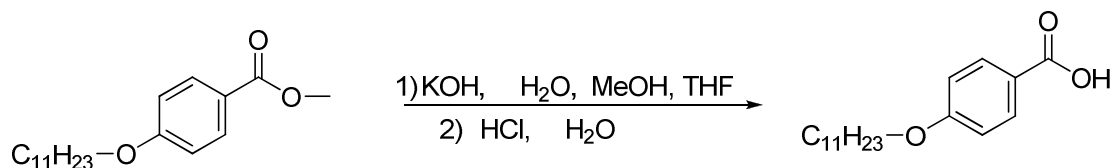
$^1\text{H-NMR}$ (CDCl_3) δ : 8.06 (d, Ar), 6.93 (d, Ar), 4.02 (t, $-\text{CH}_2\text{-O-Ar}$), 1.20-1.90 (m, aliphatic), 0.88 (s, $\text{CH}_3\text{-C-}$)

$^{13}\text{C-NMR}$ (CDCl_3) δ : 172.18 (carboxyl), 163.69 (Ar), 132.32 (2C, Ar), 121.37 (Ar), 114.16 (2C, Ar), 68.27 (aliphatic), 31.79 (aliphatic), 28-30 (3C, aliphatic), 25.97 (aliphatic), 22.64 (aliphatic), 14.09 (aliphatic)

MS m/z : 249.976

EA: - experimentally: C 71.71%; H 9.04%
- calculated: C 71.97%; H 8.86%

Preparation of 4-undecyloxy benzoic acid



The synthesis and work up are similar with the method for the preparation of 4-undecyloxy benzoic acid.

Yield: 12.3 g, 60%

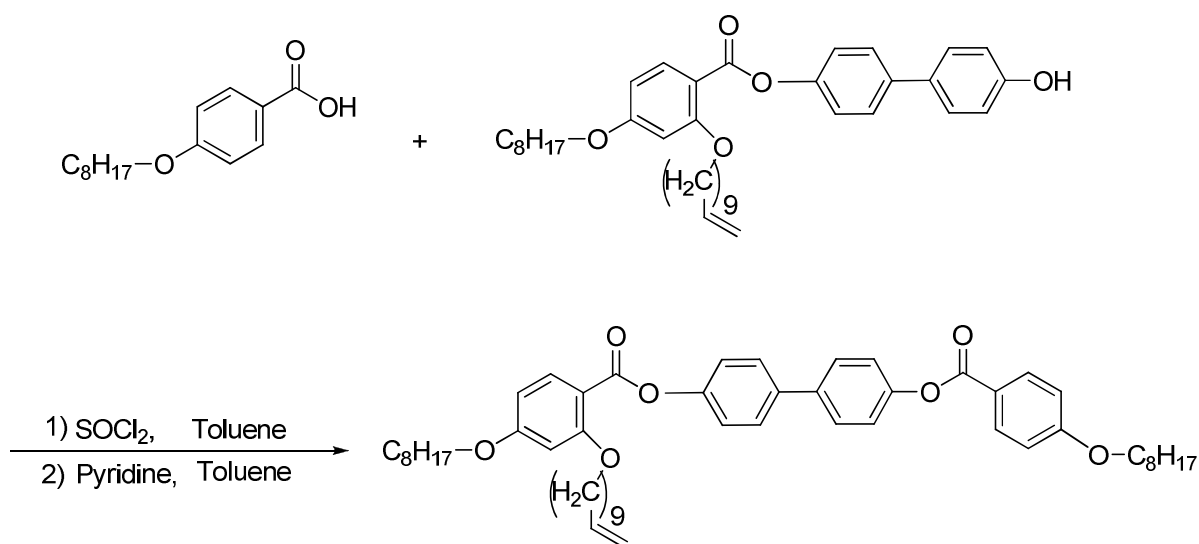
¹H-NMR (CDCl₃) δ : 8.05 (d, Ar), 6.93 (d, Ar), 4.02 (t, -CH₂-O-Ar), 1.20-1.90 (m, aliphatic), 0.88 (s, CH₃-C-)

¹³C-NMR (CDCl₃) δ : 172.18 (carboxyl), 163.68 (Ar), 132.32 (2C, Ar), 121.31 (Ar), 114.18 (2C, Ar), 68.27 (aliphatic), 31.89 (aliphatic), 28-30 (6C, aliphatic), 25.96 (aliphatic), 22.68 (aliphatic), 14.10 (aliphatic)

EA: - experimentally: C 74.01%; H 9.69%

- calculated: C 73.93%; H 9.65%

Preparation of 4'-(4-octyloxybenzoyloxy) biphenyl-4-yl-4-octyloxy-2-(undec-10-en-1-yloxy) benzoate (4RM)



4-octyloxy benzoic acid (2.2 g; 8.5 mmol) was dissolved in toluene (40 ml); thionyl chloride (12.3 ml; 170 mmol) was added and the solution heated gradually from r.t. to 80°C for 3 h, the reaction being completed after heating at reflux for 1 h. The thionyl chloride and toluene were distilled off. A solution of 4'-hydroxy-4-yl-4-octyloxy-2-(undec-10-en-1-yloxy) benzoate (5 g; 8.5 mmol) and pyridine (13.7 ml; 170 mmol) in toluene (40 ml) was added to the residue. The mixture was heated to 80°C overnight and the reaction completed after heated to reflux for 1 h.

Ice/water (80 ml) and ether/hexane=1/1 (80 ml) were added. The phases were separated and the aqueous layer extracted with chloroform (2 X 60 ml). The combined organic layers were dried with MgSO_4 and the solvents distilled off. The residue was purified by column chromatography (CH_2Cl_2 /hexane=1/1).

Yield: 4.9 g, 70%

¹H-NMR (CDCl₃) δ: 8.16 (d, Ar), 8.04 (d, Ar), 7.60 (d, Ar), 7.27 (d, Ar), 6.98 (d, Ar), 6.51 (m, Ar), 5.78 (m, -CH=C), 4.95 (dd, CH₂=CH-), 4.04 (m, -CH₂-O-), 2.01 (m, -CH₂-CH=CH₂), 1.20-1.90 (m, aliphatic), 0.89 (m, CH₃-C-)

¹³C-NMR (CDCl₃) δ: 164.50 (carboxyl), 164.41 (carboxyl), 164.09 (Ar), 163.51 (Ar), 161.62 (Ar), 150.66 (Ar), 150.43 (Ar), 139.14 (Ar), 138.16 (Ar), 137.74 (Ar), 134.42 (Ar), 132.25 (2C, Ar), 128.07 (2C, Ar), 128.01 (2C, Ar), 122.25 (2C, Ar), 122.04 (2C, Ar), 121.43 (Ar), 114.25 (2C, Ar), 114.06 (Ar), 111.13 (Ar), 105.22 (ethylene), 100.13 (ethylene), 68.86 (aliphatic), 68.27 (aliphatic), 22-34 (21C, aliphatic), 14.07 (2C, aliphatic)

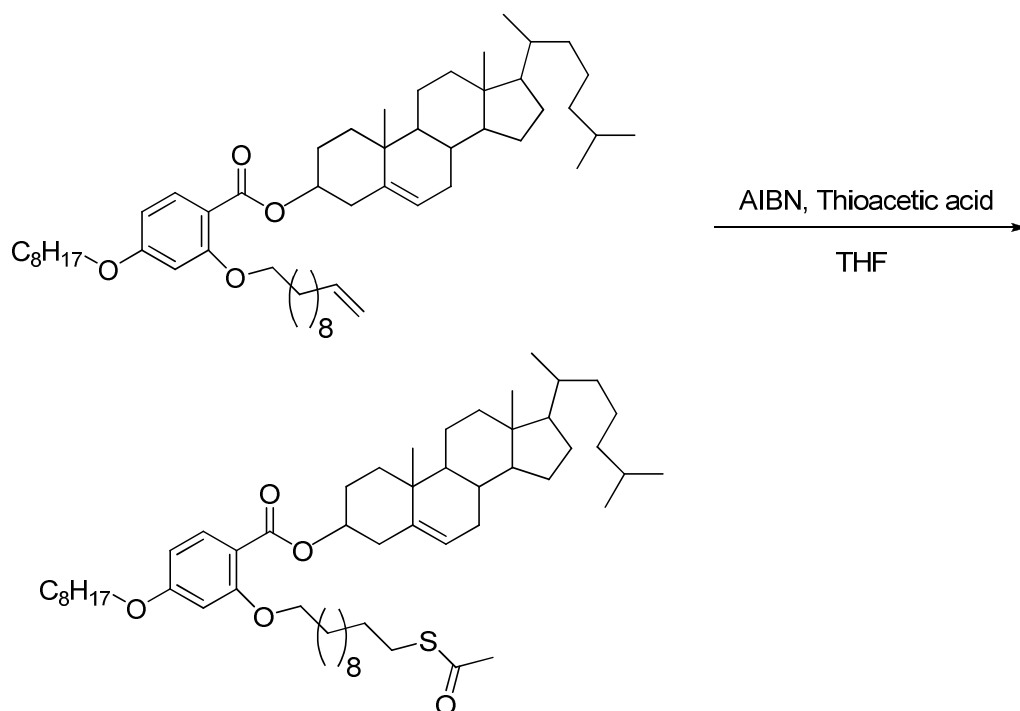
MS m/z: 841.759

EA: - experimentally: C 77.81%; H 8.81%

- calculated: C 77.71%; H 8.61%

Phase transition temperatures: Cr 80 N 140 Iso

Preparation of M1-TA material



Using dry glassware (overnight in the oven), M1 (1 g; 1.27 mmol) was dissolved in dry tetrahydrofuran (THF) (15 ml). Azobisisobutyronitrile (AIBN) (0.3 g; 1.83 mmol) was added in small excess and the solution kept under nitrogen atmosphere. Thioacetic acid (0.26 ml; 3.66 mmol) was added and the solution heated gradually from room temperature to 70°C for 5 h. After the completion of the reaction, the volatile compounds were distilled off using a vacuum pump. The residue was purified by column chromatography (CH₂Cl₂/hexane=2/1).

Yield: 0.9 g, 80%

¹H-NMR (CDCl₃) δ: 7.79 (d, Ar), 6.43 (d, Ar), 6.42 (s, Ar), 5.40 (d, chol-CH=C-), 4.82 (q, chol-CH-O-), 3.97 (t, -CH₂-O-), 2.85 (t, -CH₂-S-C=O), 2.44 (dd, chol-CH₂-C=C-), 2.31 (s, CH₃-C=O), 1.00-1.90 (m, chol H), 0.91 (d, chol-CH₃-CH-), 0.86 (d, chol-(CH₃)₂-CH-), 0.68 (s, CH₃-C-)

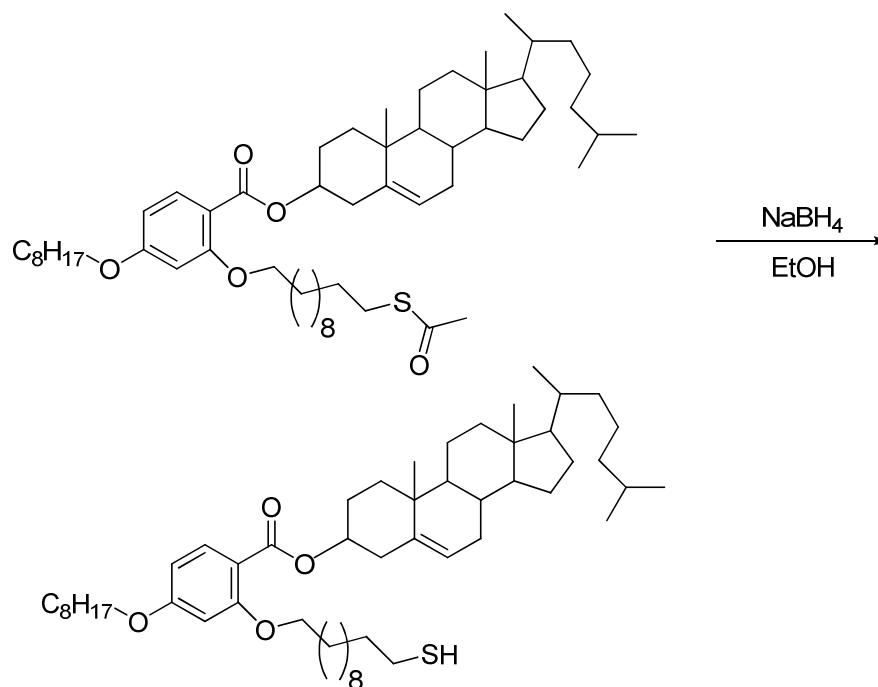
¹³C-NMR (CDCl₃) δ: 165.64 (carboxyl), 163.44 (Ar), 160.56 (Ar), 139.90 (Ar), 133.61 (Ar), 122.49 (Ar), 119.04 (carboxyl-S), 112.50 (Ar), 104.90 (ethylene), 100.11 (ethylene), 71.92 (cyclohexane), 68.73 (aliphatic), 68.14 (aliphatic), 56.65 (cyclopentane), 56.07 (cyclohexane), 49.99 (2C, cyclohexane), 42.27 (cyclopentane), 18-40 (6C, cyclohexane), 18-40 (26C, aliphatic), 18-40 (3C, cyclopentane), 14.07 (aliphatic), 11.82 (aliphatic)

MS m/z: 885.897 (+ ²³Na)

EA: - experimentally: C 74.87%; H 10.94%; S 3.08%

- calculated: C 76.51%; H 10.51%; S 3.71%

Preparation of M1-SH material



A solution of M1-TA (0.5 g; 0.58 mmol) in dry ethanol (EtOH) (6 ml) is heated gradually from r.t. to 70°C. 10 equivalents of sodium borohydride (NaBH₄) (0.22 g; 5.8 mmol) are added portion wise. The reaction is left at 70°C for an hour. After the completion of the reaction, the reaction mixture was poured into ice water and extracted with ether, 3 times. Then, ether layer washed with brine and dried over MgSO₄. The solution was concentrated and the residue purified by column chromatography (CH₂Cl₂).

Yield: 0.3 g, 65%

¹H-NMR (CDCl₃) δ: 7.79 (d, Ar), 6.44 (d, Ar), 6.43 (s, Ar), 5.40 (d, chol-CH=C-), 4.82 (q, chol-CH-O-), 3.97 (t, -CH₂-O-), 2.52 (q, -CH₂-SH), 2.44 (dd, chol-CH₂-C=C-), 1.00-1.90 (m, chol H), 0.91 (d, chol-CH₃-CH-), 0.86 (d, chol-(CH₃)₂-CH-), 0.68 (s, CH₃-C-)

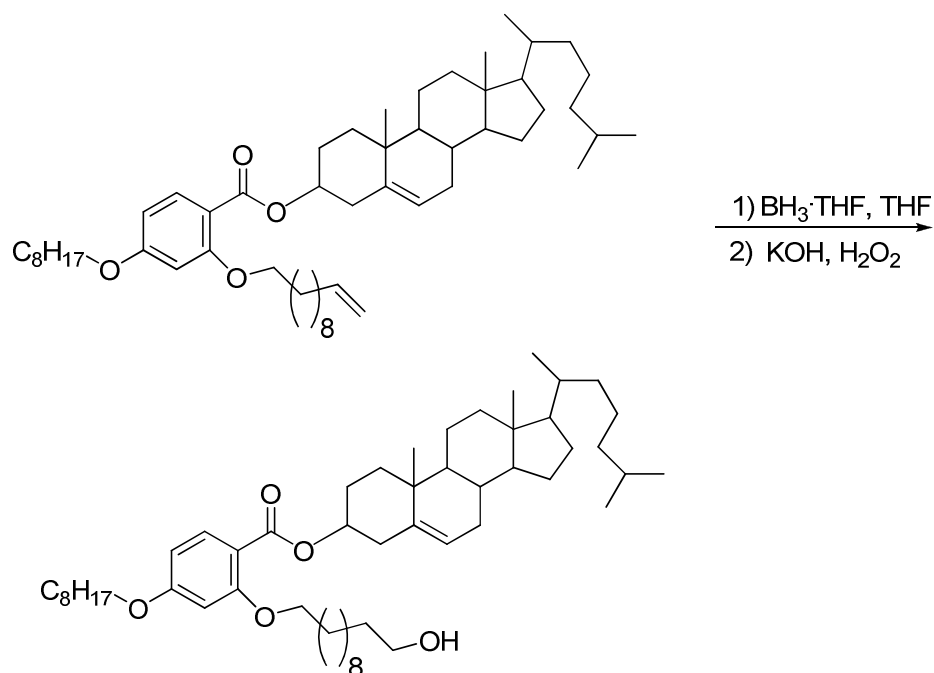
¹³C-NMR (CDCl₃) δ: 168.72 (carboxyl), 166.66 (Ar), 163.80 (Ar), 143.07 (Ar), 136.86 (Ar), 125.62 (Ar), 116.27 (Ar), 108.08 (ethylene), 103.28 (ethylene), 77.00 (cyclohexane), 71.89 (aliphatic), 71.31 (aliphatic), 59.86 (cyclopentane), 59.34 (cyclohexane), 53.22 (2C, cyclohexane), 45.55 (cyclopentane), 21-43 (6C, cyclohexane), 21-43 (25C, aliphatic), 21-43 (3C, cyclopentane), 17.33 (aliphatic), 15.06 (aliphatic)

EA: - experimentally: C 77.71%; H 11.08%; S 3.64%

- calculated: C 77.50%; H 10.80%; S 3.90%

Phase transition temperatures: T_g -15 N* 51 Iso (on cooling)

Preparation of M1-OH material



M1 (1 g; 1.27 mmol) was dissolved in dry tetrahydrofuran (THF) (10 ml). A solution of borane 1M in THF (BH_3) (1.3 ml; 1.3 mmol) was added and the solution kept under nitrogen atmosphere, over night, at room temperature. An aqueous solution of 3M potassium hydroxide (KOH) (1.3 ml) and 30% hydrogen peroxide (H_2O_2) (1.1 ml) was added and the solution was left stirring for 2 h. After that, the mixture was added to 30 ml of brine and 30 ml of ether. The organic phase was washed with water, twice, and brine and dried over MgSO_4 . The filtrate was concentrated and the residue was purified by column chromatography, using a short column (CH_2Cl_2).

Yield: 0.4 g, 40%

$^1\text{H-NMR}$ (CDCl_3) δ : 7.71 (d, Ar), 6.37 (d, Ar), 6.35 (s, Ar), 5.32 (d, chol- $\text{CH}=\text{C}$ -), 4.75 (q, chol- CH-O -), 3.89 (t, $-\text{CH}_2\text{-O}$ -), 3.55 (t, $-\text{CH}_2\text{-OH}$), 2.37 (dd, chol- $\text{CH}_2\text{-C}=\text{C}$ -), 1.00-1.90 (m, chol H), 0.80 (d, chol- $\text{CH}_3\text{-CH}$ -), 0.78 (d, chol- $(\text{CH}_3)_2\text{-CH}$ -), 0.61 (s, $\text{CH}_3\text{-C}$ -)

¹³C-NMR (CDCl₃) δ: 168.87 (carboxyl), 166.74 (Ar), 163.86 (Ar), 143.08 (Ar), 136.92 (Ar), 125.68 (Ar), 116.25 (Ar), 108.15 (ethylene), 103.31 (ethylene), 77.12 (cyclohexane), 71.94 (aliphatic), 71.36 (aliphatic), 66.03 (aliphatic-OH), 59.91 (cyclopentane), 59.38 (cyclohexane), 53.27 (2C, cyclohexane), 45.52 (cyclopentane), 21-43 (6C, cyclohexane), 21-43 (24C, aliphatic), 21-43 (3C, cyclopentane), 17.36 (aliphatic), 15.08 (aliphatic)

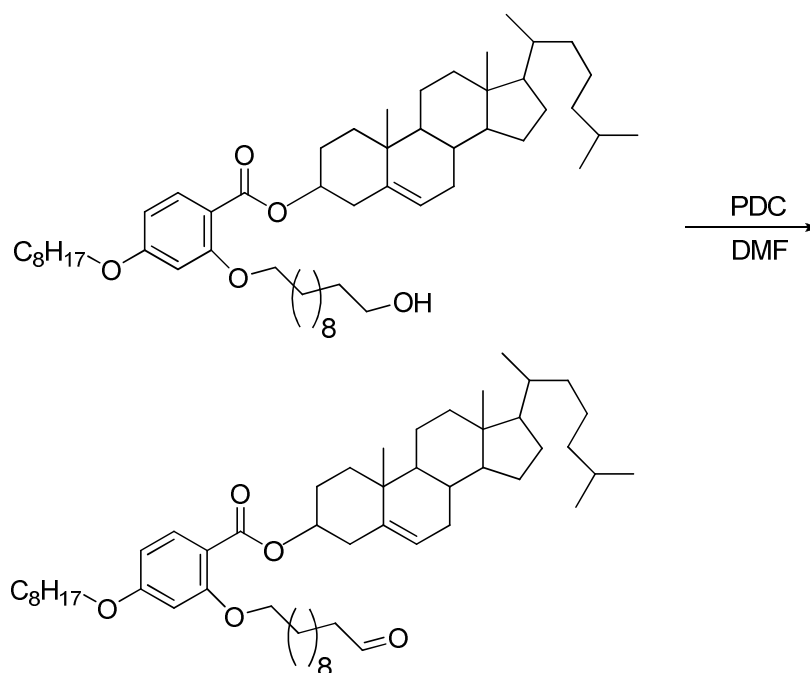
MS m/z: 827.997 (+ ²³Na)

EA: - experimentally: C 78.90%; H 11.26%

- calculated: C 79.05%; H 11.01%

Phase transition temperatures: T_g -6 N* 52 Iso (on cooling)

Preparation of M1-COH material



M1-OH (0.25 g; 0.31 mmol) was dissolved in dimethylformamide (DMF) (4 ml), dried over night on sodium sulphate or molecular sieves or barium oxide. Pyridinium dichromate ((C₅H₅NH⁺)₂Cr₂O₇⁻) (PDC) (0.41 g; 1.1 mmol), 3 equivalents, was added portion wise and the solution kept overnight, at room temperature. After that, the mixture was added to 7-10 volumes of water and extracted with ether, 3 times. The organic phase was dried over MgSO₄. The filtrate was concentrated and the residue was purified by column chromatography (ethyl acetate (EA)).

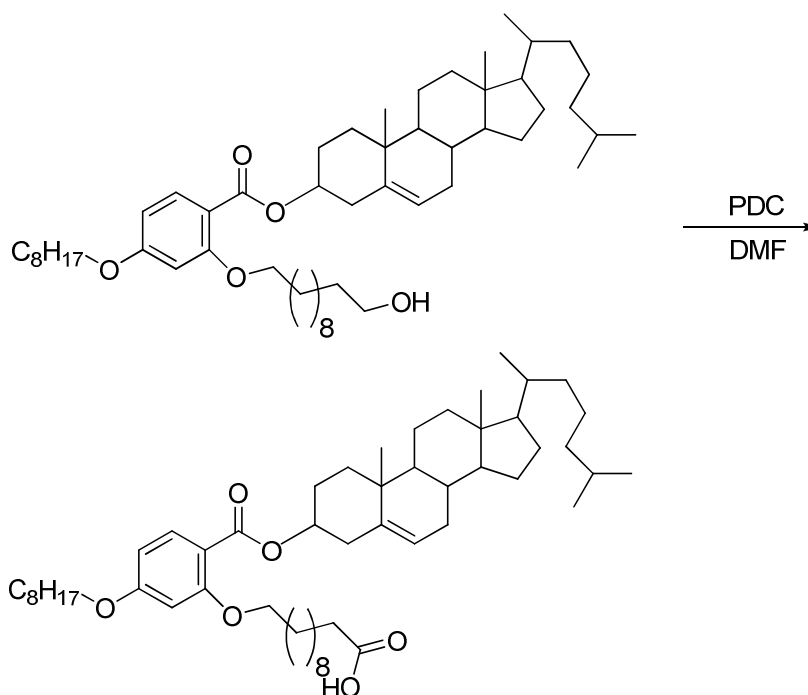
Yield: 0.2 g, 70%

¹H-NMR (CDCl₃) δ: 9.76 (s, -CH=O), 7.79 (d, Ar), 6.44 (d, Ar), 6.43 (s, Ar), 5.39 (d, chol-CH=C-), 4.82 (q, chol-CH-O-), 3.97 (t, -CH₂-O-), 2.42 (dd, chol-CH₂-C=C-), 2.41 (dd, -CH₂-C=O), 1.00-1.90 (m, chol H), 0.86 (d, chol-CH₃-CH-), 0.85 (d, chol-(CH₃)₂-CH-), 0.68 (s, CH₃-C-)

$^{13}\text{C-NMR}$ (CDCl_3) δ : 206.01 (aldehyde), 168.76 (carboxyl), 166.60 (Ar), 163.72 (Ar), 143.05 (Ar), 136.76 (Ar), 125.58 (Ar), 116.21 (Ar), 108.04 (ethylene), 103.28 (ethylene), 77.00 (cyclohexane), 71.86 (aliphatic), 71.29 (aliphatic), 59.79 (cyclopentane), 59.23 (cyclohexane), 53.14 (2C, cyclohexane), 45.52 (cyclopentane), 21-43 (6C, cyclohexane), 21-43 (24C, aliphatic), 21-43 (3C, cyclopentane), 17.21 (aliphatic), 14.97 (aliphatic)

MS m/z : 825.825 (+ ^{23}Na)

Preparation of M1-COOH material



M1-OH (0.25 g; 0.31 mmol) was dissolved in dimethylformamide (DMF) (20 ml), dried over night on sodium sulphate or molecular sieves or barium oxide. Pyridinium dichromate ($(\text{C}_5\text{H}_5\text{NH}^+)_2\text{Cr}_2\text{O}_7^-$) (PDC) (1.15 g; 3.1 mmol), 10 equivalents, was added portion wise and the solution kept at room temperature, for 4 days. After that, the mixture was added to 7-10 volumes of water and

extracted with ether, 3 times. The organic phase was dried over MgSO_4 . The filtrate was concentrated and the residue was purified by column chromatography (CH_2Cl_2).

Yield: 0.2 g, 75%

$^1\text{H-NMR}$ (CDCl_3) δ : 7.79 (d, Ar), 6.45 (d, Ar), 6.43 (s, Ar), 5.39 (d, chol- $\text{CH}=\text{C}$ -), 4.82 (q, chol- CH-O -), 3.97 (t, $-\text{CH}_2\text{-O}$ -), 2.45 (dd, chol- $\text{CH}_2\text{-C}=\text{C}$ -), 2.34 (t, $-\text{CH}_2\text{-C}=\text{O}$), 1.00-1.90 (m, chol H), 0.86 (d, chol- $\text{CH}_3\text{-CH}$ -), 0.85 (d, chol- $(\text{CH}_3)_2\text{-CH}$ -), 0.68 (s, $\text{CH}_3\text{-C}$ -)

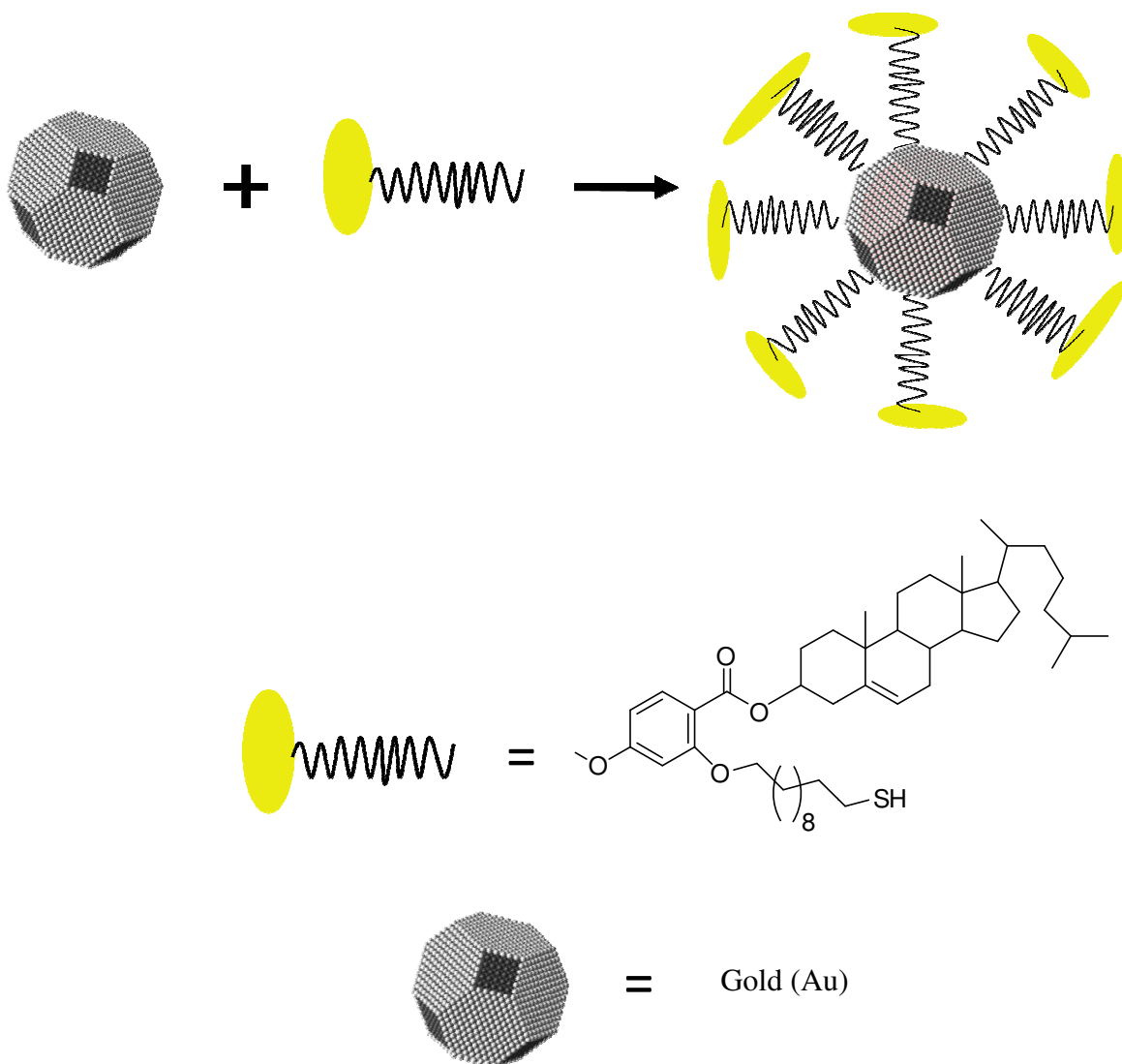
$^{13}\text{C-NMR}$ (CDCl_3) δ : 182.62 (carboxyl), 168.77 (carboxyl), 166.57 (Ar), 163.69 (Ar), 143.00 (Ar), 136.73 (Ar), 125.55 (Ar), 116.15 (Ar), 108.01 (ethylene), 103.22 (ethylene), 76.50 (cyclohexane), 71.83 (aliphatic), 71.25 (aliphatic), 59.76 (cyclopentane), 59.20 (cyclohexane), 53.10 (2C, cyclohexane), 45.50 (cyclopentane), 21-43 (6C, cyclohexane), 21-43 (24C, aliphatic), 21-43 (3C, cyclopentane), 17.17 (aliphatic), 14.92 (aliphatic)

MS m/z : 841.841 (+ ^{23}Na)

EA: - experimentally: C 77.69%; H 10.43%
- calculated: C 77.70%; H 10.58%

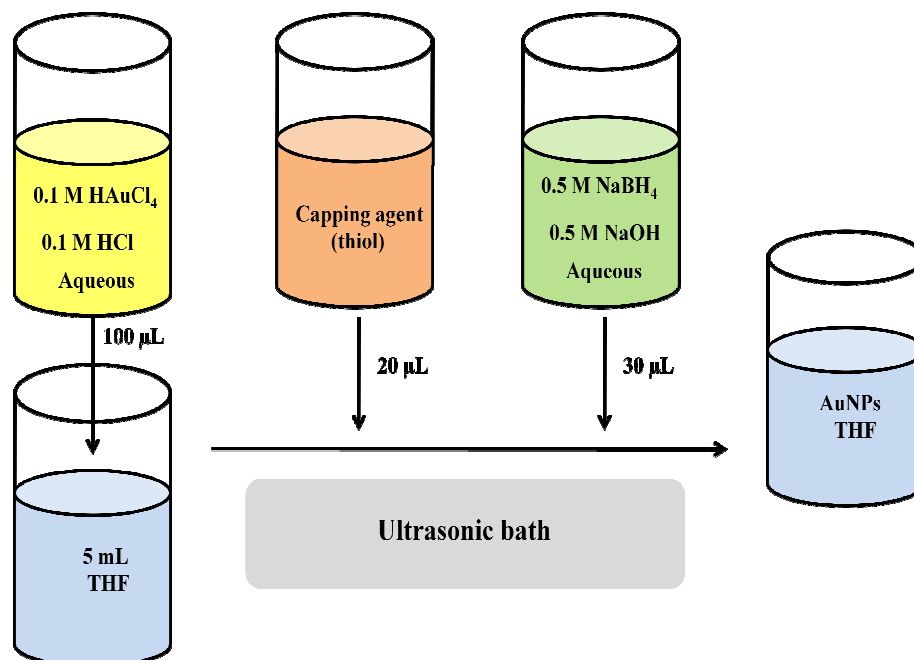
Phase transition temperatures: Tg 3 X 10 X 61 N* 67 Iso

Preparation of Au-NPs coated with M1



40 ml of THF were added to an Erlenmeyer flask on ultrasonic bath and an aqueous solution of 0.1M chloroauric acid (HAuCl_4) / 0.1M hydrochloric acid (HCl) (5.91 ml) previously prepared was added into the flask. Then, a solution of M1-SH (272.6 mg) in THF was added, followed by the reducing aqueous solution composed of 0.5M sodium borohydride (NaBH_4) / 0.5M sodium hydroxide (NaOH) (3.32 ml). The ratio between the Au and the functionalised mesogen was 2 to 1. Immediately after the addition of the reducing solution the colour changed to brown. The reaction was kept in ultrasonic bath for 15 min. In order to purify the Au-NPs a more complex, expensive and time consuming procedure was involved. The solution was concentrated and passed through bio beads SX-1 (Bio-

Rad[®]), twice, using as the mobile phase dichloromethane. Afterwards, the residue was washed twice under centrifugation with acetone/ethanol mixtures. The residue was concentrated and prepared for further characterisation.



Yield: ~20%

¹H-NMR (CDCl₃): The ¹H-NMR exhibits broad peaks and the disappearance of the peak for -CH₂-SH at 2.52 ppm, can be followed.

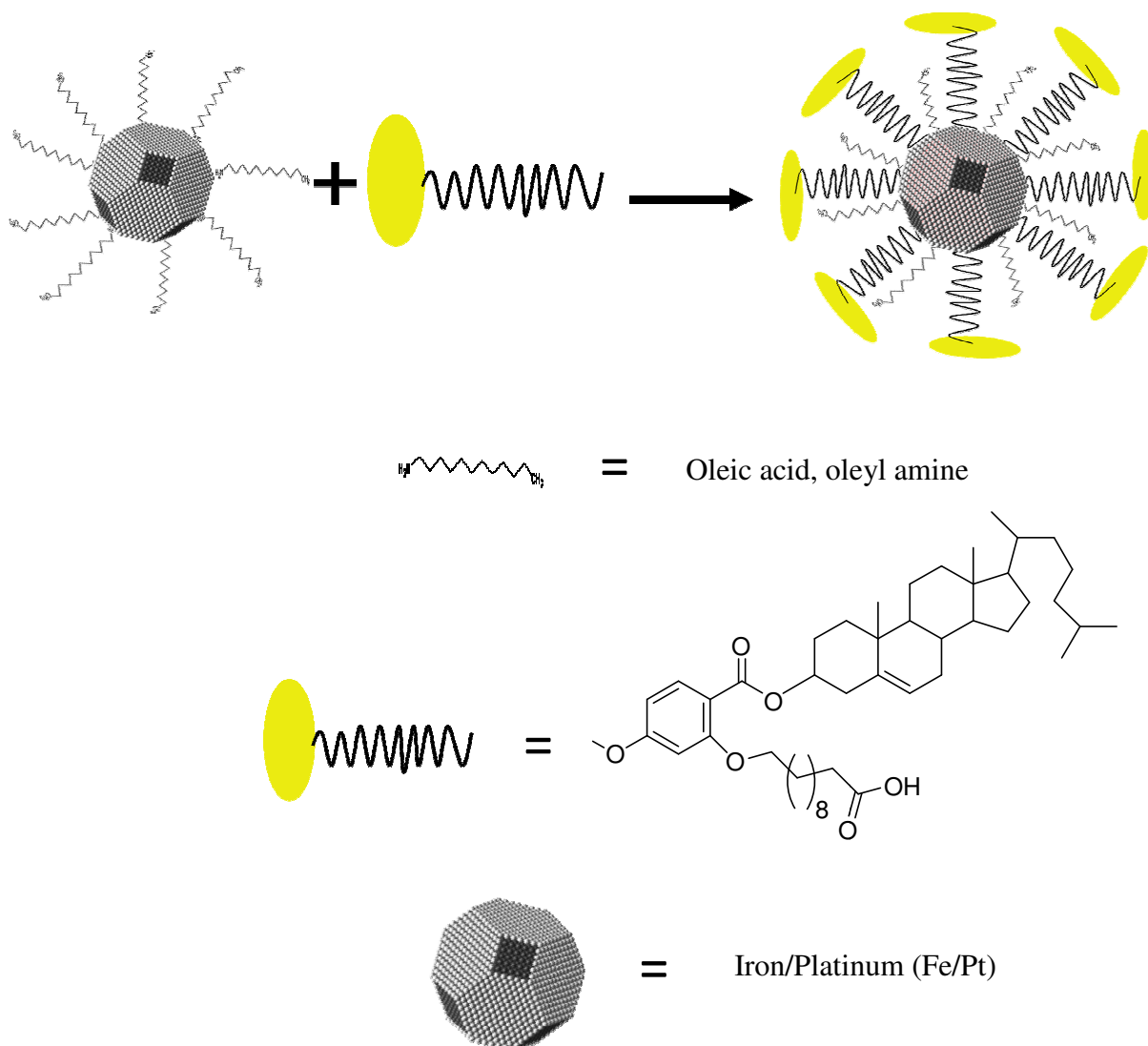
GPC: in THF, peak at 14.2 ml

EA: - experimentally: C 52.14%; H 6.81%; S 1.94%

Phase transition temperatures: T_g -10 N* 35 Iso (on cooling)

NOTE: The synthetic procedure is similar in all cases when the coating is made with materials functionalised with thiol (-SH) group.

Preparation of Fe/Pt-NPs coated with M1



A platinum precursor (platinum acetylacetonate) ($\text{Pt}(\text{acac})_2$) (394 mg; 1.0 mmol), a iron precursor (iron pentacarbonyl) ($\text{Fe}(\text{CO})_5$) (0.26 ml; 2.0 mmol) and a reducing agent (1,2-hexadecanediol) (780 mg; 3 mmol) are added to a high boiling point solvent (octyl ether) (40 ml) and the flask kept under nitrogen atmosphere. Capping agents, oleic acid (286 mg; 1 mmol) and oleyl amine (276 mg; 1 mmol) were added into the flask before the mixture was first heated to 100°C and subsequently to 286°C for 30 min to remove low-boiling components under a flowing stream of nitrogen. At this time the solution turned black. The mixture was allowed to heat up to refluxing temperature for 1 h. After cooling to room temperature, the black solution was precipitated by adding pure ethanol (300

ml) into the mixture followed by centrifugation. The yellow-brown supernatant was discarded and the solid kept. In order to remove the free unreacted capping agents/surfactants (oleic acid and oleyl amine) several cycles of washing with ethanol and centrifugation were performed. The black solid was dispersed in dichloromethane.

A Fe/Pt NPs solution from the black mixture in DCM (corresponding to 100 mg capped NPs) and M1-COOH material (0.3 mmol) were added in DCM and heated under reflux for several days, under a nitrogen atmosphere. If the mesogen can withstand higher temperatures, the mixture can be heated under reflux in toluene for several hours in order to have better quality NPs.

In order to purify the coated Fe/Pt-NPs a similar procedure like in the case of Au-NPs was involved. The solution was concentrated and passed through bio beads SX-1 (Bio-Rad[®]), twice, using as the mobile phase THF. Afterwards, the residue was washed twice under centrifugation with acetone/ethanol mixtures. The residue was concentrated and prepared for further characterisation.

Yield: ~20%

¹H-NMR: The NMR spectroscopy cannot be used due to the presence of the Iron (Fe) in the composition of Fe/Pt NPs.

Phase transition temperatures: T_g 0 N* 40 Iso (on cooling)

NOTE: The synthetic procedure is similar in all cases when the coating is made with materials functionalised either with acid or amine group.

IV.2. SYNTHESIS. DISCUSSION

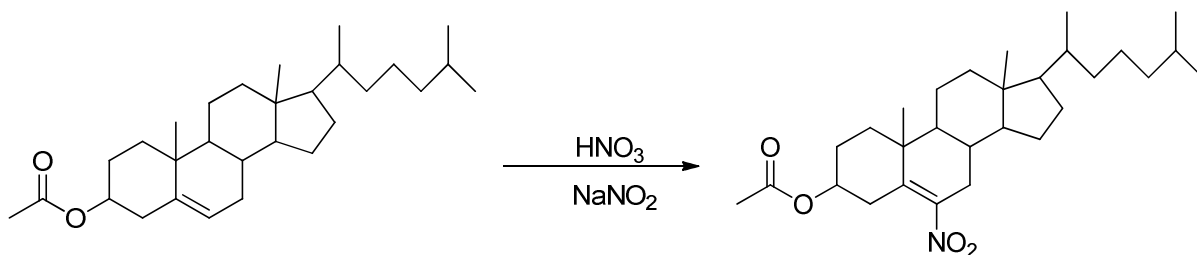
One of the targets for the research performed was to validate and improve techniques and synthetic procedures towards obtaining room temperature chiral liquid crystals, therefore issues, problems, difficulties and/or solutions regarding the synthesis, characterisation and their related procedures were discussed.

The work consisted in the preparation of cholesterol-based intermediates.

Following the logical route for the synthesis of the mesogen M1 and M2, their attachment to silsesquioxanes, the functionalization of M1 and its attachment to gold and iron/platinum NPs, issues are accordingly discussed.

We start by protecting the hydroxyl group by forming the cholesterol ester, followed by nitration and then converting into a ketone. Then the ketone was converted to a diol in a Grignard reaction. This product was esterified using the undecyloxy benzoic acid under acidic conditions and dehydrated forming the cholesterol derivative.

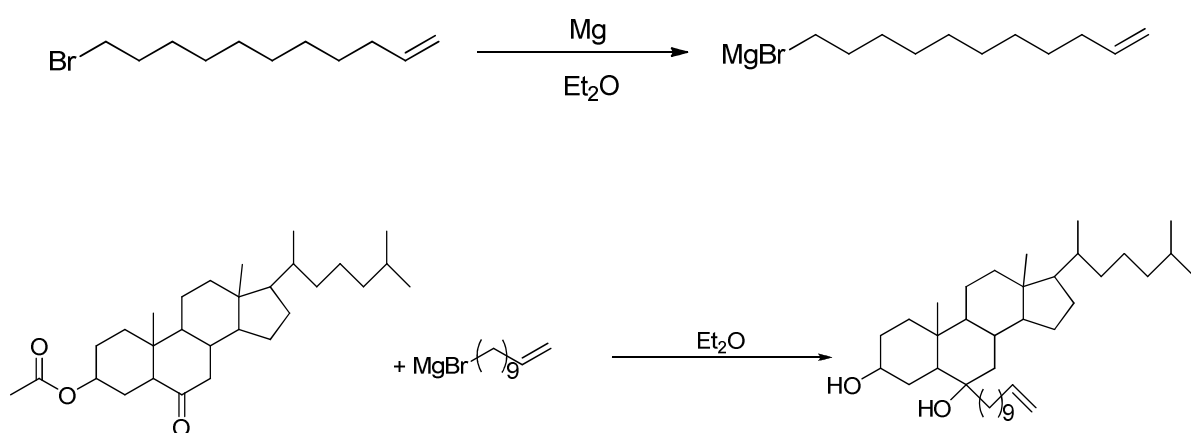
The first step involved the **nitration reaction** of the cholesterol acetate through a substitution reaction at the cholesterol alkenic carbon in order to a further side-on functionalise of the cholesterol moiety. Sodium nitrite is used as catalyst and nitric acid as solvent and nitration agent.



The nitration reaction is difficult to control in terms of yield; it can vary between a few percents and as much as 90% [106]. As the nitration is usually a highly exothermic reaction under quite harsh conditions, by-products are

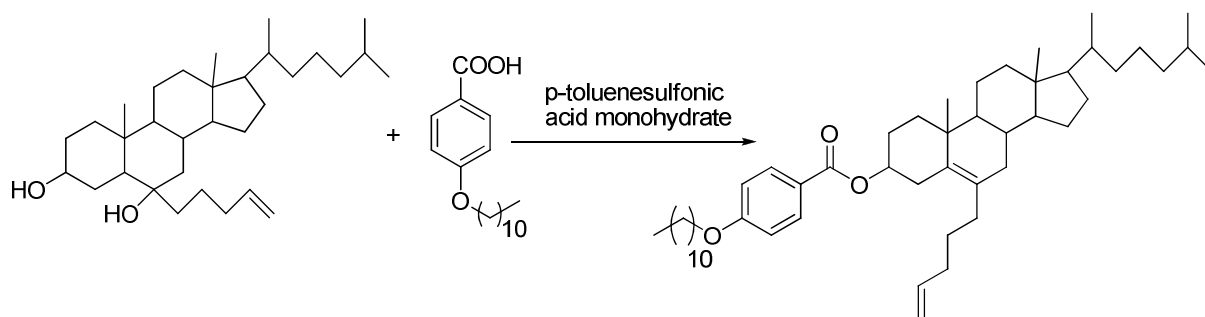
formed, thus reducing the overall yield of the reaction; also, one important issue is the purification of the materials. As recrystallisations are almost always employed, this is decreasing the yield. The route towards the optimal yield was a long iterative process and involved the optimisation of parameters such as the reaction time, the process of addition of reagents, work-up, purification) in order to achieve the yield of around 50% at all times.

The **Grignard precursors** used to prepare the cholesterol diols were challenging to prepare in a good yield and good quality, challenging to handle for the next step of the synthetic route. This was the reaction with a cholesterol ketone.

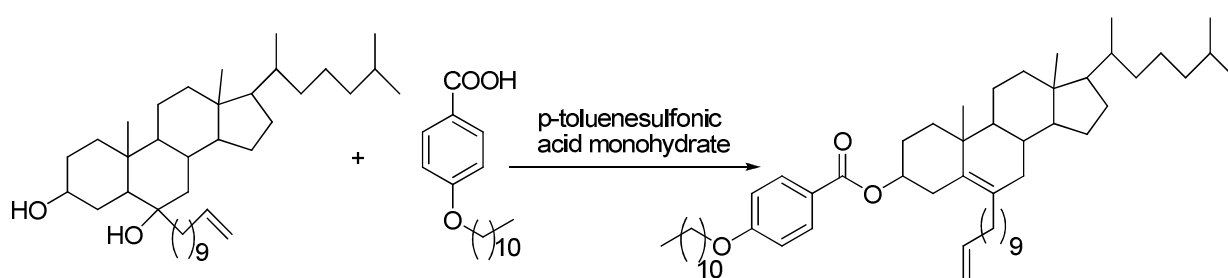


The main issue was the sensitivity of the reagents towards moisture.

Preparing the **MX** and **M2** materials, which they have similar synthetic route, was problematic, as the reaction proceeded in low yields (less than 10%). The synthetic path for these materials involves an esterification and elimination performed as a one pot reaction, under acidic conditions.



In order to identify what causes this low yield, all reaction parameters were checked and every possible problem eliminated, one at a time. In the literature [107], this reaction is performed in CHCl_3 , but toluene was used as solvent with no identifiable inconvenience even though the boiling temperature of toluene is 110°C comparing to 61°C of chloroform. Every starting material that was used should be stable at that temperature. The advantage was the use of the Dean-Stark trap method helping eliminate the water formed and move the esterification equilibrium towards the ester formation. The reaction development was followed by TLC. The formation of a new species was observed. It was assumed that there might be a problem with the catalyst used. The next step was to use chloroform as solvent and a drying agent (possible molecular sieves) for removing the water.

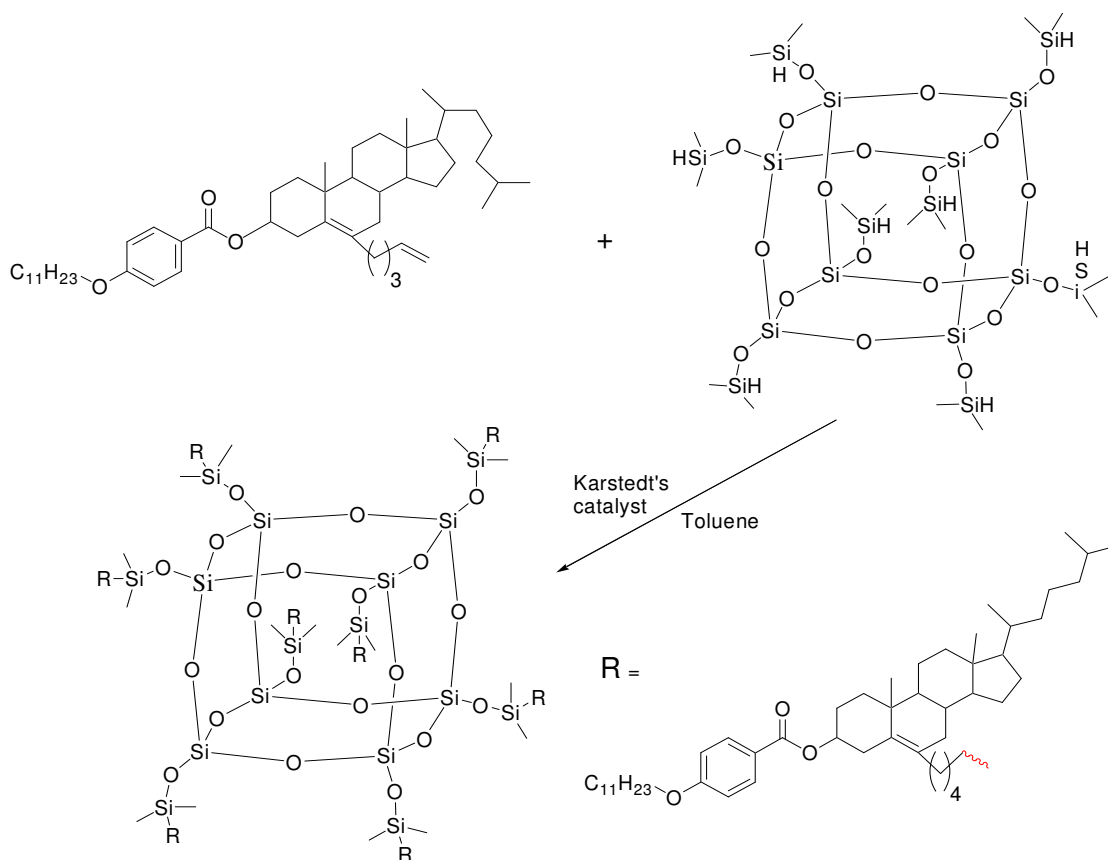


As the synthesis is quite similar, the same problem was encountered for the synthesis of 4-undecyloxy-6-pentenylcholestanol.

To solve the problem of low yields, the reaction was performed in chloroform and for removing the formed water, activated molecular sieves were

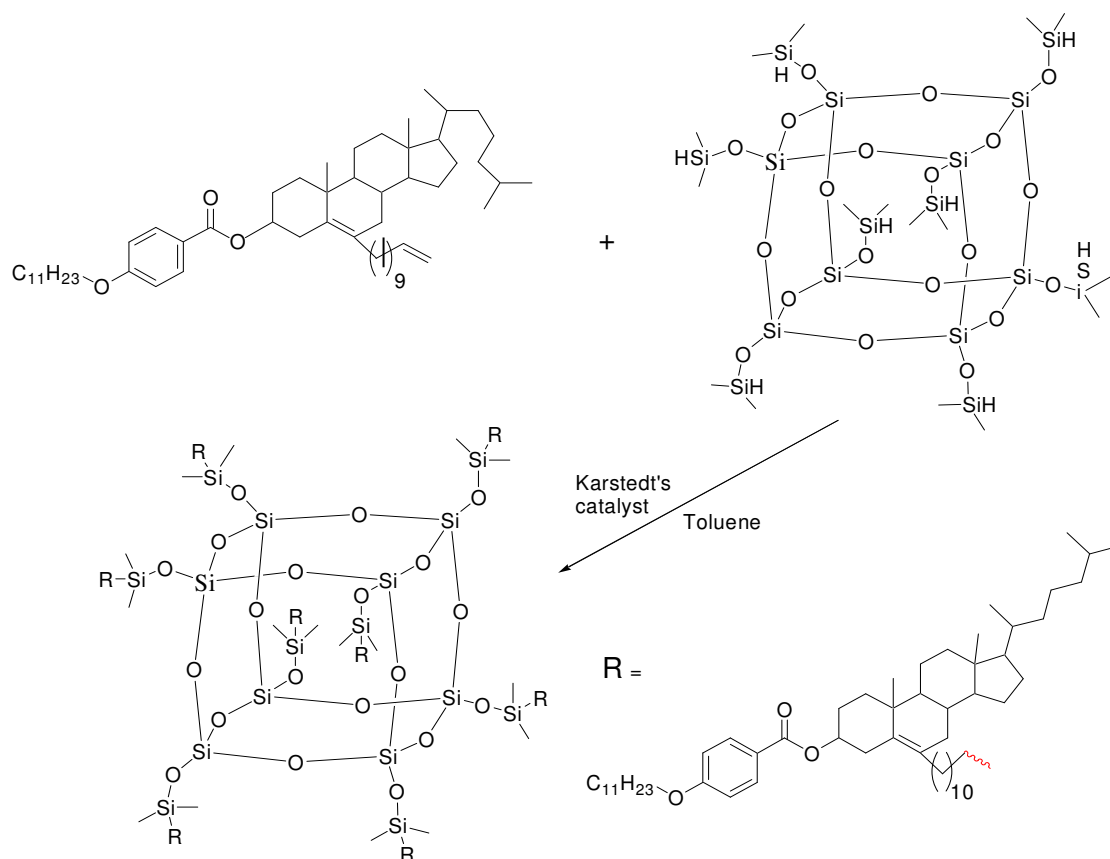
used. The reaction was left reacting at 60°C, for 6 days. It was found to be important that the temperature does not exceed 80°C, as the dehydration of the secondary alcohol takes place at higher temperatures. The reaction was checked by TLC. The activated molecular sieves were added starting at the fourth day of reaction when equilibrium was reached. This was found to give the best yields. From then onwards small portions of activated molecular sieves were added every day until no change was observed (day 6). Thereafter, the work-up was relatively easy and resulted in the desired material obtained in an acceptable yield of 60%.

For the preparation of **C-M2-X**, the issue was that no octo-substituted product was formed. As the cause for this lack of reactivity the length of the lateral alkyl chain was identified. It was considered that the selected pentyl spacer is too short and steric hindrance prevents product formation. A solution was an increase of the chain length of the spacer group separating the cholesteryl moiety and silsesquioxane group.



For the hydrosilylation particular attention is required in the selection of the reaction temperature; if it is too high, the Karstedt's catalyst induces unwanted side-reactions: the formation of isomeric olefins, reduced alkenes or dehydrocondensation adducts.

For the synthesis of **C-M2** the reaction sequence is the same as discussed for the synthesis for C-M2-X material.



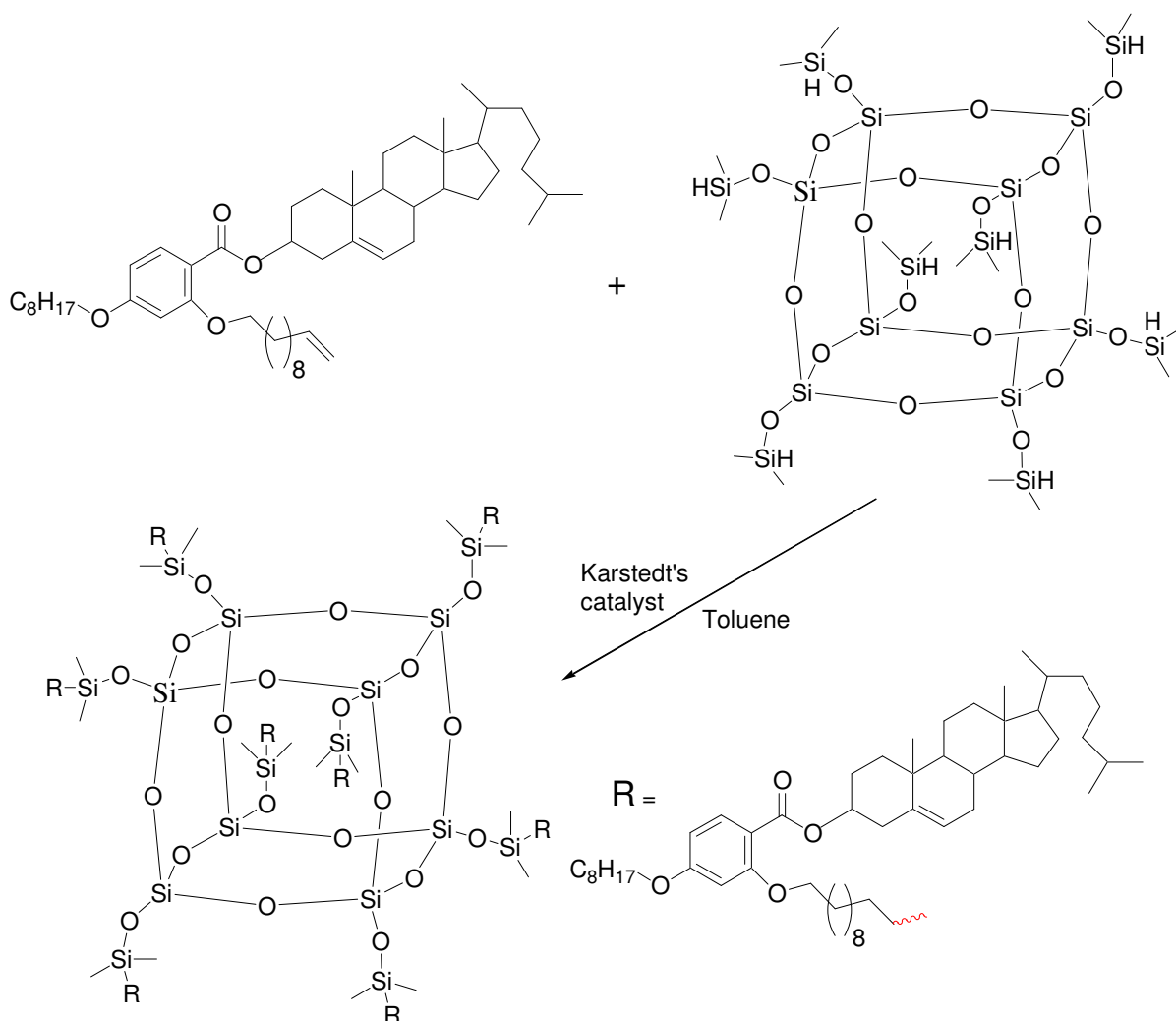
The formation of the product was monitored by the disappearance of the signal of the protons of the terminal double bonds at 5.78 ppm and at 4.92 ppm respectively, in the 1H -NMR spectra. Additionally, the signal of the S-H group ($H(CH_3)_2Si-O$) at 4.72 ppm disappeared with the progressing reaction.

Additional purity checks was performed using GPC as the preferred method. A single peak was observed except the reference peak (toluene as internal reference).

An overall reaction yield for the hydrosilylation of 45% was observed. This is equal to a reaction of around 5.6% per group.

Synthesis of the **M1** mesogens involves in the initial step the alkylation of dihydroxy methyl benzoate first in *para* position and then in *ortho* position in a Williamson reaction, followed by the removal of the methyl group protecting the carboxylic acid. This product was esterified with cholesterol giving the other cholesterol based mesogen M1 [108].

For **C-M1** material, the synthetic procedure is the same as discussed for the synthesis for C-M2-X and C-M2 materials.

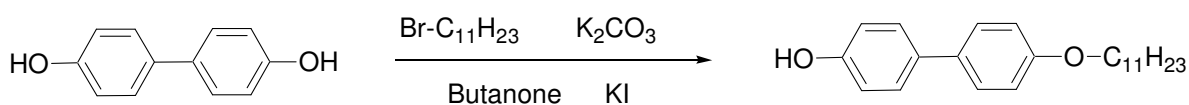


The difference in structure between the monomer (M1) and the C-M1 material can be observed in the $^1\text{H-NMR}$ and $^{13}\text{C-NMR}$ spectra of the two

compounds. Thus, the C-M1 material's ^{13}C -NMR spectra does not exhibit the signals for carbons (δ : 139.27 ppm, 114.03 ppm) for the double bond of M1 used in the reaction for the connection to the cubic silsesquioxane. Moreover, the specific proton from the siloxane group eliminated during reaction must be absent in the ^1H -NMR spectra, $\text{H}(\text{CH}_3)_2\text{Si-O-}$ at δ : 4.72 ppm.

Additionally, the presence of the C-M1 can be confirmed by the ^{29}Si -NMR spectrum. Generally, the ^{29}Si -NMR spectrum contains a broad background signal for the glass NMR tube at δ : -100.00 ± 10.00 . This drawback can be overcome by running a blank sample and subtracting it from normal spectrum. Running a ^{29}Si -NMR has a few shortcomings. The collection of the spectra is time consuming because in most cases a blank spectrum has to be run and extracted. Or, if the signal which is to be traced is in the same region as the blank spectrum (δ : -84 $-\text{Si-H}$), an alternative solution has to be tried. An option to avoid this would be the use of a teflon NMR tube or even a sapphire NMR tube, but this is extremely expensive and therefore not used in everyday research. In the current research those solutions couldn't be employed.

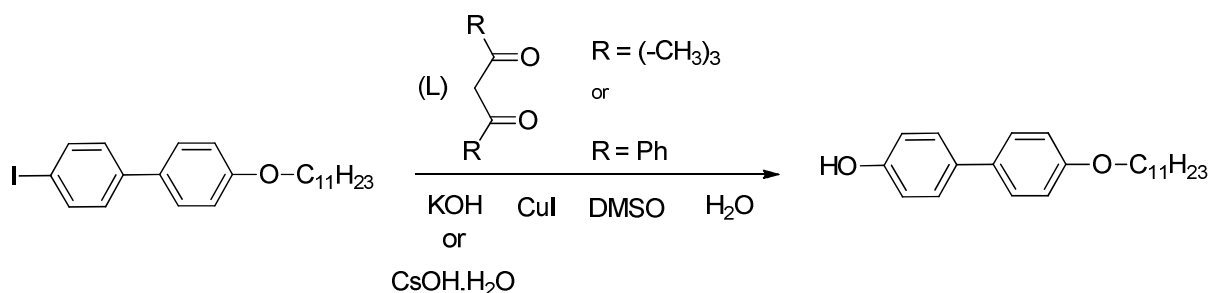
Important materials used as classic nematogens in mixtures with the already prepared materials, were **3RM** and **4RM**. One intermediate for preparing these materials is 4-hydroxy-4'-undecyloxybiphenyl.



Purification is performed by recrystallisation from THF with ethanol.

Nevertheless, it was very difficult to separate; the difference in polarity between the final product and the disubstituted biphenol is very small, so column chromatography is not the best procedure for purification. Thus, alternative synthetic routes for preparing of 4-hydroxy-4'-undecyloxybiphenyl had to be found.

Hence, one viable way was considered to be through an iodo-intermediate which was prepared rather easy and in high yield (more than 90%) and subsequently substituted to 4-hydroxy-4'-undecyloxybiphenyl.



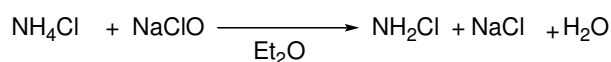
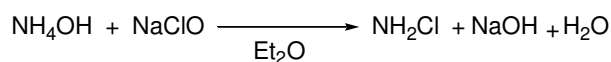
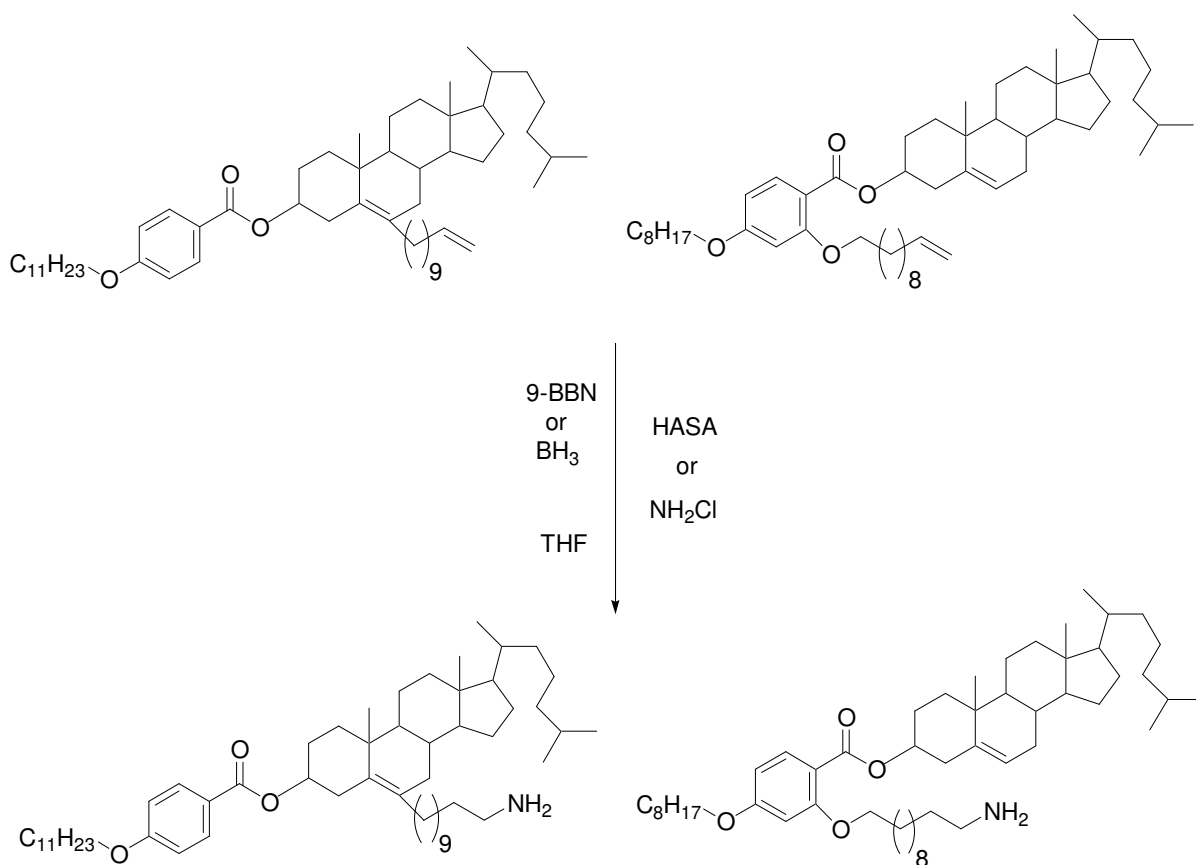
One of the literature procedures which was explored was the following: after three standard cycles of evacuation and back-filling with nitrogen a Schlenk tube equipped with a magnetic stirring bar was charged with 0.1 eq. CuI, 3 eq. of a nucleophile (KOH or CsOH·H₂O), 1 eq. aryl iodide and 0.5 eq. of a ligand (dibenzoylmethane or 2,2,6,6-tetramethyl-3,5-heptadione). The tube was evacuated and back-filled with nitrogen, followed by DMSO and water, in 1/1 ratio. The tube was sealed under positive pressure of nitrogen, stirred and heated to 130-150°C for 24 h. After cooling to room temperature, CH₂Cl₂ was added and HCl (37%). The mixture was stirred for 2 h. The reaction mixture was filtered through a plug of celite[®], the filter cake being further washed with dichloromethane. The filtrate was washed twice with water. Gathered aqueous phases were extracted with dichloromethane for five times. The organic layers were to be gathered, dried over Na₂SO₄, filtered and concentrated in vacuum to yield the crude product. Purification was to be carried out by column chromatography [109].

Although the procedure looks fairly simple and easy, the reaction temperature could not exceed 110°C, lower than the temperature needed for a successful reaction. The lack of proper heating equipment (heating mantle to fit the Schlenk tube) to ensure the control to higher temperatures made this procedure unattractive.

Another solution for the preparation of 4-hydroxy-4'-undecyloxybiphenyl, was the initially considered mono substituting Williamson

reaction. However, this option was discarded due to difficulty of purification of the resulting compound. After the exploration of a number of solvents for recrystallisation, a rather complicated sequence of recrystallisations made possible to separate the product from the starting material and the disubstituted by-product. Ethanol and THF were used as recrystallisation solvents.

In order to attach the M1 to iron/platinum nanoparticles, the mesogen must be first functionalised to ensure a ligand exchange with the capping agents, oleic acid and oleyl amine. Therefore, M1 must contain as functional group either carboxylic acid or amine group. Initially, the amine group terminated M1 was considered the target molecule. Thus, a synthetic path was to be found to convert a terminal double bond into an amine group. The synthesis of **M1- and M2-based amines** was very difficult and time consuming and implied a large number of test reactions. Basically, two hydroboration agents were used: borane (BH₃) and 9-borabicyclo (3.3.1) nonane (9-BBN); and two amine group bearing compounds such as chloramine (NH₂Cl) and hydroxylamine-*O*-sulfonic acid (HASA) were used. There were a number of initial concerns such as the cleavage of the ester bond, the amination of the cholesterol double bond or borane being a strong hydroboration agent.



Chloramine is unstable in water so it has to be synthesised *in situ*, at -10°C.

Synthesis of chloramine: there are two main procedures to prepare fresh chloramine [110].

1.

The reaction flask was maintained at -11°C. 20 ml of a 2.28 mol/l ammonium chloride solution were introduced into the reactor. A 2.07 mol/l sodium hypochlorite solution was prepared, the sodium hydroxide concentration of which is 0.12 mol/l. 20 ml of the prepared solution, cooled to -15°C, were subsequently

introduced drop wise into the reactor. The ratio of the ammonium chloride concentration to the sodium hypochlorite concentration ($[\text{NH}_4\text{Cl}]/[\text{NaOCl}]$) was equal to 1.1. The addition lasted 15 min and was carried out using a dropping funnel. The temperature of the reaction medium settled at -7°C with stirring. For cooling the ice baths, a mixture of salt and ice was used.

2.

The procedure was the same as above, with the difference that instead of NH_4Cl , aqueous ammonia was used.

Reaction of organoboranes with freshly prepared chloramine. In a flask, the alkene was dissolved in THF and the flask was flushed with nitrogen. A solution of borane (BH_3) or 9-BBN (9-Borabicyclo(3.3.1)nonane) in THF was injected in the flask (exothermic reaction). After 1 h, water was added to destroy residual hydride, followed by 3M aqueous sodium hydroxide. The amination was accomplished by adding the freshly prepared chloramine solution. After 1 h at r.t., the reaction was complete.

The work-up was carried out in two ways:

1. The reaction mixture was acidified with hydrochloric acid and the acidified solution extracted with ether. The solution was made strongly alkaline with sodium hydroxide and the amine extracted with ether.
2. The solvent is removed and the residue purified by column chromatography.

Reaction of organoboranes with hydroxylamine-O-sulfonic acid. The alkene was dissolved in THF. After flushing with nitrogen the hydroboration was accomplished by a solution of borane (BH_3) or 9-BBN (9-Borabicyclo (3.3.1) nonane) in THF. Solid hydroxylamine-O-sulfonic acid was added to the solution and the reaction mixture was heated under reflux for 3 h. The work-up was the same as mentioned above in the chloramine procedure [111].

From the total of 6 possible cases, only two of them were studied: in one of them, the chloramine was prepared from NH_4Cl and in the other case, HASA was used. In both cases, as hydroboration agent, 9-BBN was used. These two procedures were selected due to reagent availability. Only in the reaction when chlorine was used as the leaving group, a very low yield (less than 10%) of

amine was obtained. It had to be considered that chlorine might be a better leaving group than sulfonic acid, under these conditions.

A change to borane as hydroboration agent might improve the reaction. A concern was the attack of the borane on the cholesterol moiety's double bond, but no such by-products and intermediates were observed. Using HASA instead of chloramine, efforts were made to increase the low yield of the previous procedure. These efforts included the increase of the solubility of HASA. As HASA has a low solubility in THF at the reaction temperatures, the solvent was changed to diglyme. Even under these conditions, the reaction was not successful.

The difficulty of preparing amine terminated M1 in reproducible and viable yields, made necessary to rethink the synthetic route for attaching M1 to Fe/Pt NPs. Therefore, a different path to achieve this was to use a carboxylic acid as a terminal group. Further functionalisation of the M1 is needed and M1-COOH was synthesised through a single intermediate in good yields.

First, a one pot hydroboration-oxidation reaction was involved in preparing the alcohol M1 derivative (M1-OH) and then in a very selective oxidation the carboxylic acid, both with good yields.

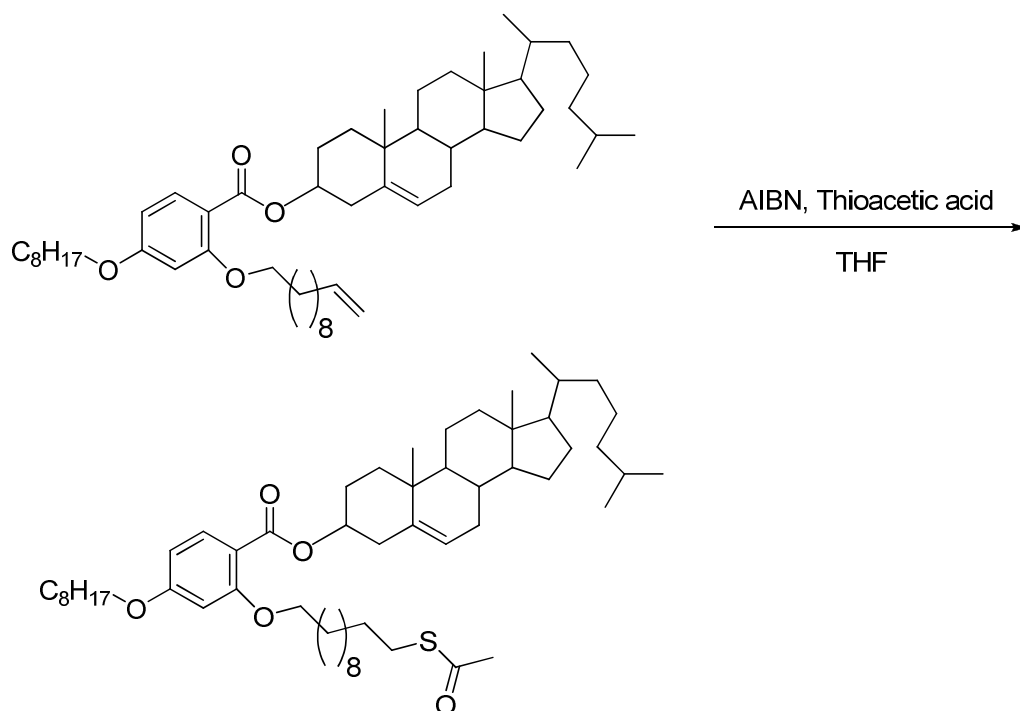
In order to attach the M1 to gold nanoparticles, M1 must undergo some transformations which make this coordination possible. Generally, gold has an increased affinity towards sulphur, hence the necessity for the M1 to be terminated in a sulphur containing group, such as thioacetate, thiol or even disulfide [112].

Recently, the preparation of self-assembly monolayers (SAMs) at gold surface using the thioacetate group was demonstrated [113]. The SAMs prepared using this method were not as ordered or densely packed as the SAMs prepared using free thiol compounds. Thioacetates need longer times to absorb on the gold surfaces than the thiols.

The M1 thiol, **M1-SH**, can be prepared in two steps: first, the M1 thioacetate intermediate (**M1-TA**) must be synthesised and then hydrolysed to M1-SH.

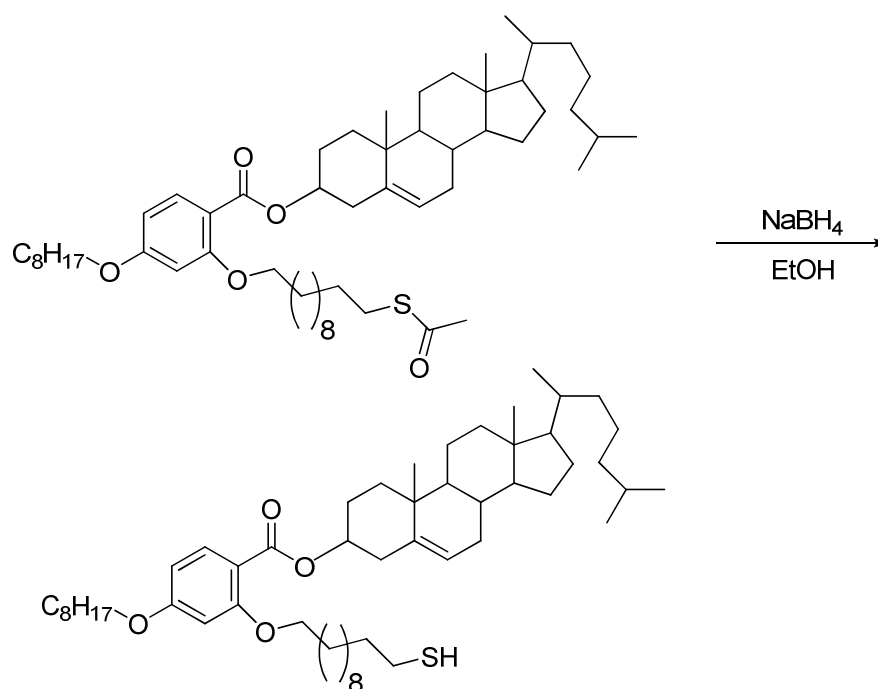
The intermediate thioacetate is synthesised using thioacetic acid and AIBN in a free radical mediated nucleophilic addition. This reaction proceeded

well and was optimised until a yield of 80% was achieved. The parameters which were improved were: the temperature and the ratios between the reagents.



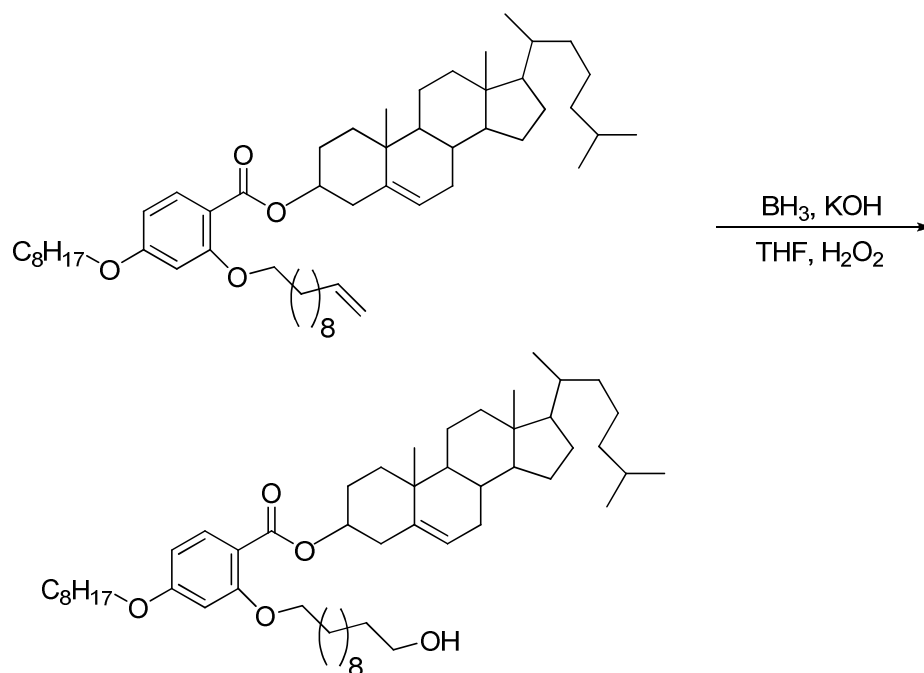
The next step, the transformation to the desired thiol, was challenging. Initially, sodium thiomethoxide (NaSMe) in methanol at room temperature [114] was used to hydrolyse the thio ester bond to thiol, but it was not successful and the starting material was recovered. There was also a one-pot reaction to convert the double bond into a thiol group using in first step as radical initiator, AIBN and UV light. The alkene was reacting in these conditions with triphenylsilanethiol. The next step involved the hydrolysis with trifluoroacetic acid (TFA) [108,115]. The hydrolysing agent was too strong and the cleavage of the ester bond was recorded. Other procedures used strong hydrolysing agents such as sodium hydroxide, potassium hydroxide, potassium carbonate; hence there were not suitable for the M1-TA [112]. A mild hydrolysing agent was considered to be sodium borohydride. At room temperature and in THF and water [116], no change to the M1-TA could be seen.

A successful procedure for the M1-TA to undergo a hydrolysis, with large excess of NaBH₄ (10 eq.) in ethanol to give the thiol (M1-SH) was found [117].

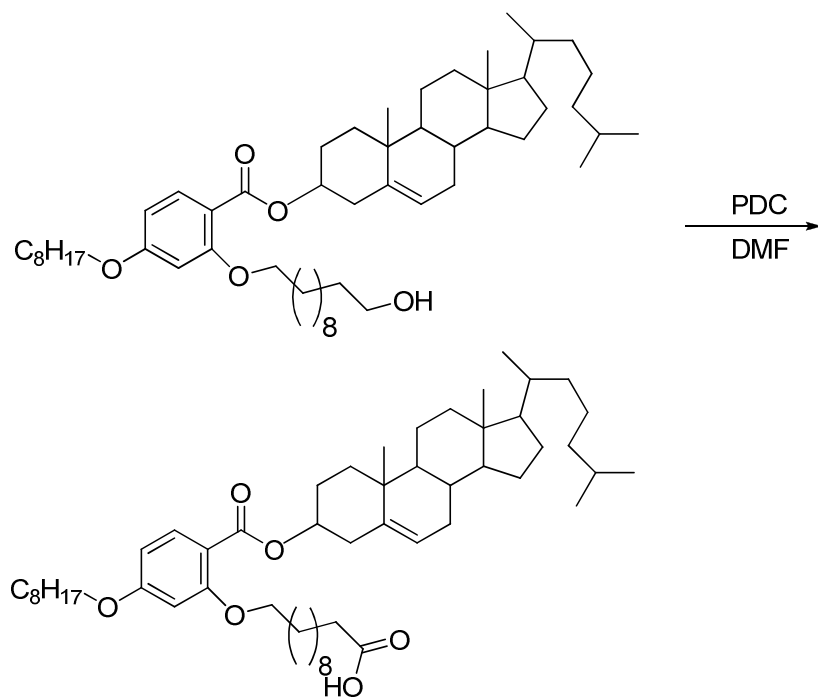


As the M1-TA has low solubility, the reaction temperature was kept high, close to the boiling temperature of the solvent. Controlling the reaction parameters ensured the reaction has a satisfying yield, up to 65%. The cleavage of the ester bond in the product was judged as a potential risk, but no sign of by-products could be observed. The resulting free M1 thiol can be used immediately or alternatively can be stored for long periods of time, at room temperature. M1-SH is a viscous white liquid and a very stable compound at room temperature.

For the synthesis of **M1-OH** intermediate to the final carboxylic acid terminated M1 (M1-COOH), a one pot hydroboration-oxidation reaction was used and this proceeded with an acceptable yield (40%).



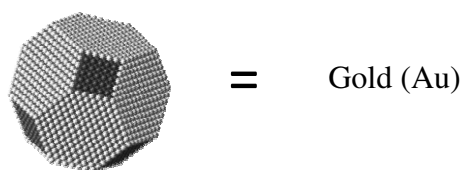
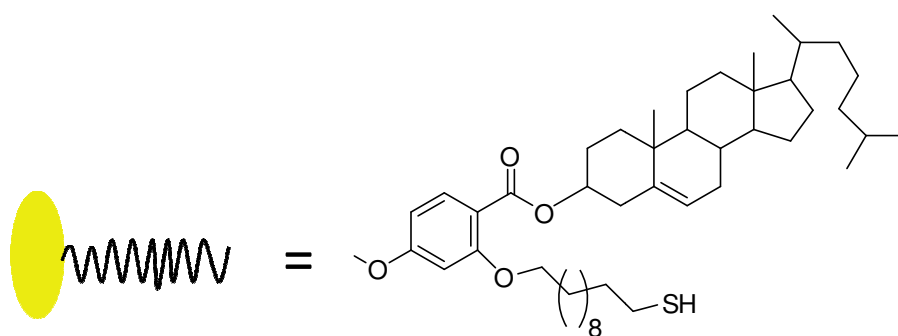
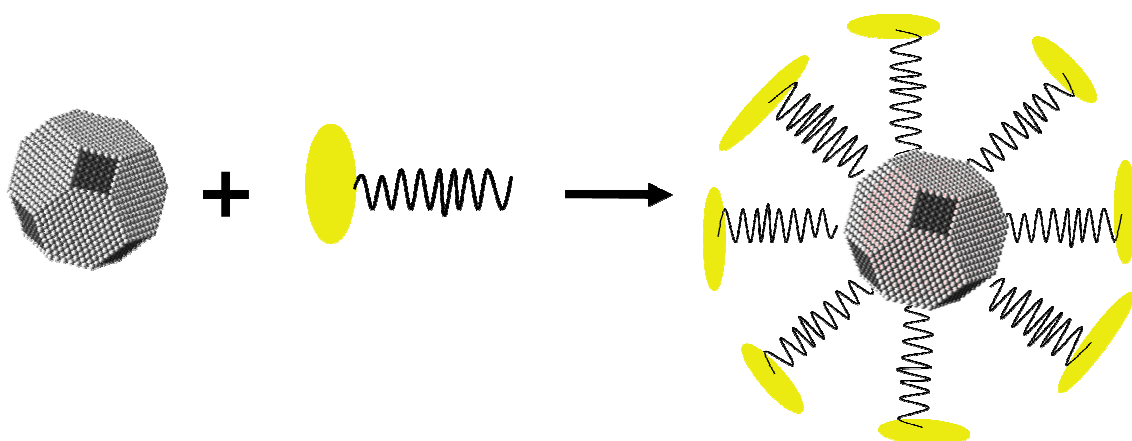
The next step, was the oxidation of M1-OH to **M1-COOH** through a very selective oxidation using pyridinium dichromate ($(\text{C}_5\text{H}_5\text{NH}^+)_2\text{Cr}_2\text{O}_7^-$) (PDC) in DMF [118].



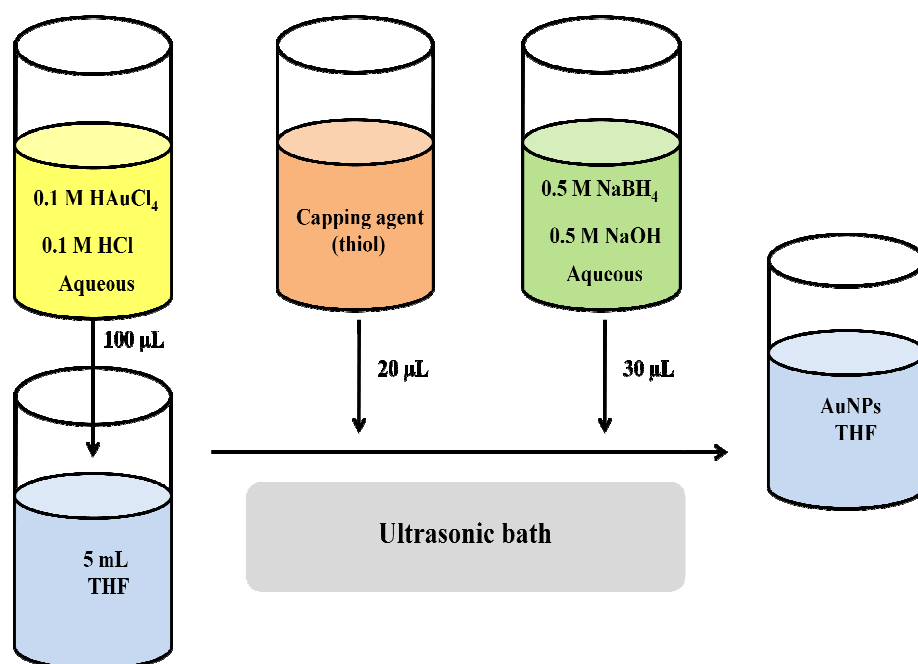
It was observed that PDC in excess up to 4 eq. oxidised just to the M1 aldehyde. Increasing the amount of PDC to 10 eq. resulted in the M1-COOH material being prepared in good yield (70%). Overall, this synthesis is relatively easy to perform with the shortcoming that it takes up to one week for the reaction to reach the maximum conversion.

As the M1 is functionalised to a thiol in order to be coordinated to **Au-NPs**, the next step is to prepare the Au-NPs. There are two principle ways to prepare the M1 capped gold nanoparticles: the most widely used method is by preparing Au-NPs covered with a capping agent (hexane thiol) and then a ligand exchange is performed [101]. This method so-called Brust-Schiffrin, since its discovery in 1994, was extensively used for preparing gold nanoparticles capped with a large number of ligands. The method is a variation of the Turkevich method for preparing gold nanoparticles, in the early 50's [119]. These NPs were also used in doping liquid crystal mixtures. NPs obtained using this method are monodispersed, the size can be controlled and they are stable in the appropriate solvent. In order to prepare the NPs with the desired organic moiety attached implies an additional step which can alter the narrow size distribution, have both the initial ligand and the organic molecule attached which can modify drastically the NPs' properties and not the least it adds additional steps into work up these NPs lowering the yield and quality of NPs.

In order to avoid all the shortcomings of the Brust-Schiffrin method, a second method was developed. The method was originated at the University of Hull and came out of C.-H. Yu's work in materials chemistry. This completely new route for synthesising the gold NPs consists in capping the Au-NPs directly with M1-SH. The procedure was preferred because it also eliminates one step of purification which for NPs is the most time consuming and challenging of all.



This new method produces NPs with a quite narrow size distribution. There are different procedures to synthesize Au-NPs with different sizes. They are relatively easy and the reaction time is quite reduced compared to the procedures previously used. A number of explorative reactions were performed in order to identify the ratio between the Au precursor and M1-SH for the desired ligand coverage and for the reaction to be reproducible. For the best results, the chosen Au to M1-SH ratio was 2 to 1.



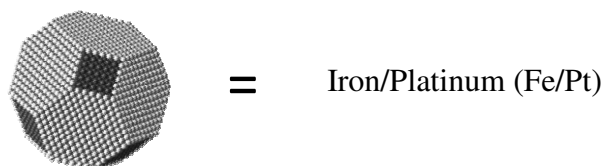
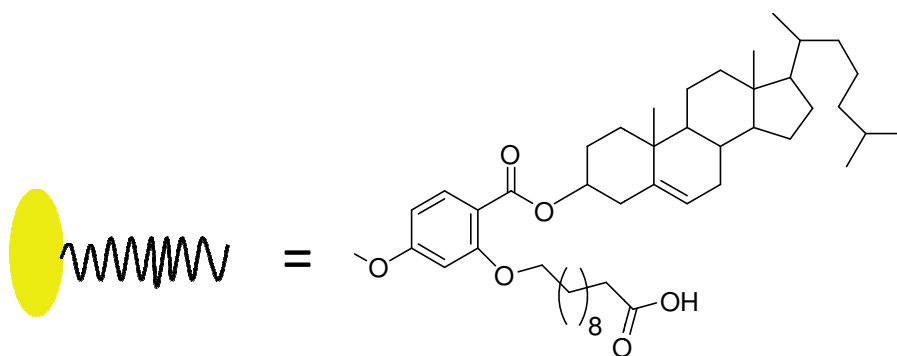
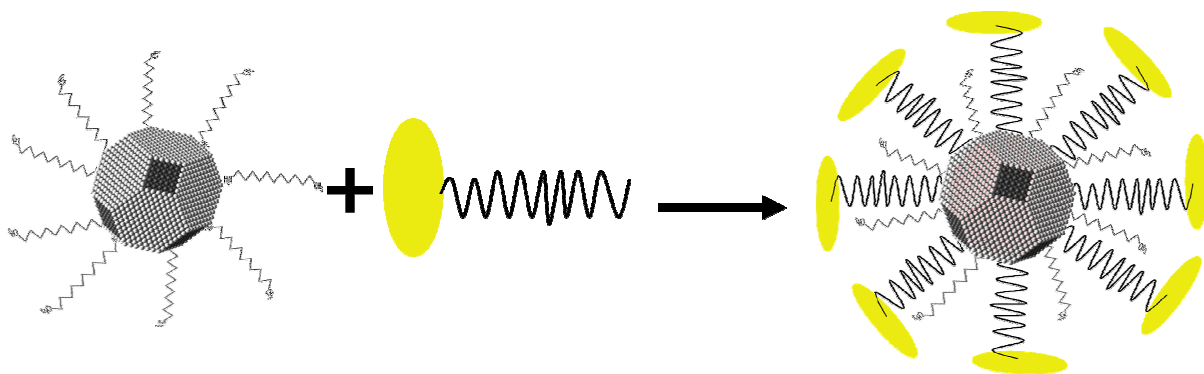
After the preparation of the M1-Au NPs which is completed in a matter of minutes, the most difficult part is to purify the LC NPs. A variation of size exclusion chromatography was used. A tall glass column was packed with polystyrene beads (BioRad, SX series) with cross-linkage of various percentages. Depending on the type of bio beads and the molecular weight of NPs that needed separation, the right percentage of cross-linkage was used. The mobile phase used for the purification of M1-Au NPs was dichloromethane. The NPs layer was reintroduced in the column for separation, even for a third time if necessary. A number of purification/washing cycles (2 or 3) using the centrifuge were involved. The solvent mixture for washing the NPs was composed of acetone and ethanol. After all these tedious procedures, column and centrifuge, pure M1-Au NPs with narrow size distribution were obtained. Full characterisation was performed, including purity checks by GPC. This new procedure is faster and reliable and gives pure NPs with readily controlled sizes ranging from 1 nm to 10 nm and bigger.

For the preparation of M1 ligand covered **Fe/Pt NPs** a carboxylic acid or an amine functionalized mesogen was needed. As discussed above, a procedure to prepared M1-COOH was found, taking into account that there is an easy to cleave ester bond in the target compound. The synthesis is straightforward and in good yields.

This new category of NPs, Fe/Pt, was prepared using a so-called polyol process, because the reducing agent is a polyol or a diol. In this case was 1,2-hexadecanediol. The Pt precursor is platinum acetylacetonate, the Fe precursor is iron pentacarbonyl. Adding the capping agents (oleic acid, oleyl amine), they are all mixed in a high boiling point solvent such as octyl ether, around 300°C and reacted for 1 h until the solution turned black. Then the NPs are washed with ethanol and precipitated using a centrifuge.

The mesogen is added to a solution of Fe/Pt NPs in DCM, and then heated under reflux for a few days. If the mesogen can withstand higher temperatures, the mixture can be heated under reflux in toluene for several hours for high quality nanoparticles. In order to purify the coated Fe/Pt NPs a similar procedure like in the case of Au NPs was involved. The solution was concentrated and passed through bio beads SX-1 (Bio-Rad®), twice, using as the mobile phase THF. Afterwards, the residue was washed twice under centrifugation with acetone/ethanol mixtures. The residue was concentrated and prepared for further characterisation.

The synthetic procedure and work-up are similar in all cases when the coating is made with materials functionalised either with acid or amine group.



The novelty for both NPs systems, gold and iron/platinum covered with M1, is that the mesogen is chemically bonded to the metallic NP. Until recent, most of the research on LC NPs was based on simply mixing the NPs with the mesogens, but not chemically bonding them to NPs.

NOTE: - the frequency of radio waves used for ^1H NMR analysis was 400 MHz
 - the frequency of radio waves used for ^{13}C NMR analysis was 101 MHz

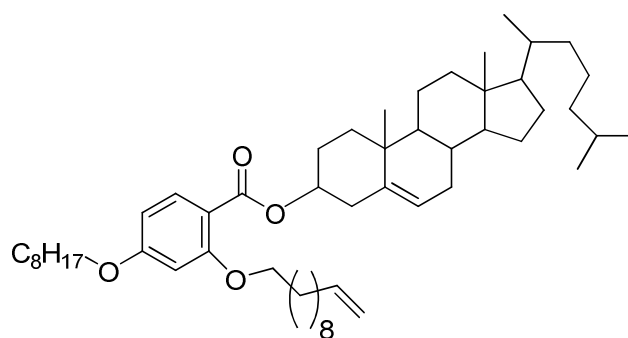
CHAPTER V

PROPERTIES. DISCUSSION OF PROPERTIES

A limited number of examples of monomeric liquid crystal polyhedral silsesquioxane materials have been reported and in all of them the cholesteric group is attached end-on (or “terminally”) [1-4]. Two cholesterol groups containing mesogens were designed and synthesised.

Expected to promote exclusively chiral nematic phase behaviour in these mesogens, as well as low melting points and low transition temperatures, the cholesterol groups were designed to be attached “laterally” (side-on) to the silsesquioxane cores by hydrosilylation.

V.1. Material M1



Liquid crystal and thermal properties

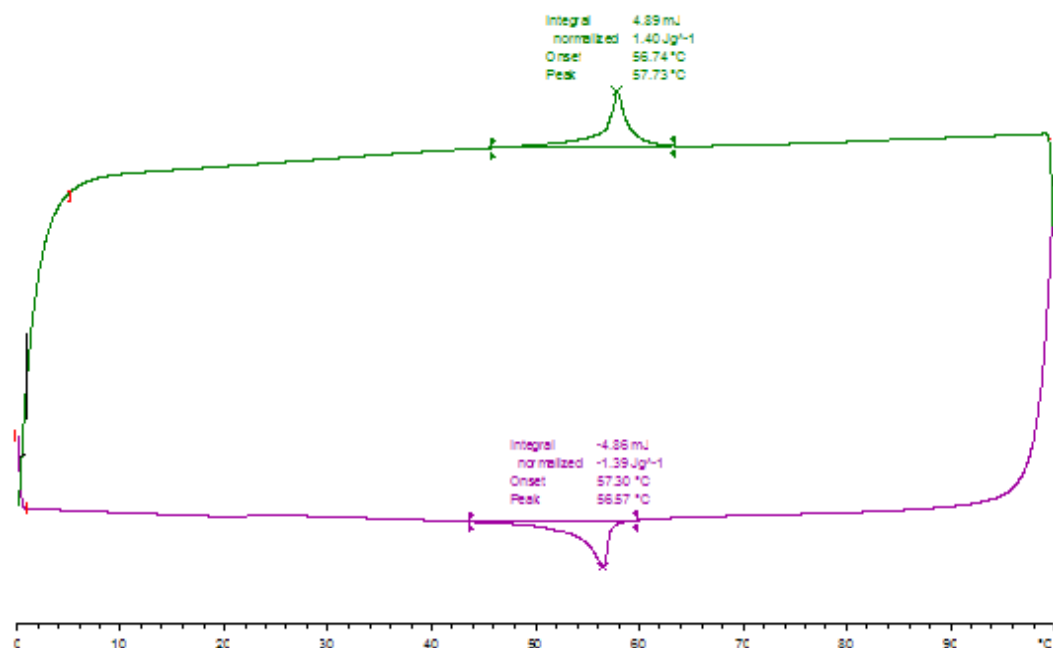


Fig. V.1. DSC trace for material M1

In Fig. V.1., the DSC trace for the material M1 is presented. A full cycle of heating and cooling which exhibits a transition from chiral nematic to isotropic liquid, with the onset temperature of 56°C. As the initial DSC instrument had a limitation in terms of the temperature range, a different DSC instrument was used to find the transition temperature to crystal, or in our case to glass. The glass transition temperature was found to be -25°C.

M 1	Tg -25 N* 57 Iso
------------	-------------------------

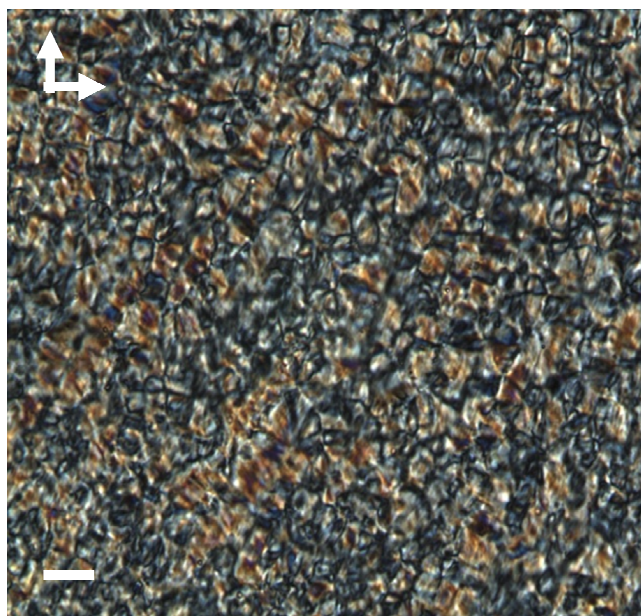


Fig. V.2. OPM, pseudo fan shape texture at 56°C.

A poorly developed fan-shaped like texture typical for cholesteric material is shown in Fig. V.2.

Optical properties

Table V.1. Optical properties (optical rotation)

Material	a	[a] degree (g ⁻¹ ml dm ⁻¹)
M 1	- 0.052	- 4.777

The specific rotation was calculated using the following equation:

$$[a] = a / c \times l$$

[a] = specific rotation;

a = optical rotation;

c = concentration (g/ml);

l = length of the cell (dm).

For optical rotation measurements an automatic polarimeter was used with the cell length of 0.25 dm.

Based on the optical rotation angle measurements performed on the material M1, a levorotatory behaviour can be deduced. The chiral M1 rotates the plane of polarised light towards the left, as the observer looks to the light source.

UV spectroscopy

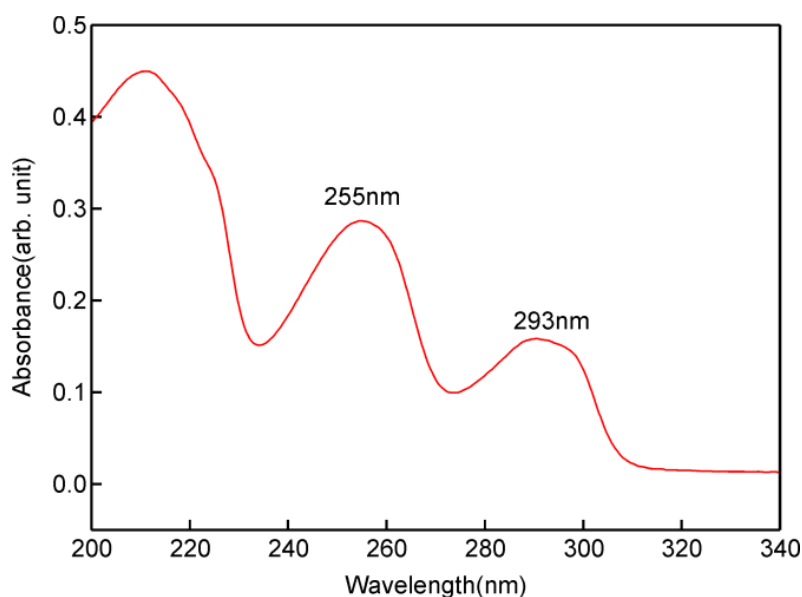


Fig. V.3. UV spectra of M1 mesogen

Fig. V.3. shows a UV spectrum for the material M1 and exhibits 2 absorption bands of medium intensity above 250 nm with no major absorption at shorter wavelength (200 – 250 nm). The 255 nm absorption band is for the *para* substituted benzenic ring. The extra absorption band at 293 nm is for the *meta* substituent at the benzenic core.

CD spectroscopy

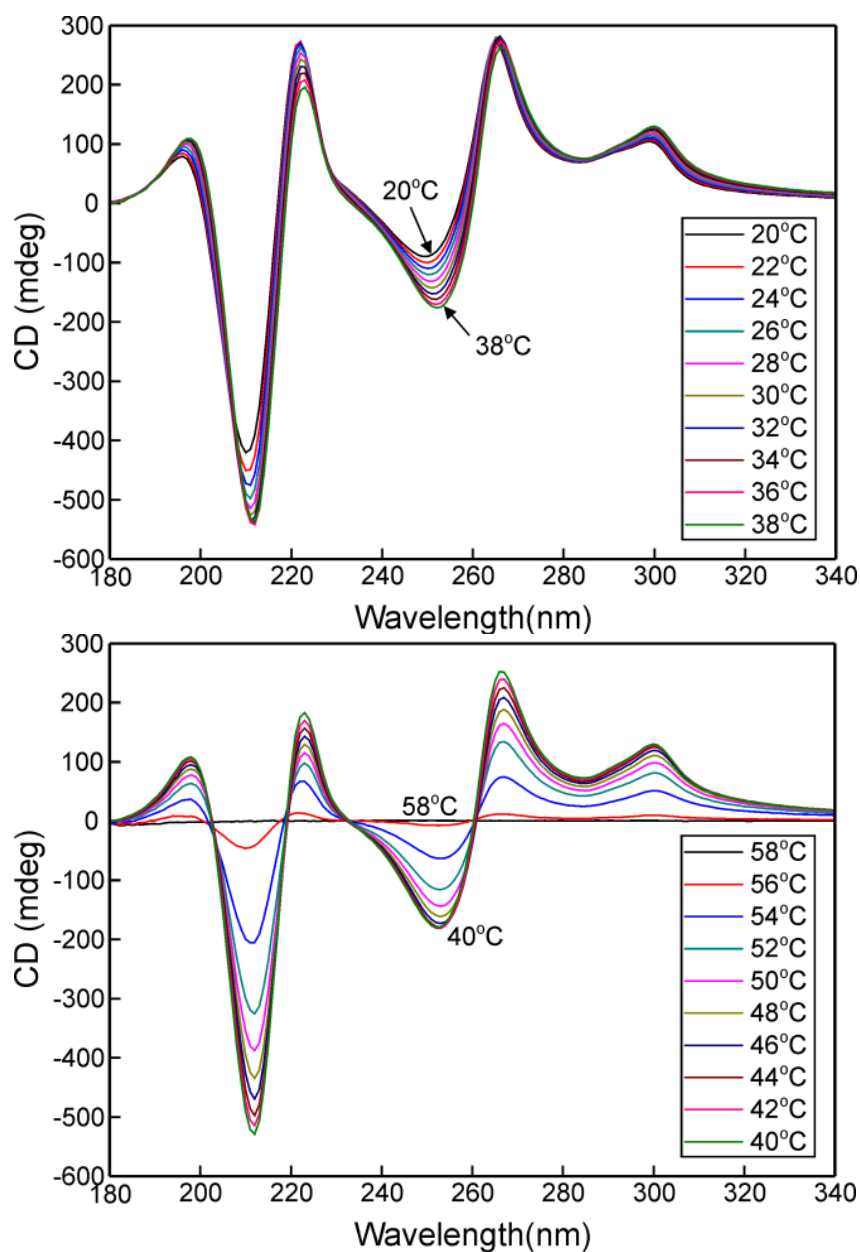


Fig. V.4. CD spectra of M1 mesogen

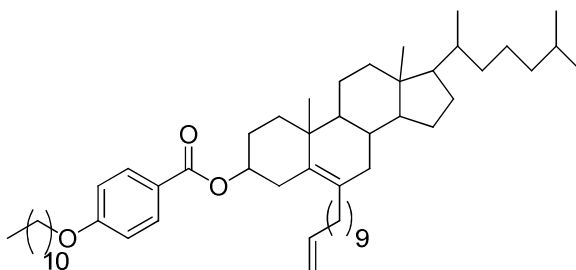
Circular dichroism monitors the subtle alterations in structure such as the conversion of M1 from crystal to liquid crystal and subsequently to isotropic liquid. It measures the temperature dependence of the structure of M1 going through all the enumerated stages.

The samples were analysed in the form of films.

Cholesterol is a natural product with eight chiral centres. For the end-on attachments to the cholesteryl unit through the C3 carbon, only the nature of the substituent gives the handedness of the cholesteric phase. Some examples of substituents and the corresponding handedness are the following: for a right-handed mesophases the substituents must be -H, -OH, -F, -Cl, -Br and for a left-handed phase bulkier substituents are needed such as -I, acetate, nonanoate and others [120]. For expressing the changes in handedness, the cholesteryl chiral centres are not involved, as it has the same absolute configuration regardless the substituent.

In the wavelength region where light is absorbed (255 nm) a negative Cotton effect is observed. The signal intensity decreases as the temperature rises and finally disappears when the material M1 suffers an isotropic transition. As the temperature is increased, the Cotton effect is less visible as the structure is less chiral. A second and positive Cotton effect for the second absorption band at 293 nm is observed. The CD spectrum for M1 presents a number of other features, positive and negative. It is assumed to be for the cholesteryl chiral centres.

V.2. Material M2



Liquid crystal properties and thermal properties

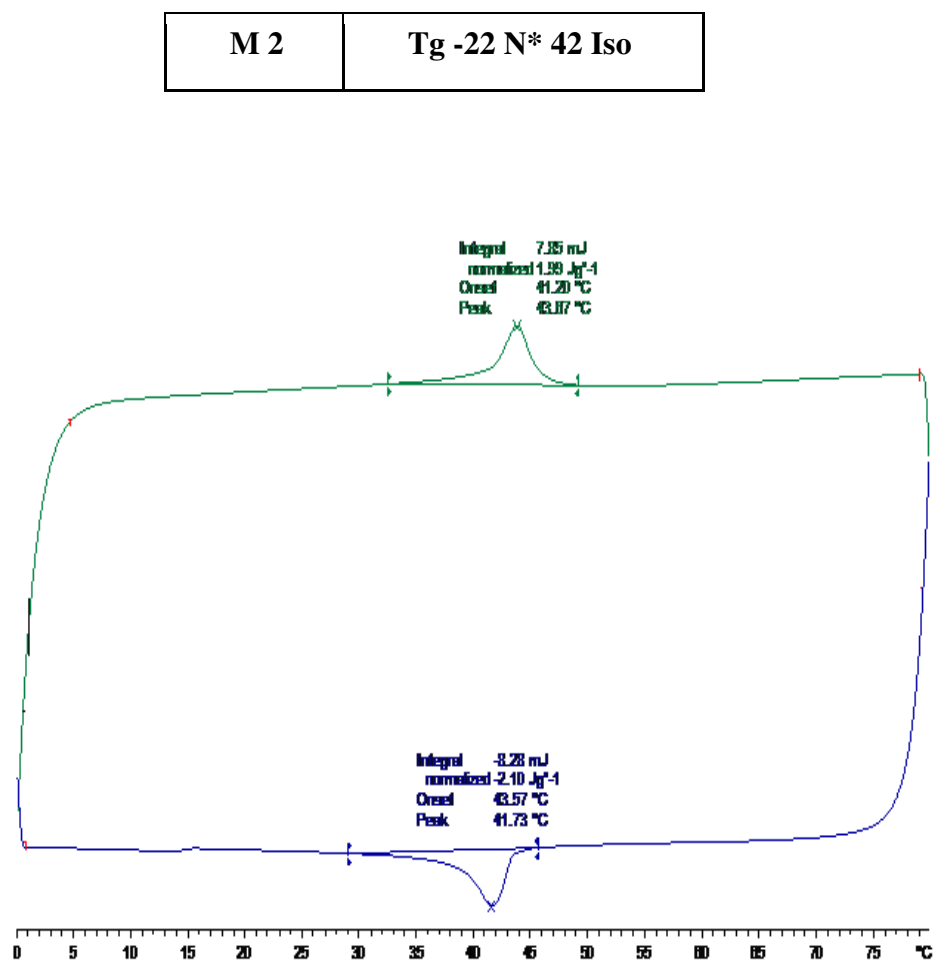


Fig. V.5. DSC trace for material M2

In Fig. V.5., the DSC trace for the material M2 is presented. A full cycle of heating and cooling which exhibits a transition from the chiral nematic phase to isotropic liquid, with the onset temperature of 42°C is shown. As the initial DSC instrument had a limitation in terms of the temperature range, a different DSC instrument was used to find the transition temperature to crystal, or in our case to glass. The glass transition temperature was found to be -22°C.

Optical properties

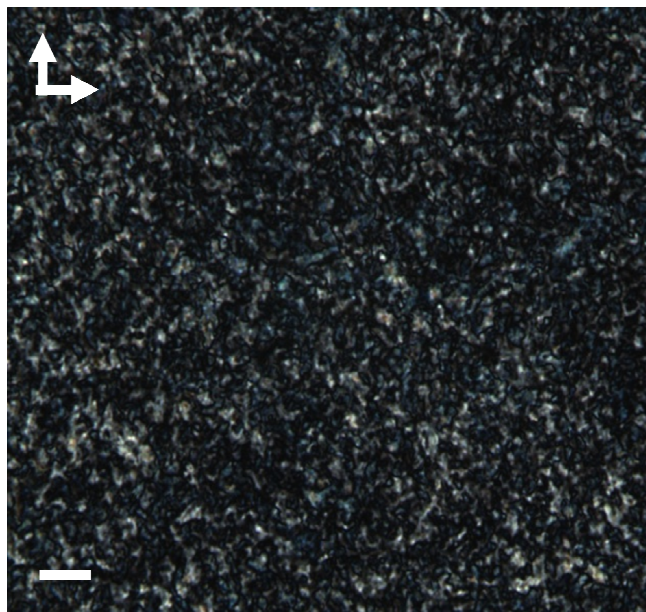


Fig. V.6. OPM, pseudo fan shape texture at 42°C, for mesogen M2

A poorly developed fan-shaped like texture typical for cholesteric material is shown in Fig. V.6.

Table V.2. Optical properties (optical rotation)

Material	a	[a] degree (g ⁻¹ ml dm ⁻¹)
M 2	+ 0.060	+ 9.160

The specific rotation was calculated using the following equation:

$$[a] = a / c \times l$$

[a] = specific rotation;

a = optical rotation;

c = concentration (g/ml);

l = length of the cell (dm).

For optical rotation measurements an automatic polarimeter was used with the cell length of 0.25 dm.

From the optical rotation angle measurements performed on the material M2, a dextrorotatory behaviour can be observed. The chiral M2 rotates the plane of polarised light towards the right, as the observer looks to the light source.

UV spectroscopy

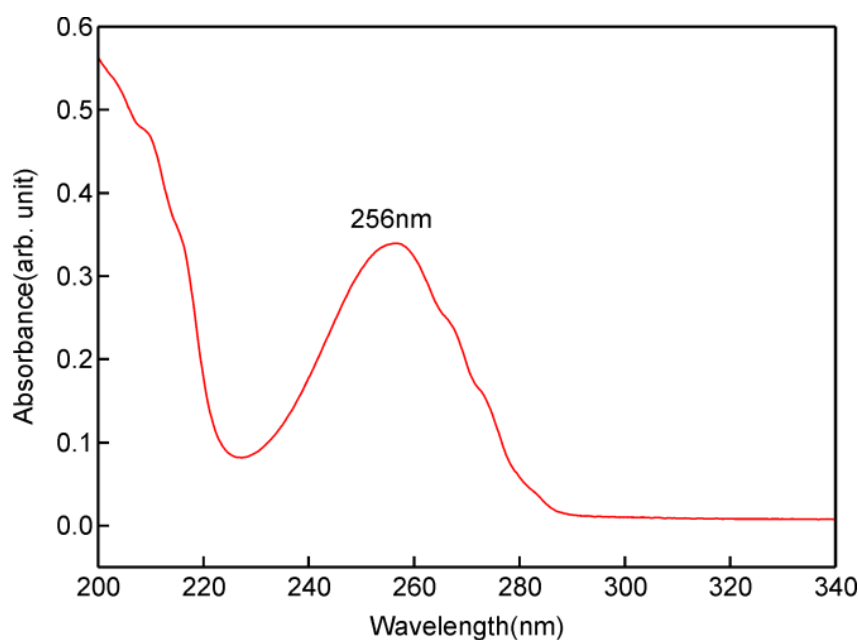


Fig. V.7. UV spectra of M2 mesogen

Fig. V.7. shows a UV spectrum for the material M2 and exhibits one absorption band of medium intensity with a maximum at 256 nm, with no major absorption at shorter wavelengths (200 – 250 nm). The 256 nm absorption band is for the *para* substituted benzenic ring. No other extra absorption band could be observed.

CD spectroscopy

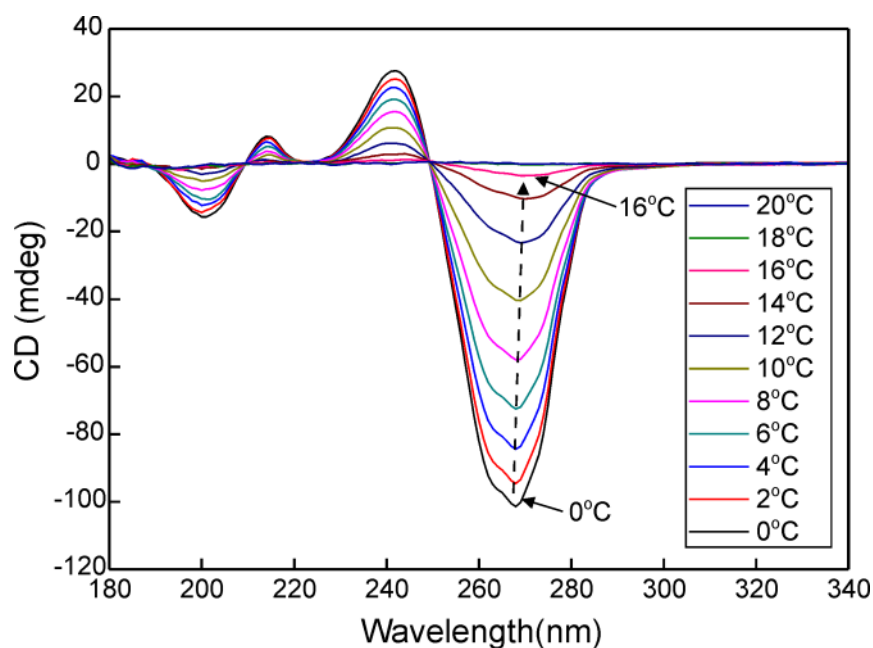


Fig. V.8. CD spectra of M2 mesogen

Circular dichroism monitors the subtle alterations in structure such as the conversion of M2 from crystal to liquid crystal and subsequently to isotropic liquid. It measures the temperature dependence of the structure of M2 going through all the enumerated stages.

The samples were analysed in the form of films.

Cholesterol is a natural product with eight chiral centres. For the end-on attachments to the cholesteryl unit through the C3 carbon, only the nature of the substituent gives the handedness of the cholesteric phase. Some examples of substituents and the corresponding handedness are the following: for a right-handed mesophases the substituents must be $-H$, $-OH$, $-F$, $-Cl$, $-Br$ and for a left-handed phase bulkier substituents are needed such as $-I$, acetate, nonanoate and others [120]. For expressing the changes in handedness, the cholesteryl chiral centres are not involved, as it has the same absolute configuration regardless the substituent.

In the wavelength region where light is absorbed (256 nm) a positive Cotton effect is observed. The signal intensity decreases as the temperature rises

and it starts to be insignificant when the material M2 reaches the temperature of around 20°C. As the temperature is increased, the Cotton effect is less visible as the structure is less chiral. The CD spectrum for M2 presents a number of other features, positive and negative, similar to the CD spectrum for M1 material. It is assumed to be for the cholesteryl chiral centres.

Conclusions to M1 and M2 materials

The combination of silsesquioxane cores, which are known to promote microphase separation in liquid crystal materials, and cholesterol groups containing mesogens, has not yet been explored to any great extent.

In order to investigate this issue, two cholesterol group containing mesogens were designed and synthesized. To promote exclusively chiral nematic phase behaviour in these mesogens, as well as low melting points and low transition temperatures, the cholesterol groups were designed to be attached “laterally” to the silsesquioxane cores by hydrosilylation, resulting in materials with liquid crystal phase at room temperature.

As to the thermal and LC properties of these mesogenic groups, they exhibit LC phases at room temperature, with low melting points. Now, if the transition temperatures are to be compared, it can be seen a difference of 15°C of the clearing point, just by changing the position of the connecting alkyl chain. For both mesogens the DSC results were fully reproducible.

The OPM textures for both materials are poorly developed fan-shaped like texture for cholesterics.

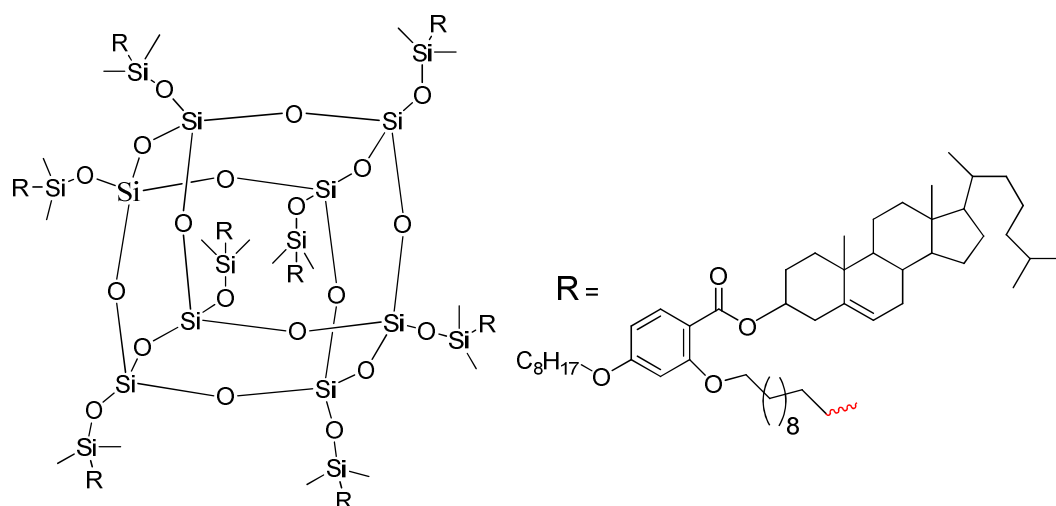
In terms of chiroptical properties of the two mesogens, the material M1 has a CD signal intensity of a factor of 5 larger than the material M2. The two materials rotate the plane of polarised light in opposite directions, material M1 being levorotatory and respectively, M2 is dextrorotatory. As optical rotation depends on the concentration of the sample, the specific rotation is taken into account when comparing the two compounds. Just by changing the position of the alkyl chain from the benzenic ring to the cholesteryl moiety, the plane of polarised light is rotated in opposite directions, towards left and subsequently, towards right.

As the temperature is increased the intensity of the CD signal decreases, the superstructures become less chiral. Heating the samples towards the clearing point the Cotton effect disappears and also the other CD spectra features.

V.3. Material C-M1

A small number of monomeric liquid crystal polyhedral silsesquioxane materials containing the cholesterol group have been reported and in all of them the mesogenic group is attached terminally (or “end-on”) [31,103]. Two cholesterol groups containing mesogens were designed and synthesised.

It was planned that the materials should exhibit exclusively chiral nematic liquid crystalline phase behaviour, as well as low melting points and low transition temperatures. Thus the compounds were designed to be attached laterally (“side-on”) to the silsesquioxane cores by a hydrosilylation reaction.



Liquid crystal properties and thermal properties

C-M1	Tg 22 N* 36 Iso
------	-----------------

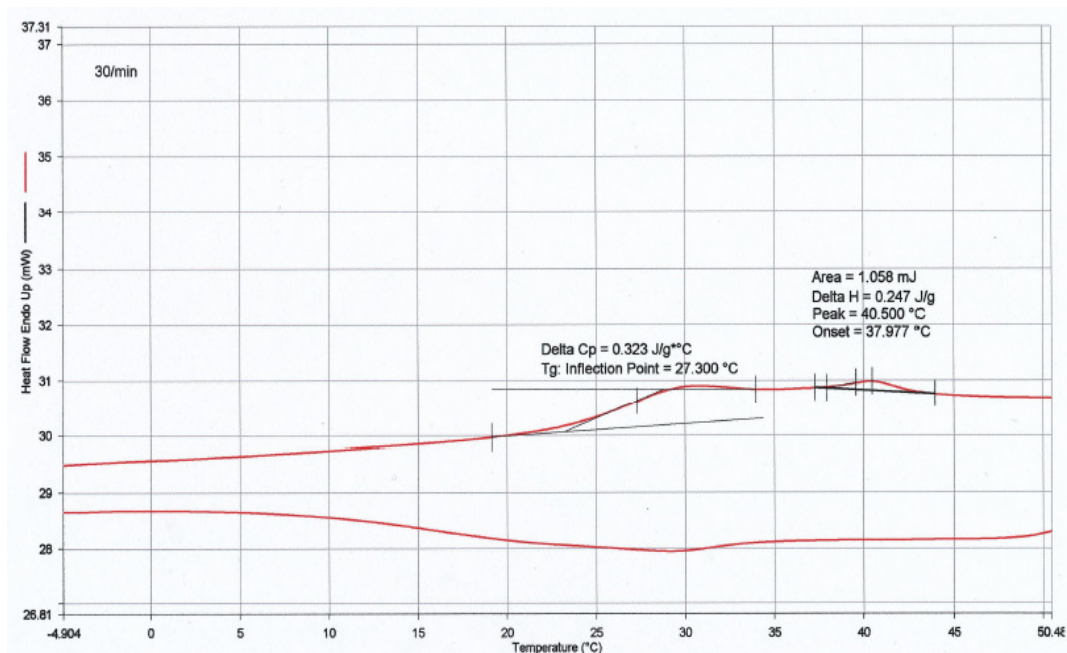


Fig. V.9. DSC trace for material C-M1

Fig. V.9. shows a complete cycle of a DSC measurement and on the heating run, two transitions, a glass transition and a phase transition are detectable. The transition temperature for this material is lower (36°C) than the one for the mesogen M1, as expected. It can also be seen that a glass transition close to room temperature, at 22°C, occurs.

Optical properties

Table V.3. Optical properties (optical rotation)

Material	a	[a] degree (g ⁻¹ ml dm ⁻¹)
C-M1	- 0.014	- 1.266

The specific rotation was calculated using the following equation:

$$[\alpha] = a / c \times l$$

[a] = specific rotation;

a = optical rotation;

c = concentration (g/ml);

l = length of the cell (dm).

For optical rotation measurements an automatic polarimeter was used with the cell length of 0.25 dm.

From the optical rotation angle measurements performed on the material C-M1, a levorotatory behaviour can be observed. The chiral C-M1 rotates the plane of polarised light towards the left, as the observer looks towards the light source.

X-Ray diffraction

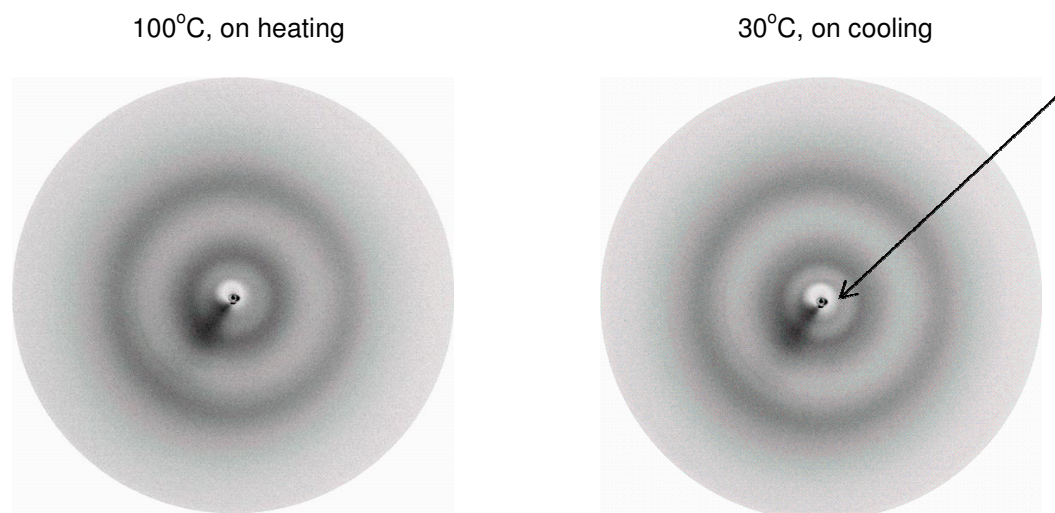
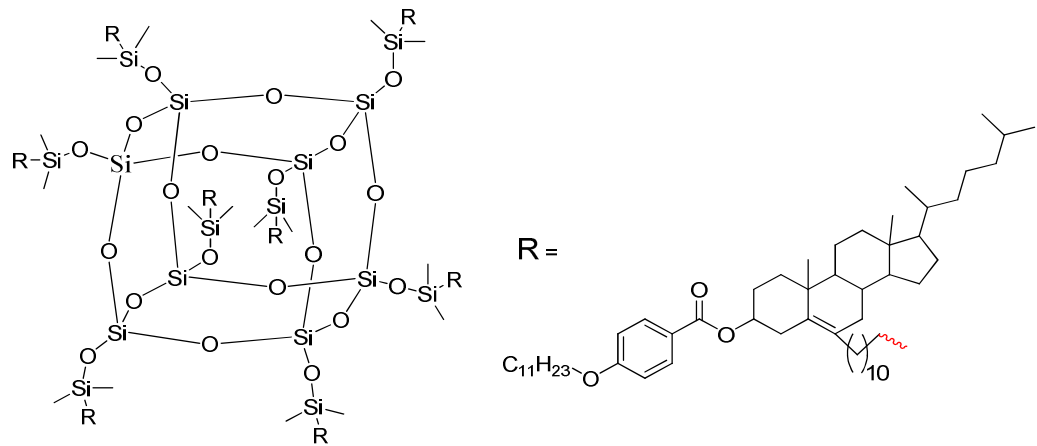


Fig. V.10. X-ray diffractograms for material C-M1

In the X-ray diffractograms of the samples of C-M1, an extra signal in the small angle region was observed.

V.4. Material C-M2



Liquid crystal properties and thermal properties

C-M2	T _g 10 N* 22 Iso
------	-----------------------------

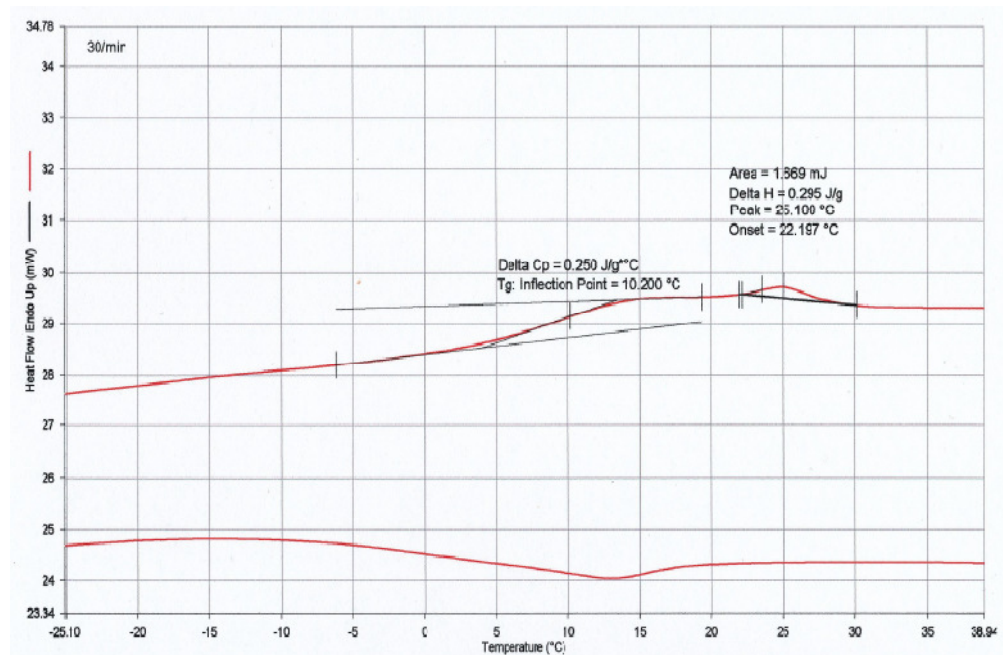


Fig. V.11. DSC trace for material C-M2

Fig. V.11. shows a complete cycle of a DSC measurement and on the heating run, two transitions, a glass transition and a phase transition are detectable. The transition temperatures for these materials are lower (22°C) than the ones for the mesogens, as expected. We can see also glass transition close to room temperature, at 10°C.

Optical properties

Table V.4. Optical properties (optical rotation)

Material	a	[a] degree (g⁻¹ ml dm⁻¹)
C-M2	+ 0.051	+ 7.208

The specific rotation was calculated using the following equation:

$$[\alpha] = a / c \times l$$

[a] = specific rotation;

a = optical rotation;

c = concentration (g/ml);

l = length of the cell (dm).

For optical rotation measurements an automatic polarimeter was used with the cell length of 0.25 dm.

From the optical rotation angle measurements performed on the material C-M2, a dextrorotatory behaviour can be observed. The chiral C-M2 rotates the plane of polarised light towards the right, as the observer looks to the light source.

Conclusions for C-M1 and C-M2 materials

The combination of silsesquioxane cores, which are known to promote microphase separation in liquid crystal materials, and cholesterol groups containing mesogens, has not yet been explored to any great extent.

In order to investigate this issue, two cholesterol group containing mesogens were designed and synthesized and attached “laterally” to the silsesquioxane cores by hydrosilylation, resulting in materials with liquid crystal phase at room temperature.

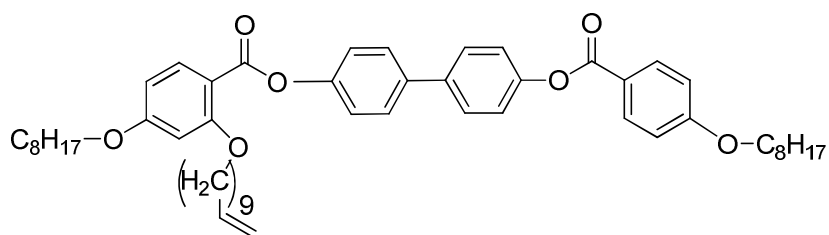
As to the thermal and LC properties of these materials, they exhibit LC phases at room temperature, with low melting points. Now, if the transition temperatures are to be compared, it can be seen a difference of 13°C of the clearing point, using one monomer of the other. The liquid crystal phase interval is quite narrow, around 12 degrees. For both materials the DSC results were reproducible.

In terms of chiroptical properties the two materials rotate the plane of polarised light in opposite directions, material C-M1 being levorotatory and respectively, C-M2 is dextrorotatory, as the correspondent monomers.

When the materials were checked under OPM, to identify the eventual LC phases, both samples were optically isotropic, no birefringence could be seen. This was contrary to expectations where helical superstructure or a simple cholesteric phase was expected, but OPM, DSC and XRD proved the existence of a possibly highly ordered phase or a short pitch cholesteric phase.

Considering that the DSC measurements show clearly a transition, other methods were involved to explain the behaviour of these structures: contact experiments and phase diagrams of binary mixtures between the mesogens and the final compounds and known nematogens, but also miscibility experiments between the mesogen and a known nematogen.

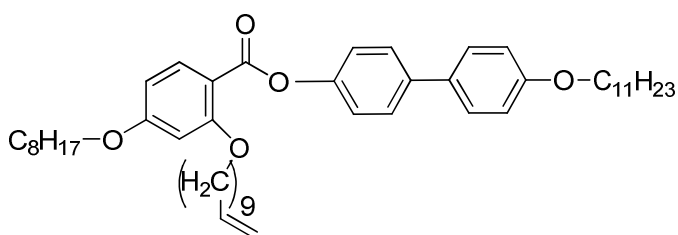
V.5. Material 4RM



4RM	Cr 80 N 140 Iso
-----	-----------------

As a nematic compound the molecule 4RM, shown above, was chosen. It was selected as it has a lateral side-chain of similar length; moreover, the length of the mesogenic group is similar to that of the cholesteric mesogen M1.

V.6. Material 3RM



3RM	Cr 26 N 62 Iso
-----	----------------

As a nematic compound for mixtures with the C-M1, 3RM was chosen. It was selected as it is a nematogen with the transition temperature close to those of the CM1 and also this is the reason why the 4RM was not used.

V.7. Binary mixtures

Further exploration of these structures was needed, phase diagrams of different mixtures between these mesogens and the cubic structures and known nematic structures were calculated.

Contact experiments: C-M1 and 4RM

Contact experiments were made between C-M1 and cholesteric material M1.

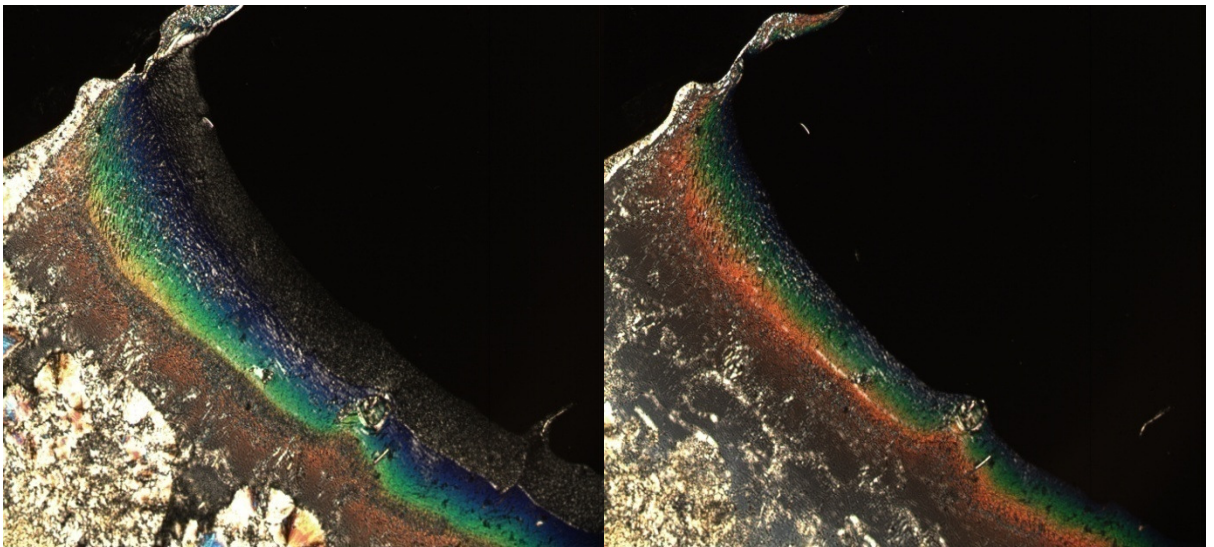


Fig. V.14. Contact experiment between C-M1 and 4RM

When mixing with the cholesteric mesogen slow and very little mixing is observed. An answer could be that the CM1 has a very short pitch

cholesteric phase; being shorter than the wavelength of visible light, as it cannot be seen under the OPM, as previously stated.

In Fig. V.14., images from two different experiments are shown. A variation in colour with a gradient from the blue towards the red as the cholesteric helix unwinds. Hence, the pitch of the helix increases and the selective reflection of visible light is observed.

M1 / 4RM phase diagram

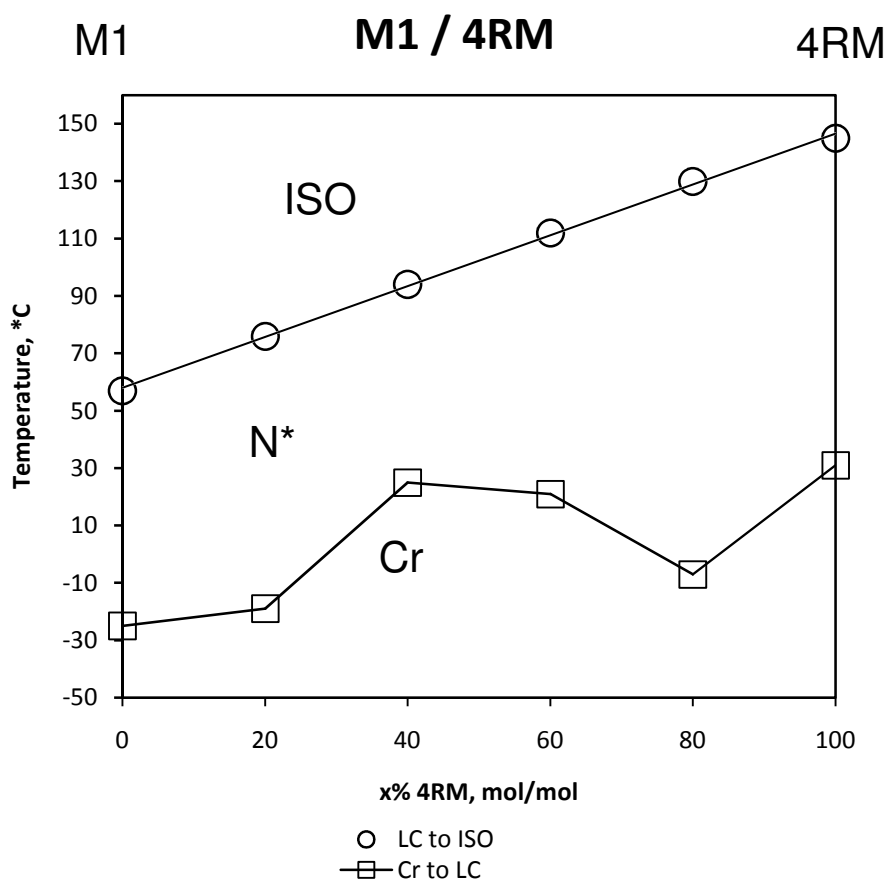


Fig. V.12. Phase diagram of the mixtures between M1 and 4RM

Phase diagrams of defined mixtures between M1, the cholesteric LC, and a nematogens were performed. The transition temperature from the chiral nematic to the isotropic state develops linearly with the addition of 4RM, as it was expected.

C-M1 / 3RM phase diagram

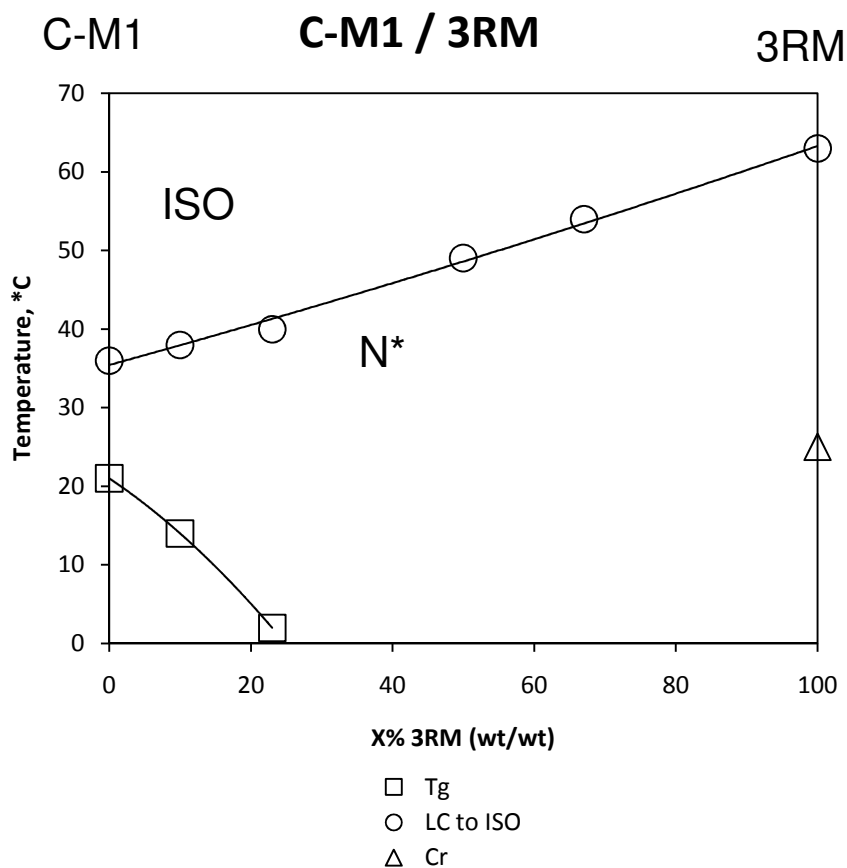


Fig. V.13. Phase diagram of the mixtures between C-M1 and 3RM

Defined mixtures were prepared by dissolving the compounds in dichloromethane (DCM). After removing the solvent, the samples were melted and mixed again to insure the homogeneity of the samples.

The mixtures of C-M1 with 3RM were prepared to understand the phase structure and phase behaviour of C-M1 better.

The materials were investigated by OPM and DSC; the transitions shown in Fig. V.13. are based on mixtures starting from 10% 3RM and continuing to increase the amount of 3RM.

A number of trends can be observed. Adding 3RM to C-M1 results in a lowering of the glass transition temperature. On adding 3RM to C-M1, the liquid crystal to isotropic transition was observed to increase monotonically.

No phase separation could be observed. The OPM texture observed in mixtures up to 90% 3RM showed clearly a formation of a cholesteric (N^*) phase.

Miscibility experiments: M1 and 4RM

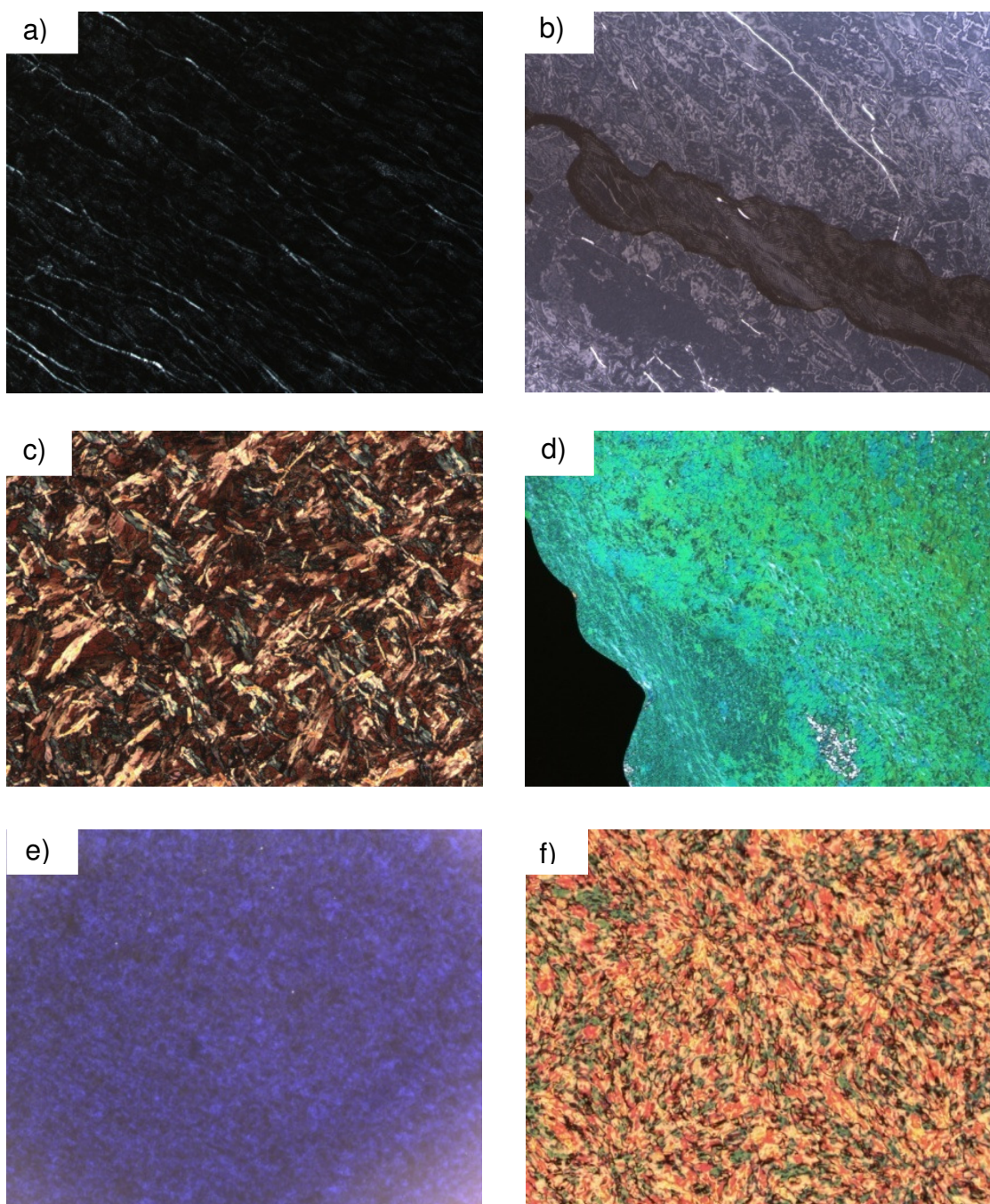


Fig. V.15. OPM images of: a) M1; b) 20% M1 in 4RM; c) 40% M1 in 4RM; d) 60% M1 in 4RM; e) 80% M1 in 4RM; f) 4RM

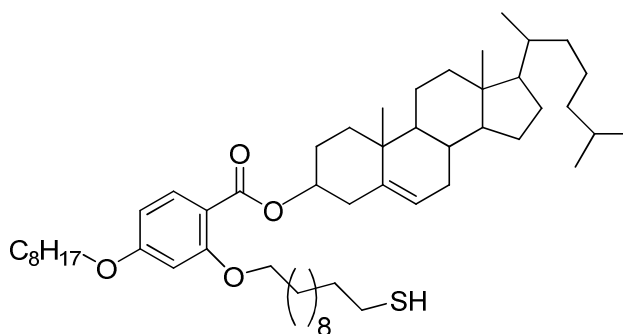
The OPM images of the mixtures between M1, which is cholesteric and 4RM, a nematic, show a variation in texture and colour as we increase the amount of M1, from 20% to 80% in increments of 20, and modify the pitch length, thus the change in colour.

Conclusions

The LC silsesquioxanes do not show birefringent OPM textures, however contact and miscibility studies with nematics show the formation of cholesteric phase behaviour. The absence of a miscibility gap in these mixtures suggests the formation of a cholesteric phase with very short pitch helix (shorter than the wavelength of the visible light, ~400nm). These results are in agreement with DSC and XRD data confirming the formation of a low ordered LC phase.

No pitch length calculations could be performed as no finger print texture was observed.

V.8. Material M1-SH



Liquid crystal and thermal properties

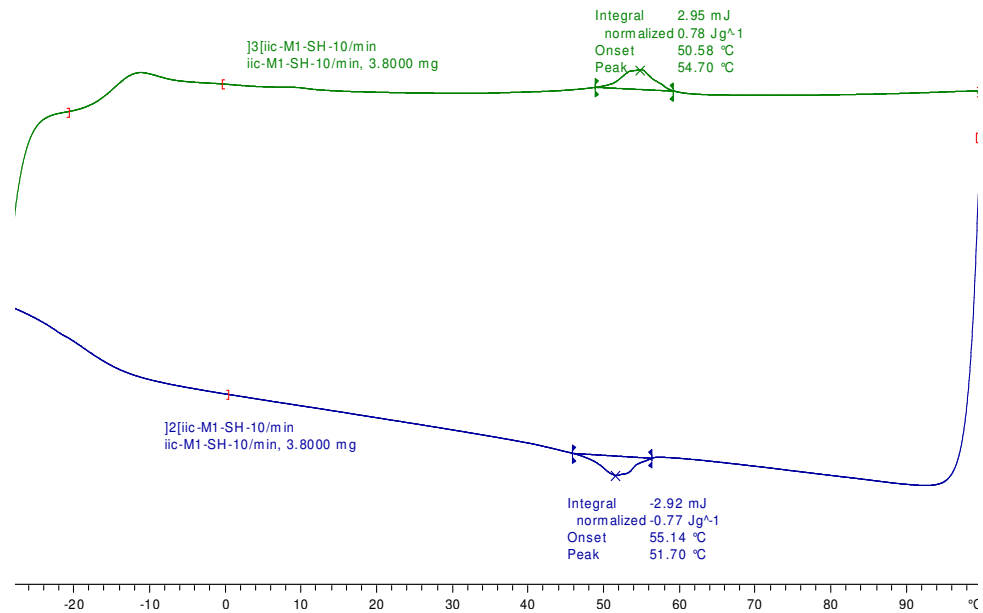


Fig. V.16. DSC trace for material M1-SH

In Fig. V.16., the DSC trace for the material M1-SH is presented. A full cycle of heating and cooling which exhibits a transition from chiral nematic to isotropic liquid, with the onset temperature of 51°C, recorded on the heating run. The glass transition temperature was found to be -15°C.

M1-SH	Tg -15 N 51 Iso
--------------	------------------------

V.9. M1 covered gold NPs (M1-AuNPs)

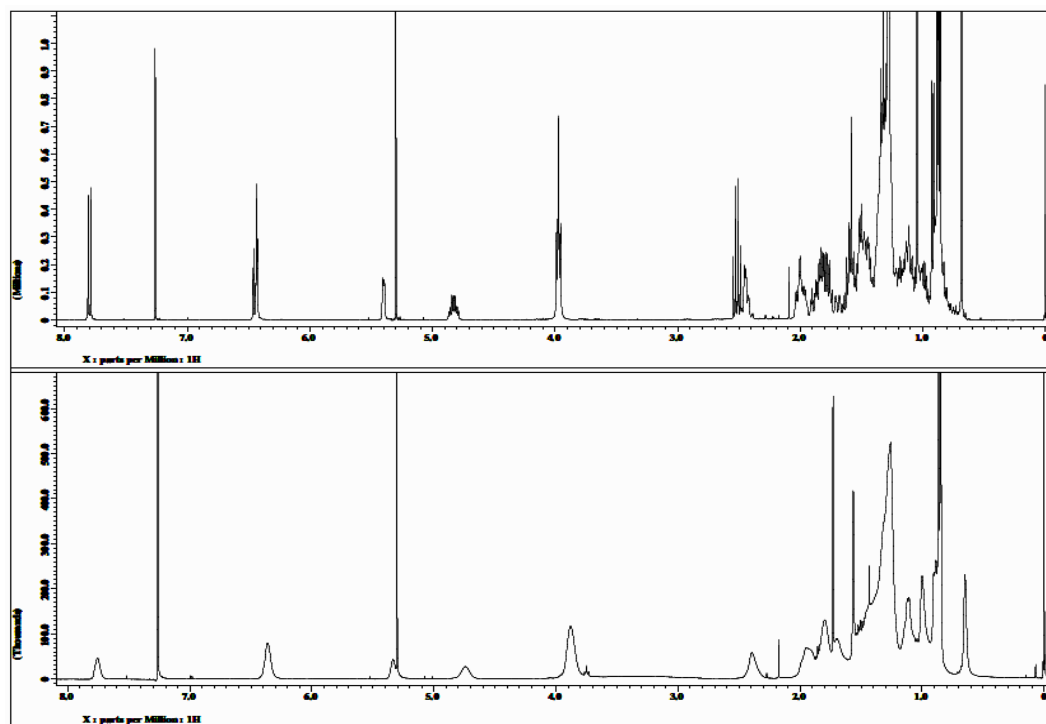


Fig. V.17. ^1H NMR spectra comparison of the free ligand (M1-SH) (top) and M1-AuNP (bottom)

Observing the ^1H NMR spectra of both materials, the one for the M1-AuNP (bottom) stands out with the broadness of the peaks. They correspond perfectly to the peaks for the monomer M1-SH, but they are much less distinguishable. This is attributed to the lack of mobility for the monomeric molecules M1 bonded to the gold nanoparticles. It is also a proof that M1 has bonded to the Au NPs.

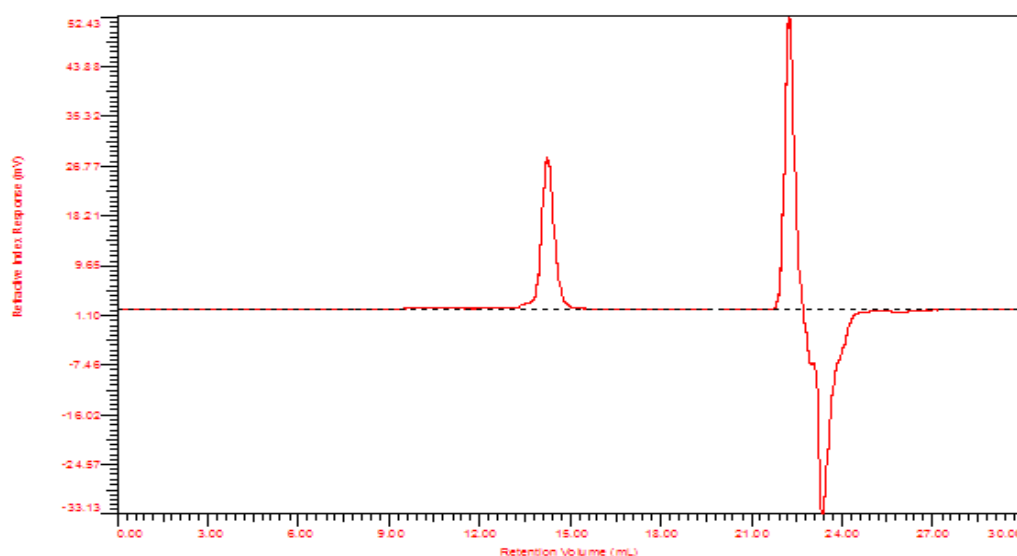


Fig. V.18. GPC retention curve of M1-AuNP

The purity of M1-AuNPs is vital for the correct characterisation of its properties including liquid crystal, thermal or optical properties. The purity was checked by GPC and as the Fig. V.18. shows, only one peak is present, except the one for the internal reference. The retention time cannot be taking into account and cannot give an exact molecular mass of the species as the NPs cannot be compared to the standard used for calibration. The standard is polystyrene beads which are spherical in morphology, hence very different than the structure of the M1-Au NPs.

Liquid crystal properties and thermal properties

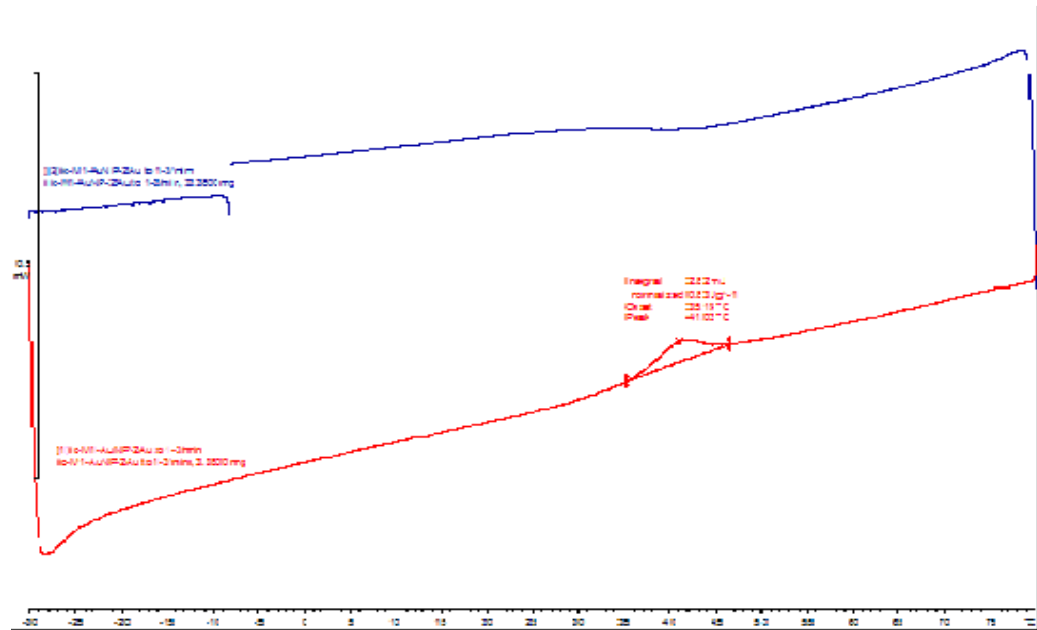


Fig. V.19. DSC trace of M1 ligand covered AuNPs

In Fig. V.19., the DSC trace for the M1-AuNPs is presented. A full cycle of heating and cooling which exhibits a transition from a liquid crystal phase to isotropic liquid is shown. The onset temperature for the LC to isotropic transition is at 35°C. The glass transition temperature was recorded to be at -10°C.

M1-Au NPs	Tg -10 N* 35 Iso
------------------	-------------------------

UV spectroscopy

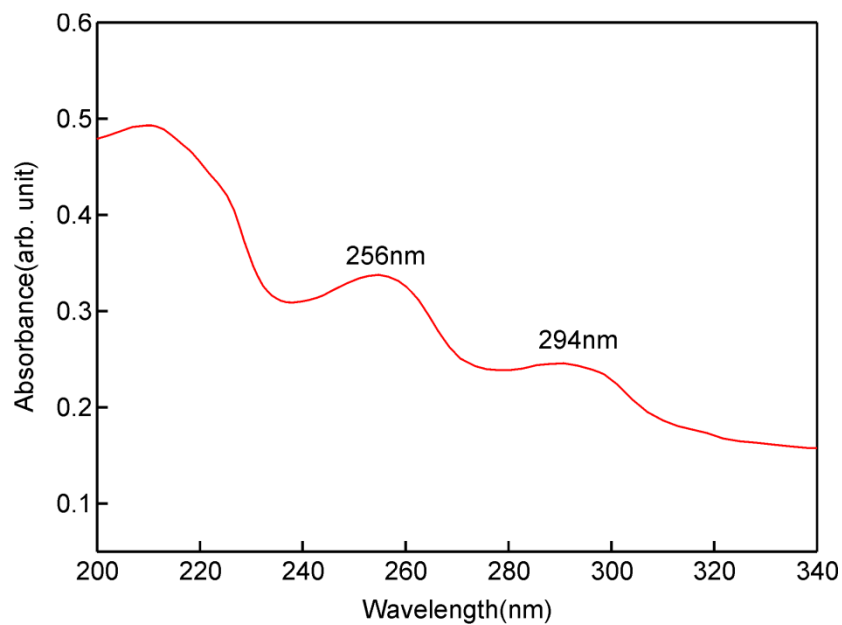


Fig. V.20. UV spectra of M1-AuNP

Fig. V.20. shows a UV spectrum for the M1-AuNPs and exhibits 2 absorption bands of medium intensity above 250 nm with no major absorption at shorter wavelength (200 – 250 nm). The spectrum is similar with the one for the material M1.

CD spectroscopy

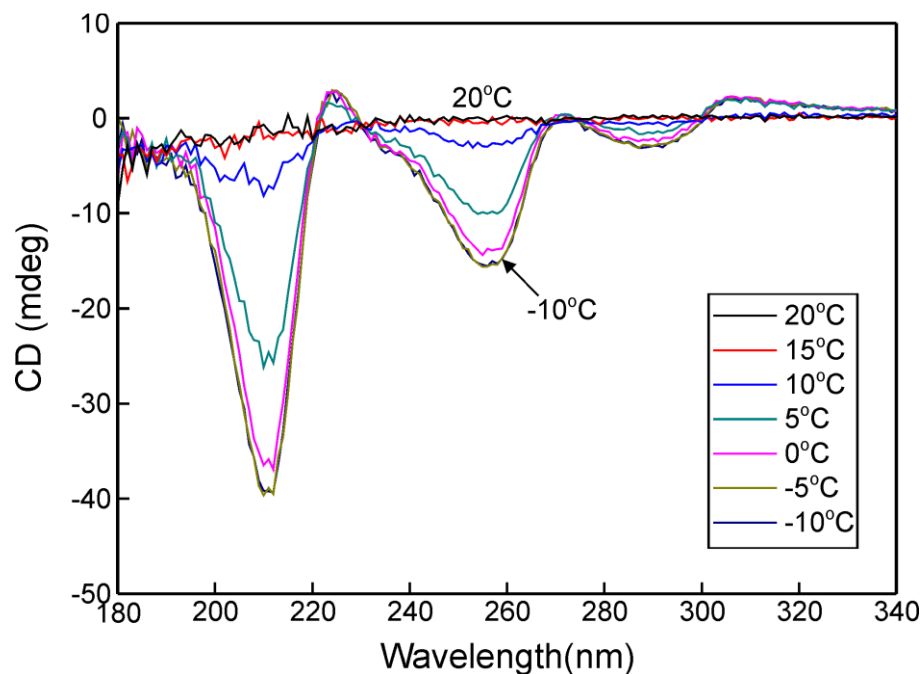


Fig. V.21. CD spectra of Au NPs coated with M1

Circular dichroism monitors the subtle alterations in structure such as the conversion of M1-AuNPs from glass to liquid crystal and subsequently to isotropic liquid. It measures the temperature dependence of the self-assembly of M1-AuNPs going through all the enumerated stages.

The samples were analysed in the form of films. They were pre-cooled in a freezer over night to -10°C .

In the wavelength region where light is absorbed (256 nm) a negative Cotton effect is observed. The signal intensity decreases as the temperature rises and it starts to be insignificant when the NPs reach the temperature of around 20°C .

Though CD measurements do not allow a direct identification of a phase structure the results indicate clearly that with increasing temperature the chirality of the LC phase is reduced and at the isotropic state only a residual small chirality could be observed.

NPs parameters calculations (TGA, TEM)

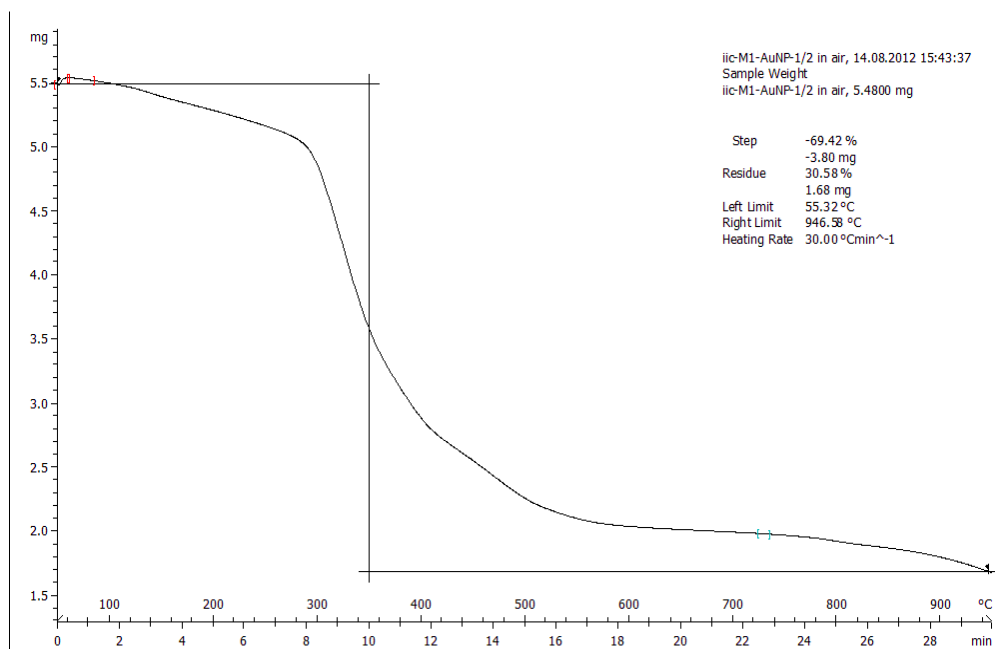


Fig. V.22. TGA trace of ligand covered AuNPs

The TGA analysis was performed in air, in order to oxidise and remove all organic material in the time set and by 900°C; when the analysis was carried out in nitrogen slow and incomplete elimination of organic material was observed. The samples were pre-dried over night in the oven to ensure the complete removal of the solvent.

The Fig. V.22. shows a slow decrease in weight above ~140°C followed by a sharp decrease in weight above 300°C and the decomposition was completed by the time the temperature reaches 500°C. These results are in line with the often observed lack of thermal stability of cholesteryl based mesogens above 140°C when it starts to decompose.

The organic materials must have been completely removed in order to identify the ration between the ligand (M1) and metallic core of the NPs.

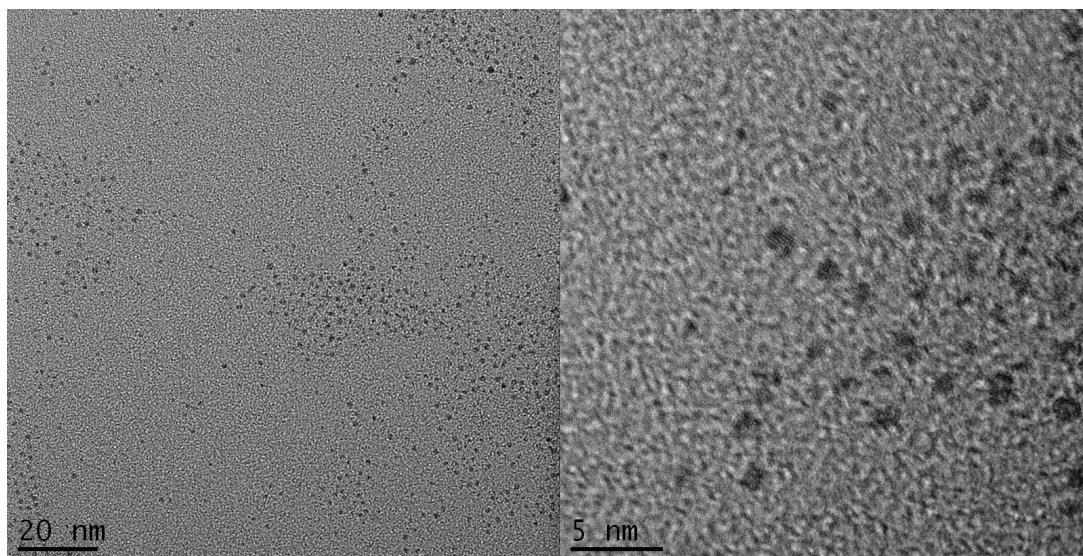


Fig. V.23. TEM images of M1-Au NPs

The sizes of M1-Au NPs were recorded using TEM showing large uniform arias and narrow size distribution.

Having the information gathered by TGA in addition to TEM analysis giving the size of the NPs, D. Astruc et al. [121] formulated equations to calculate the number of gold atoms per cluster of NPs (Eq. V.1.), number of ligands per nanoparticle (Eq. V.2.) and the average molecular weight (Eq. V.3.). These three equations are the following:

Eq. V.1. :

$$n_{\text{Au}} = \frac{4 \pi R^3}{3 V_g}$$

where: $V_g = 17 \text{ \AA}^3$ (the volume of gold atom)

$R = 7.5 \text{ \AA} = 0.75 \text{ nm}$ (the radius for 1.5 nm NPs)

Eq. V.2. :

$$N_L = \frac{n_{Au} \cdot A_{W Au} \cdot wt\%L}{M_{wL} \cdot wt\%Au}$$

where: $\frac{wt\%L}{wt\%Au} = \frac{7}{3}$

$$A_{w Au} = 196.97 \text{ (atomic weight for Au)}$$

$$M_{wL} = 820 \text{ (molecular weight for M1)}$$

Eq. V.3. :

$$\overline{M_w} = n_{Au} \cdot A_{w Au} + N_L \cdot M_{wL}$$

Table V.5. Calculations of NPs parameters

Size of M1-AuNPs	1 nm	1.5 nm	2 nm
No. of Au atoms/cluster	31	104	246
No. of ligands/NP	17	58	138
Average molecular weight	20 000	68 000	160 000

The TGA analyses were reproducible for NPs from different experiments, validating the synthetic route for obtaining the M1-Au NPs and the method of purification. The ligand coverage was similar in all cases.

The TGA and TEM results were consistent and the ligand coverage was constant at 70% of the total mass of the NP. The average diameter for the NPs was found to be 1.5 nm with narrow size distribution. From the calculations it

results that M1-Au NPs have around 104 gold atoms per NP and coverage of 58 ligands M1.

From the TEM pictures a size variation of ± 0.2 nm can be estimated, however the GPC data indicate that the material is very monodisperse.

V.10. Material M1-COOH

Liquid crystal properties and thermal properties

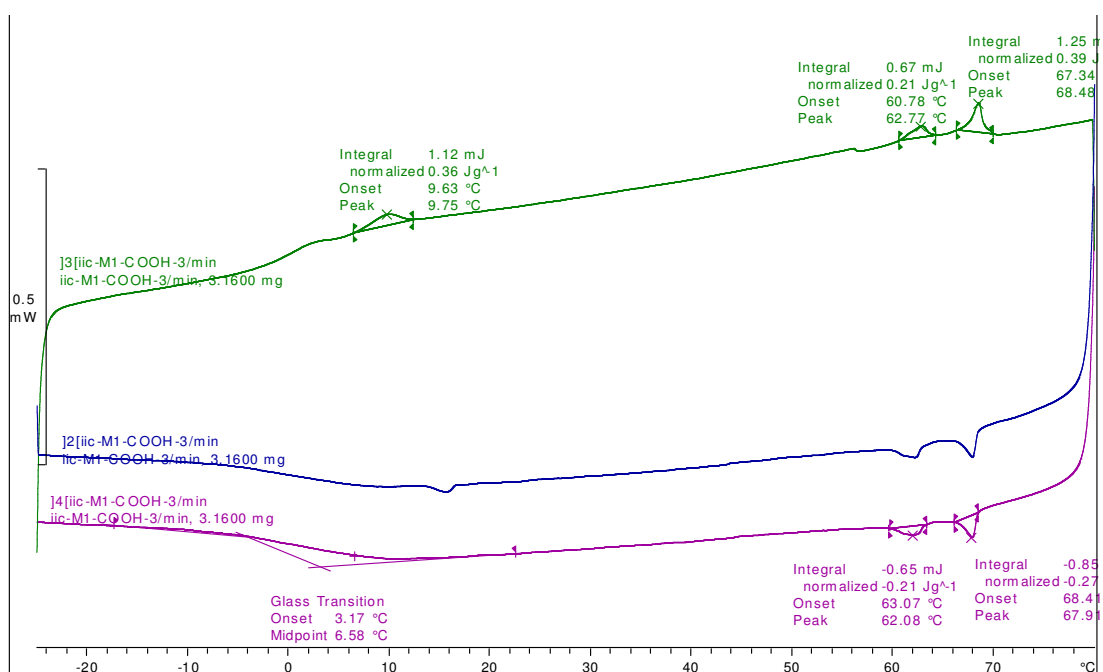


Fig. V.24. DSC trace of M1-COOH

In Fig. V.24., the DSC trace for the material M1-COOH is presented. A full cycle of heating and cooling and an additionally cooling run of 3 degrees per minute, which exhibits a number of transitions, such as a glass transition, two other transition and a transition from the liquid crystal phase to isotropic liquid, with the onset temperatures of 9°C, 61°C and subsequently 67°C. On the second cooling run the transition around 15°C it is not visible probably due to the super cooling of the sample.

M1-COOH	Tg 3 X 10 X 61 N* 67 Iso
---------	--------------------------

Nevertheless, the clearing point for M1-COOH is quite high and by attaching this system to the Fe/Pt NP it is expected that the transition of the functionalised system to decrease. The decrease of the clearing point should depend linearly on the number of M1-COOH molecules attached on the NP until the hybrid NP's properties are governed mainly by the micro segregation between the organic layer and the metallic NP.

V.11. Oleic acid/oleyl amine ligands covered iron/platinum NPs (Fe/Pt NPs)

Liquid crystal properties and thermal properties

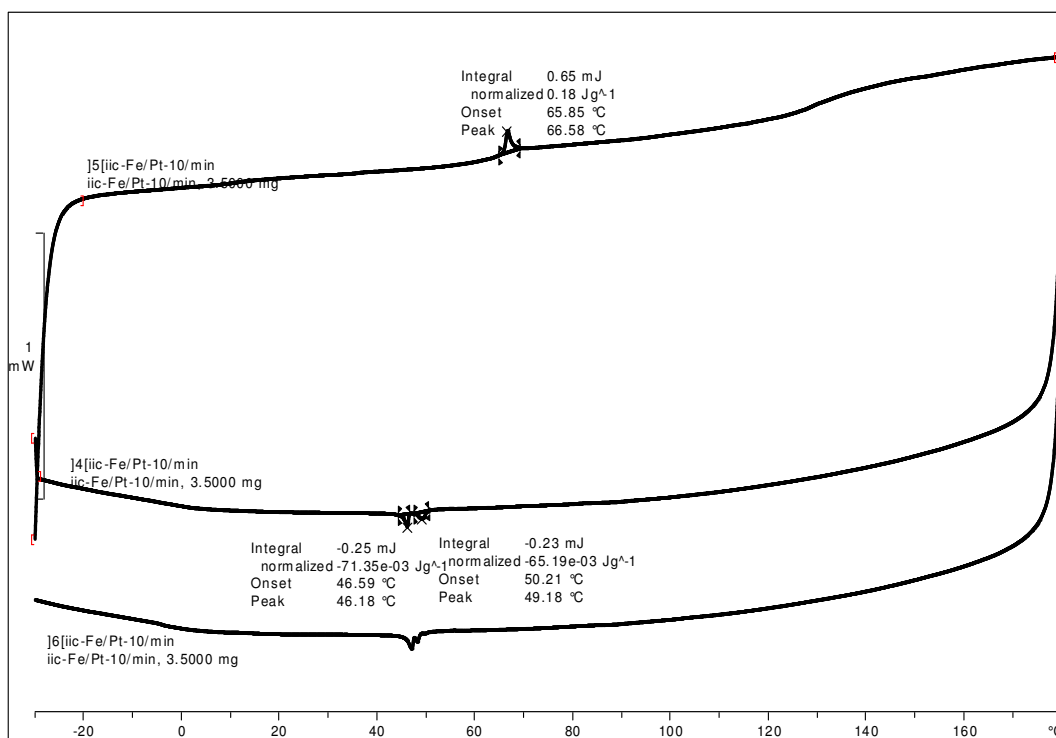


Fig. V.25. DSC trace of Fe/Pt NPs

In Fig. V.25., the DSC trace for the Fe/Pt NPs is presented. A full cycle of heating and cooling which shows a transition from a LC state to isotropic liquid can be seen. An onset temperature of 66°C, recorded on the heating run was detected. The crystal to LC or the glass transition cannot be seen on the spectra, therefore, it must be lower than -20°, the limit of the used instrument.

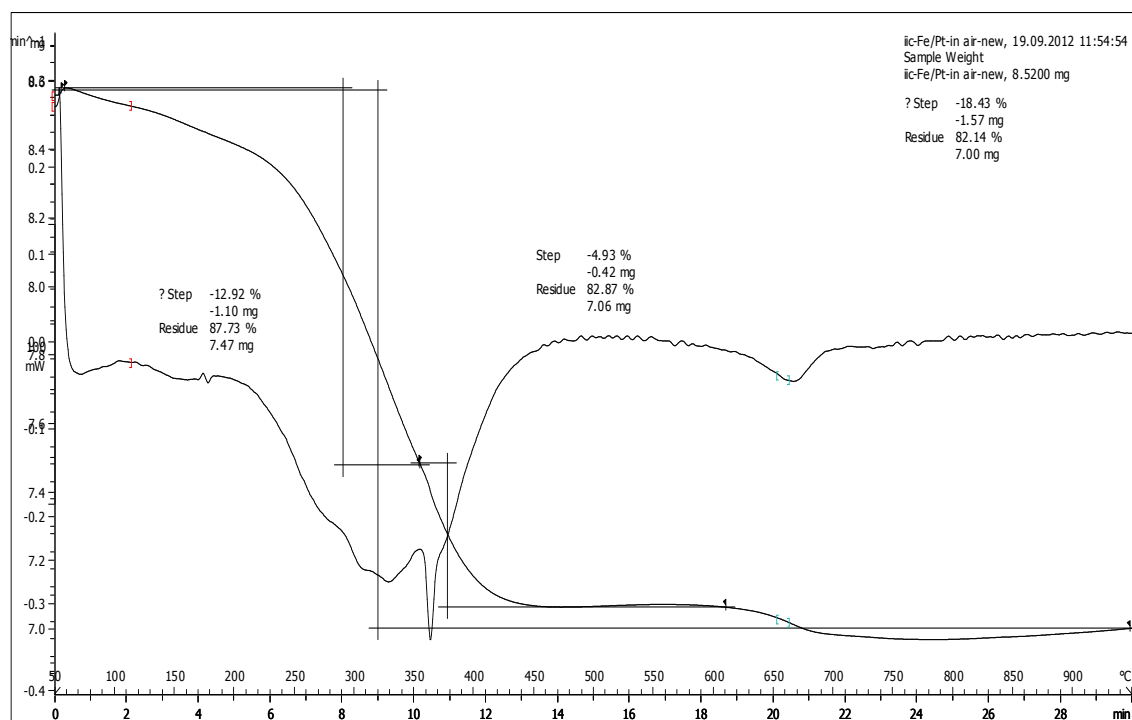


Fig. V.26. TGA spectrum of Fe/Pt NPs

The TGA analysis was performed in air, in order to oxidise and remove all organic material in the time set and by 900°C. The samples were pre-dried over night in the oven to ensure the complete removal of the solvent.

As the Fig. V.26. shows, the sample loses weight in two main steps, one for the oleyl amine (300°C) and the other for oleic acid (375°C). The removal of organic components is completed by the time the temperature reaches 450°C. There is also another visible step on the TGA trace at 675°C; it is for the conversion from the face centered cubic lattice to a more fundamental face centered tetragonal arrangement of the Fe/Pt NPs.

The organic materials must have been completely removed in order to identify the ratios between the ligands and the metallic core of the NPs. The organic compounds (oleic acid and oleyl amine) stand for 18% of the total mass of the NP. The residual percentage of pure Fe/Pt NPs is 82%.

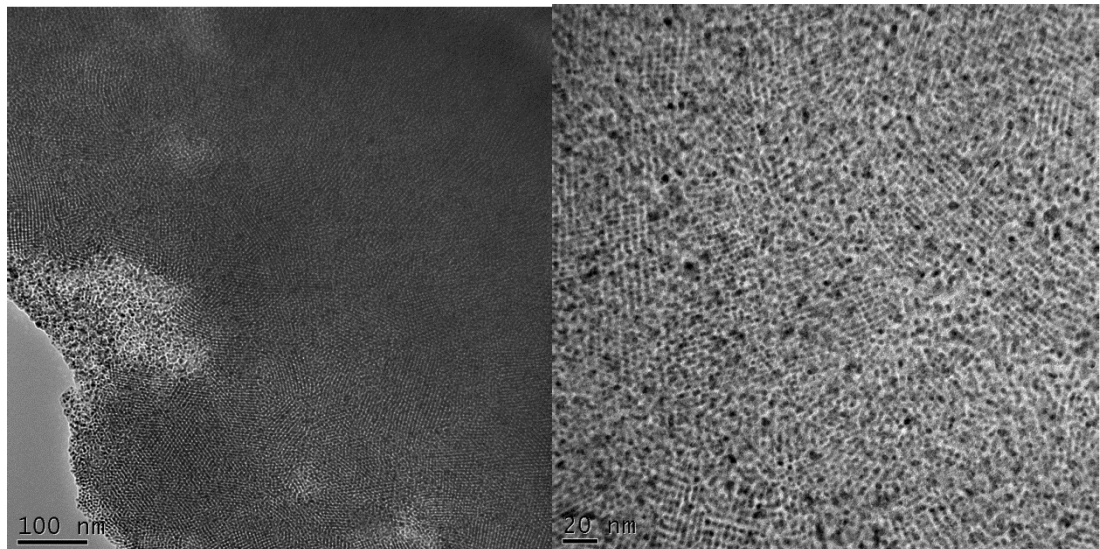


Fig. V.26. TEM images of Fe/Pt NPs

The self-assembly of Fe/Pt NPs were observed by TEM showing large uniform arias and narrow size distribution. The packing behaviour with arrays of NPs can also be seen. It was estimated that the average size for the Fe/Pt NPs was 4 nm.

V.12. M1 covered iron/platinum NPs (M1-Fe/Pt NPs)

Liquid crystal properties and thermal properties

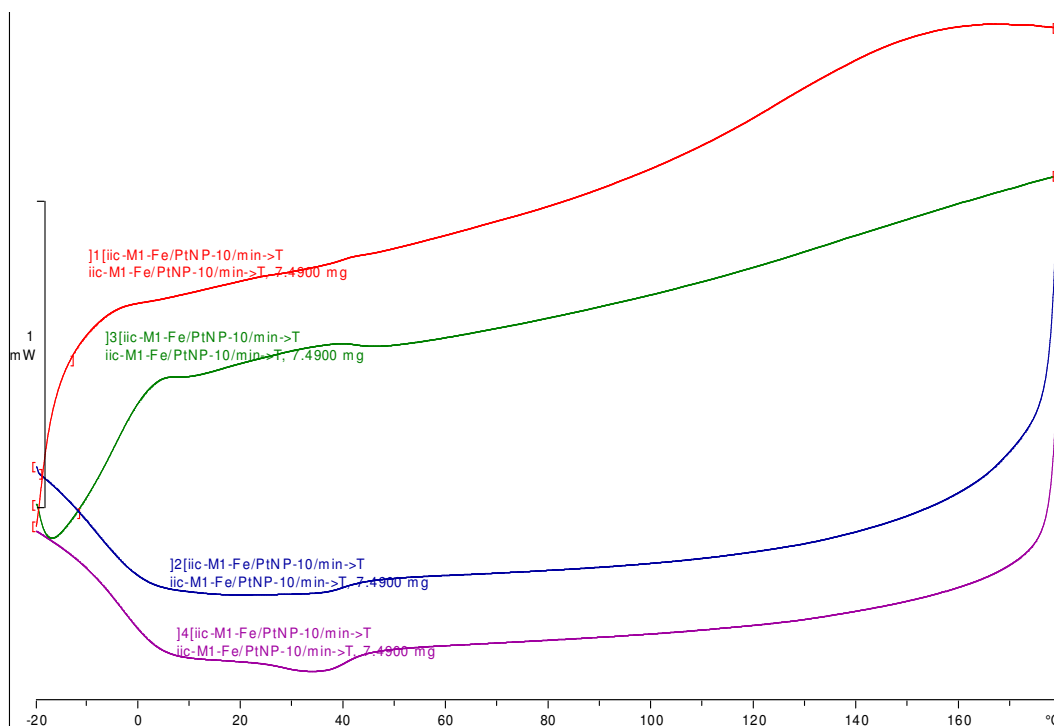


Fig. V.27. DSC trace of M1-Fe/Pt NPs

In Fig. V.27., the DSC trace for the M1-Fe/Pt NPs is presented. Two full cycles of heating and cooling showing two transitions, a glass transition at 0°C and a transition from LC to isotropic liquid are shown. The transition temperatures are in the range of 0 - 40°C. The heating rate was 10 degrees per minute.

By attaching M1 to the Fe/Pt NP it is expected that the transition of the M1 functionalised system to decrease. The decrease of the clearing point should depend linearly on the number of M1-COOH molecules attached on the NP until the hybrid NP's properties are governed mainly by the micro segregation between the organic layer and the metallic NP.

The transition temperatures are in range of room temperature, lower than the M1-COOH material and the Fe/Pt NP system, which was expected.

UV spectroscopy

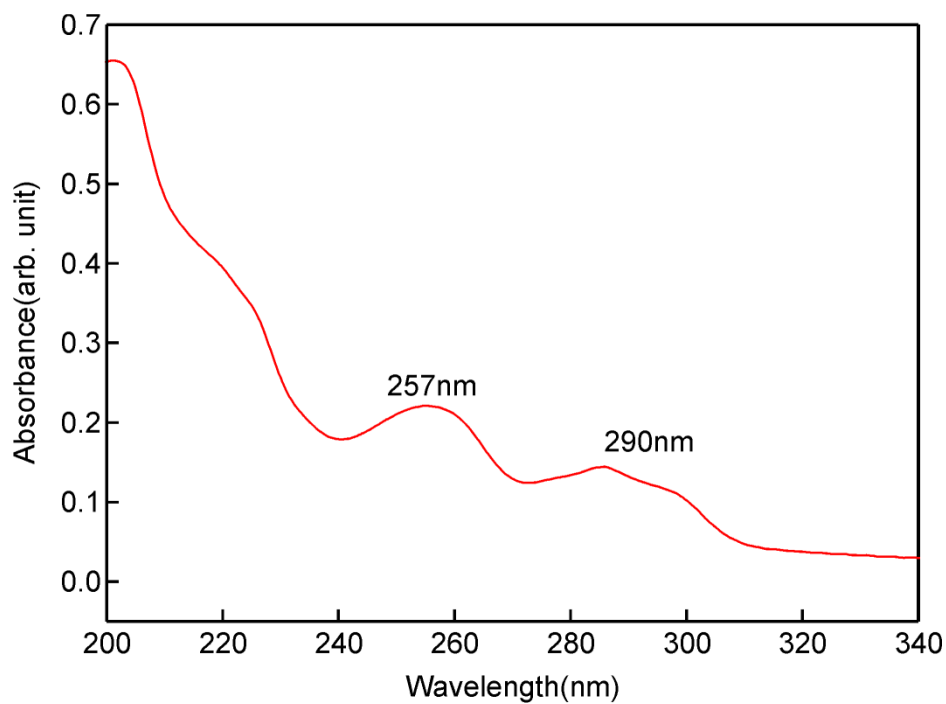


Fig. V.28. UV spectra of M1-Fe/Pt NPs

Fig. V.28. shows a UV spectrum for the M1- Fe/Pt NPs and exhibits 2 absorption bands of medium intensity above 250 nm and a low intensity absorption at shorter wavelength, 220 nm. The spectrum is similar to that recorded for the material M1.

CD spectroscopy

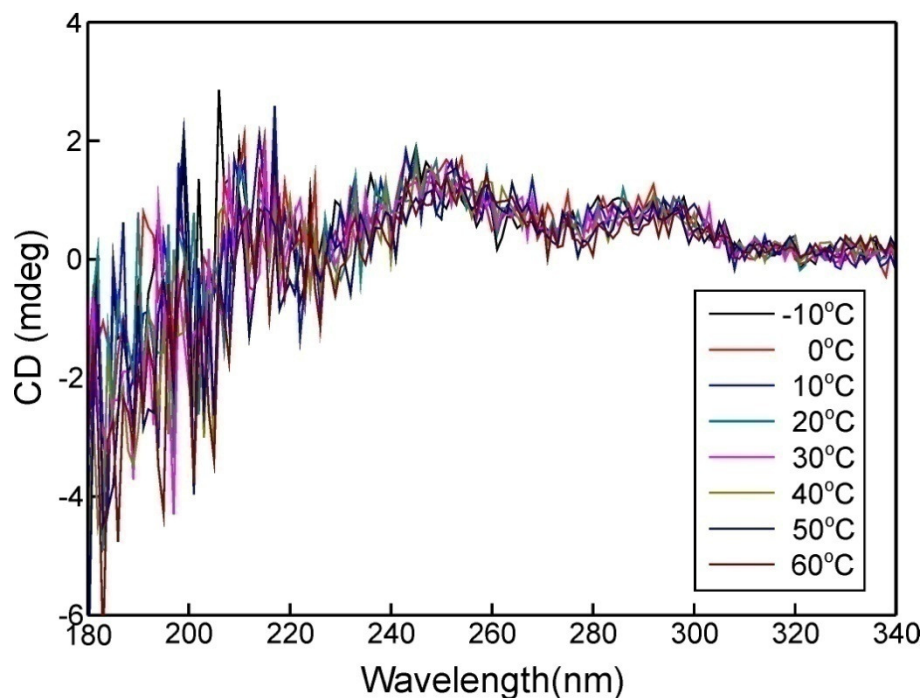


Fig. V.29. CD spectra of Fe/Pt NP coated with M1

The cells were pre-cooled in the freezer, over-night, and recorded spectra with temperature. The spectra did not change very much with increasing temperature from -10°C to 60°C ; the main features are the same, which is completely different from those of M1-AuNPs, as it was expected.

For the Fe/Pt NPs coated with M1, no significant Cotton effect could be observed. The lack of change in the CD spectra recorded at various temperatures suggests that no change in the chirality of the superstructure with changing temperature occurs.

An alternative explanation would be that the arrangement of the LC mesogens on the NPs is such that changes in chirality cannot be detected.

NPs parameters calculations (TGA, TEM)

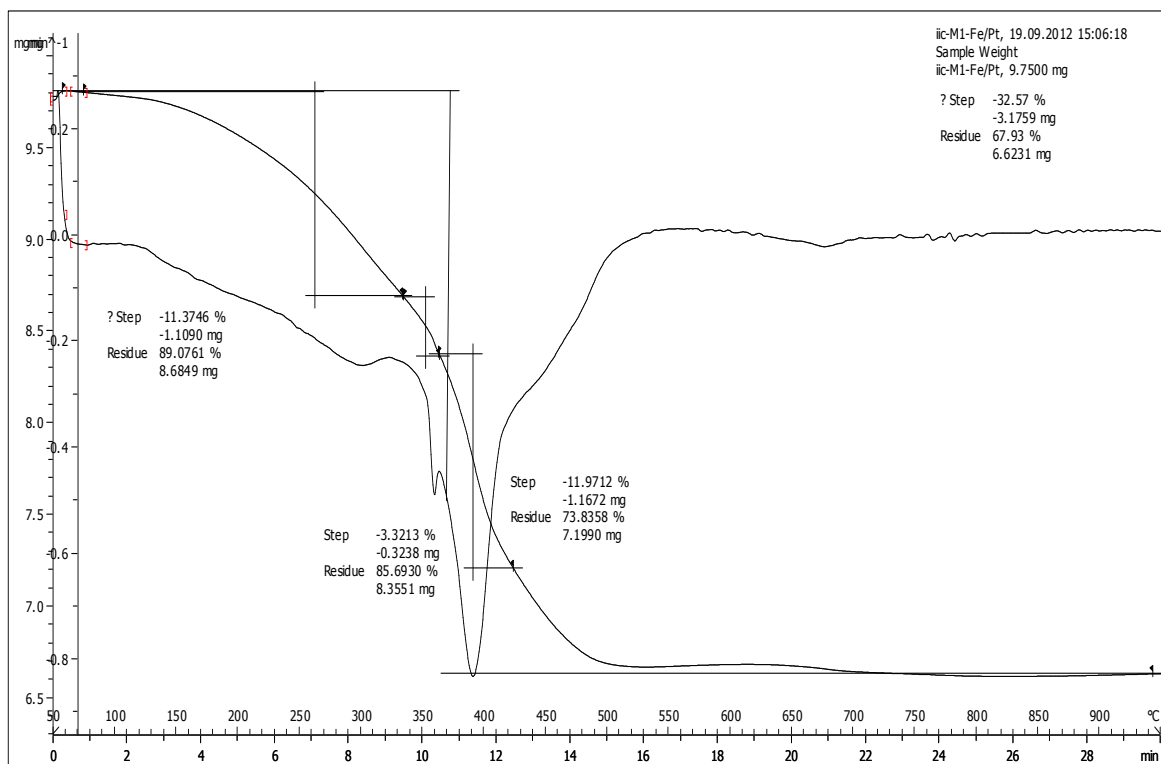


Fig. V.30. TGA spectrum of M1-Fe/Pt NPs

The TGA analysis was performed in air, in order to oxidise and remove all organic material in the time set and by 900°C. The samples were pre-dried over night in the oven to ensure the complete removal of the solvent.

As the figure show, the organic material is burnt off in three main stages, one for the oleyl amine (300°C), one for oleic acid (360°C) and the other for M1 (390°C). The removal of organic components is completed by the time the temperature reaches 500°C. There is also another visible step on the TGA trace at 675°C; it is for the conversion from the face centered cubic lattice to a more fundamental face centered tetragonal arrangement of the Fe/Pt NPs.

The organic materials must have been completely removed in order to identify the ratio between the ligand (M1) and metallic core of the NPs. The organic components (oleic acid, oleyl amine and M1) stand for 26% of the total mass of the NP and the M1 alone sums up to 6%.

In conclusion, these NP systems have the same initial loss as the Fe/Pt NPs with an extra weight loss for the M1 material. The TGA results are showing that the pure NPs are in 68% of total mass of functionalised NPs and 6% of M1.

Unfortunately, because the TEM data is missing, the calculations for the number of mesogens and ligands attached cannot be carried out. The TEM instrument was unavailable for a period of one year due to repeated technical issues. Towards the latter stages of the Ph.D., when TEM characterisation for the M1-Fe/Pt NPs was needed, the TEM was out of service.

However, considering that for the preparation of M1-Au NPs the size of NPs remained the same and with a narrow size distribution, it can be assumed that for M1-Fe/Pt NPs the same happened. An additional assumption can be made that the ratio between the iron and platinum atoms per NP is 1 to 1.

Based on these information, D. Astruc et al. [121] formulated equations to calculate the number of metallic atoms per cluster of NPs (Eq. V.1.), number of ligands per nanoparticle (Eq. V.2.). These three equations are the following:

Eq. V.1. :

$$n_{\text{Fe/Pt}} = \frac{4 \pi R^3}{3 V_g}$$

where: $V_g = 9.815 \text{ \AA}^3$ (the average volume of iron and platinum atoms)

- volume of iron atom = 8.38 \AA^3

- volume of platinum atom = 11.25 \AA^3

$R = 20 \text{ \AA} = 2 \text{ nm}$ (the radius for 4 nm NPs)

Eq. V.2. :

$$N_L = \frac{n_{\text{Fe/Pt}} \cdot A_{\text{W Fe/Pt}} \cdot \text{wt}\%L}{M_{\text{w L}} \cdot \text{wt}\%\text{Fe/Pt}}$$

where:
$$\frac{\text{wt}\%L}{\text{wt}\%Fe/Pt} = \frac{6}{68}$$

$A_{w\ Fe/Pt} = 125.46$ (average atomic weight for Fe/Pt)

- atomic weight for iron atom = 55.846

- atomic weight for platinum atom = 195.084

$M_{wL} = 820$ (molecular weight for M1)

Table V.6. Calculations of NPs parameters

Size of M1-Fe/Pt NPs	4 nm
No. of Fe and Pt atoms/cluster	3414
No. of M1 ligands/NP	46

The TGA analyses were reproducible for NPs from different experiments, validating the synthetic route for obtaining the M1-Fe/Pt NPs and the method of purification.

From the calculations it results that M1-Fe/Pt NPs have around 3414 iron and platinum atoms per NP and coverage of 46 ligands M1.

Conclusions to nanoparticles

The mesogenic moieties are covalently bonded to Au NPs and Fe/Pt NPs. The present results indicate that it is possible to prepare NPs with chiral nematic phase behaviour close to room temperature. Relationships between the size of the NPs and coverage of the NPs with mesogenic groups and the LC phase are as expected.

No OPM textures for NPs are present in the study as no birefringence could be detected.

The new method used to prepare the Au NPs can give nanoparticles with narrow size distribution. The average diameter of NPs can be controlled and for a 1.5 nm large NP, the organic layer coverage is about 70%. This means that the 1.5 nm size M1-Au NP has 104 gold atoms in its cluster and 58 molecules of M1 coordinated to the gold surface.

For Fe/Pt NPs, the initial loss of the organic compounds (oleic acid, oleyl amine) was 18% and for the M1 covered Fe/Pt NPs after a ligand exchange reaction, the total loss was 32% from which 6% is M1. The differences are clear between the initial Fe/Pt NPs and the M1 covered Fe/Pt NPs. TGA shows clearly a 6% of M1 coverage. The size and parameter calculations are not yet explored due to technical issues. Nevertheless, based on two assumptions that the NPs remain at the same size after preparation and the ration iron to platinum atoms is 1 to 1, the calculations show a number of 3414 iron and platinum atoms per NP and 46 ligands per NP.

Further characterization is needed and currently performed (XRD studies, TEM) to shed light on assembly of these NPs.

Conclusions

Table. V.7. Variation of LC properties in low molar mass compound series

Compound	LC transition	Discussion
MX	Cr 69 N* 92 Iso	<p>If the spacer is attached to the cholesteryl core compared to the benzenic ring, a decrease by 15°C of the clearing point can be observed.</p> <p>By changing the end group of the mesogenic unit, a homologous series of compounds results. Throughout the series the clearing point remains in the same temperature region. Only the glass transitions vary from one compound to the other.</p> <p>Multiple transitions can be observed for the carboxylic acid functionalised mesogen.</p>
M2	Tg -22 N* 42 Iso	
M1	Tg -25 N* 57 Iso	
M1-A	Tg 5 N* 48 Iso	
M1-SH	Tg -15 N* 51 Iso	
M1-OH	Tg -6 N* 52 Iso	
M1COOH	Tg 3 X 10 X 61 N* 67 Iso	

Table. V.8. Variation of LC properties in nanoparticle systems

Compound	No. of M1 ligands	LC transition	Discussion
C-M2	8	Tg 10 N* 22 Iso	<p>When mesogens are attached to the silsesquioxane cube, a narrow room temperature LC phase can be observed. For the M1 silsesquioxane the temperature interval is higher than the one for M2.</p> <p>For the LC NPs, the mesophase is at room temperature with low glass transitions and clearing point similar with the one for the silsesquioxane.</p>
C-M1	8	Tg 27 N* 38 Iso	
M1-Au NPs	58 (1.5 nm NP)	Tg -10 N* 35 Iso	
M1-Fe/Pt NPs	46 (4 nm NP)	Tg 0 N* 40 Iso	

CHAPTER VI

CONCLUSIONS

Chiral nematic materials, M1 and M2

In order to investigate the combination of silsesquioxane cores, which are known to promote microphase separation in liquid crystal materials, and cholesterol groups containing mesogens, two cholesterol group containing mesogens were designed and synthesized. To promote exclusively chiral nematic phase behaviour in these mesogens, as well as low melting points and low transition temperatures, the cholesterol groups were designed to be attached “laterally” to the silsesquioxane cores by hydrosilylation, resulting in materials with liquid crystal phase at room temperature.

As to the thermal and LC properties of these mesogenic groups, they exhibit LC phases at room temperature, with low melting points. Now, if the transition temperatures are to be compared, a difference of 15°C of the clearing point can be seen, just by changing the position of the connecting alkyl chain. For both mesogens the DSC results were fully reproducible.

The OPM textures for both materials are poorly developed pseudo focal conic like texture for cholesterics.

In terms of chiroptical properties of the two mesogens, the material M1 has a CD signal intensity of a factor of 5 larger than the material M2. The two materials rotate the plane of polarised light in opposite directions, material M1 being levorotatory and respectively, M2 is dextrorotatory.

As the temperature is increased the intensity of the CD signal decreases, the superstructures become less chiral. Heating the samples towards the clearing point the Cotton effect disappears as well as the other CD spectra features.

Based on the molecular structure difference between M1 and M2 in terms of UV and CD spectra, two UV absorption bands are observed for M1 and only one absorption band for M2 and respectively, positive and negative Cotton effects. The UV absorption features are due to the number of substituents at the benzenic ring, two in the case of M1 and one for M2. From the CD results, the negative Cotton effect for M1 and positive for M2 are observed.

In conclusion, new side-on chiral nematic cholesterol based compounds were prepared. Using already established methodology, the procedures were validated and optimised. The materials have a cholesteric phase at room temperature with low melting points.

Silsesquioxane based systems, C-M1 and C-M2

In order to investigate the combination of silsesquioxane cores, which are known to promote microphase separation in liquid crystal materials, and cholesterol groups containing mesogens, two cholesterol group containing mesogens were designed, synthesized and attached “laterally” to the silsesquioxane cores by hydrosilylation, resulting in materials with liquid crystal phase at room temperature.

As to the thermal and LC properties of these materials, they exhibit LC phases at room temperature, with low melting points. Now, if the transition temperatures are to be compared, a difference of 13°C of the clearing point can be seen, using one monomer of the other. The liquid crystal phase interval is quite narrow, being about 12°C. For both materials the DSC results were reproducible.

In terms of chiroptical properties the two materials rotate the plane of polarised light in opposite directions, material C-M1 being levorotatory and respectively, C-M2 is dextrorotatory, as the correspondent monomers.

When the materials were checked under OPM, to identify the eventual LC phases, both samples were optically isotropic, no birefringence could be seen. This was contrary to expectations where helical superstructure or a simple cholesteric phase was expected, but OPM, DSC and XRD proved the existence of a possibly highly ordered phase or a short pitch cholesteric phase.

Considering that the DSC measurements show clearly a transition but no birefringence, other methods were explored to explain the behaviour of these structures: contact experiments and phase diagrams of binary mixtures between the mesogens and the final compounds and known nematogens, but also miscibility experiments between the mesogen and a known nematogen.

The outcome of these studies was that the formation of cholesteric phase behaviour was observed. The absence of a miscibility gap in these mixtures

suggests the formation of a cholesteric phase with a very short pitch helix (shorter than the wavelength of the visible light, ~400nm). These results are in agreement with DSC and XRD data confirming the formation of a low ordered LC phase.

In conclusion, the side-on silsesquioxane systems are new materials and liquid crystalline at room temperature with low melting points. From the results, a mesophase with a very short pitch length is observed. Both materials are optically active.

M1 covered gold and iron/platinum nanoparticles

The mesogenic moieties are covalently bonded to Au NPs and Fe/Pt NPs. The present results indicate that it is possible to prepare NPs with chiral nematic phase behaviour close to room temperature. Relationships between the size of the NPs and coverage of the NPs with mesogenic groups and the LC phase are as expected.

No OPM textures for NPs are present in the study as no typical defect textures could be detected.

The new method used to prepare the Au NPs can give nanoparticles with narrow size distribution. The average diameter of NPs can be controlled and for a 1.5 nm large NP, the organic layer coverage is about 70%. This means that the 1.5 nm size M1-Au NP has 104 gold atoms in its cluster and 58 molecules of M1 coordinated to the gold surface. These NPs are the first chiral materials bearing chiral mesogens, with LC behaviour at room temperature.

For Fe/Pt NPs, the initial loss of the organic compounds (oleic acid, oleyl amine) was 18% and for the M1 covered Fe/Pt NPs after a ligand exchange reaction, the total loss was 32% from which 6% is M1. The differences are clear between the initial Fe/Pt NPs and the M1 covered Fe/Pt NPs. TGA shows clearly a 6% of M1 coverage. Based on two assumptions that the NPs remain at the same size after preparation and the ration iron to platinum atoms is 1 to 1, the calculations show a number of 3414 iron and platinum atoms per NP and 46 ligands per NP.

In conclusion, new chiral gold nanoparticles with laterally attached mesogens were prepared. The NPs exhibit a liquid crystal phase at room

temperature. A completely new synthetic procedure was involved. Using this method a very narrow size distribution of NPs and a control of the number of the ligands attached is observed. The chirality of these NPs is reduced with the increasing temperature. Based on the DSC results, liquid crystal iron/platinum nanoparticles are reported. It awaits confirmation by other methods. They exhibit a mesophase at room temperature. The superstructure of this mesophase is to be determined.

CHAPTER VII

OUTLOOK

The future research plans could be twofold: liquid crystal silicon based systems and liquid crystal nanoparticles.

The fundamentals of the topic have been explored and significant change in the LC phase behaviour going from a monomer to a silsesquioxane and a NP system was detected. In order to explore this transition further it would be very attractive to prepare a number of oligomers and small polymers of well defined size and topology and to investigate their properties.

For the silsesquioxane systems the investigation of the phase structure would be attractive. Moreover, the synthesis of copolymer type systems with nematogenic monomers would be attractive. This would allow exploring in more detail the chiral phase structure.

Issues to be investigated would be the change of chirality of the LC phase with temperature and the concentration of the nematogenic component and any resulting superstructure. Furthermore, these materials will continue to be studied by XRD in more depth, using SAXS with synchrotron radiation, in order to shed light of the structure of these materials. Currently, a number of the already prepared materials are with the group of Prof. G. Ungar, Sheffield, UK.

For the NP systems the investigation of the phase structure would be critical. Au NPs coated with a short chain linear carbohydrate will be interesting to analyse. Furthermore, doping Au NPs with M1 mesogen it is a good way of comparing the classical synthetic method with the one used in this research, the properties of these two classes of Au NPs, one with the mesogen coordinated to the Au NP and the other with the NPs free flowing in the nematic liquid crystal.

A study for the variation of size of NPs for plasmonic properties could be attractive and to be considered for optical applications.

A further investigation in the LC iron/platinum phase behaviour could give interesting results. Additional information on the ratio of metals Fe to Pt in the NPs can be provided by TEM through Energy Dispersive Spectroscopy (EDS).

Investigation of the magnetic properties and the behaviour of LC iron/platinum NPs when an external magnetic field is applied could complete the analysis. This study will be performed with SQUID (Superconducting Quantum Interference Device).

REFERENCES

1. P.J. Collings, M. Hird, Taylor & Francis, London, 1997, 1
2. S. Kasap, P. Capper, *Handbook of Electronic and Photonic Materials*, Springer, 2006, 917
3. D. Demus, *Liquid Crystals: Applications and Uses*, Ed. B. Bahadur, Singapore, 1990, 1
4. S. Chandrasekhar, B.K. Sadashiva, K.A. Suresh, *Paramana*, 9, 1977, 471
5. J. Billard, J.C. Dubois, T.H. Nguyen, A. Zann, *Nouveau J. Chim.*, 1978, 2, 535
6. S. Singh, *Phys. Rep.*, 1996, 277, 283
7. M.A. Bates, G.R. Luckhurst, *J. Chem. Phys.*, 1999, 110, 7087
8. K. Praefcke, Ed. by D.A. Dunmur, A. Fukuda, G.R. Luckhurst, INSPEC, London, 2001, 1
9. F. Renitzer, *Monatsh. Chem.*, 1888, 9, 421
10. H.S. Kitzerow, *Chem. Phys. Chem.*, 2006, 7, 63
11. J.W. Goodby, *Curr. Opin. Colloid Interface Sci.*, 2002, 7, 326
12. P.J. Collings, J.S. Patel, *Handbook of Liquid Crystal Research*, Oxford University Press, New York, Oxford, 1997, 1
13. S. Garoff, R. Meyer, *Phys. Rev. Lett.*, 1977, 38, 848
14. C.V. Yelamaggad, G. Shanker, U.S. Hiremath, S.K.Prasad, *J. Mater. Chem.*, 2008, 18, 2927
15. C.V. Yelamaggad, M. Mathews, T. Fujita, N. Iyi, *Liq. Cryst.*, 2003, 30, 1079
16. A.T.M. Marcelis, A. Koudijs, E.J.R. Sudholter, *Mol. Cryst. Liq. Cryst.*, 2004, 411, 193
17. C.V. Yelamaggad, G. Shanker, *Liq. Cryst.*, 2007, 34, 799
18. C. Zhang, L. Jin, B. Yin, M. Jamil, Y.J. Jeon, *Liq. Cryst.*, 2008, 35, 39
19. D.A. Tomalia, J.M.J. Frechet, *Polym. Sci. A: Polym. Chem.*, 2002, 40, 2719
20. P.R. Ashton, S.E. Boyd, C.L. Brown, S.A. Nepogodiev, E.W. Meijer, H.W.I. Peerlings, J.F. Stoddart, *Chem. Eur. J.*, 1997, 3, 974
21. O.A.N. Mathews, N. Shipway, J.F. Stoddart, *Prog. Polym. Sci.*, 1998, 23, 1
22. C.J. Hawker, *Adv. Polym. Sci.*, 1999, 147, 113

23. N. Feuerbacher, F. Vögtle, *Top. Curr. Chem.*, 1998, 197, 1
24. G.M.J. Dykes, *Chem. Technol. Biotechnol.*, 2001, 76, 903
25. U. Boas, P.M.H. Heegaard, *Chem. Soc. Rev.*, 2004, 33, 43
26. D.K. Smith, F. Diederich, *Chem. Eur. J.*, 1998, 4, 1353
27. H.F. Chow, T.K.K. Mong, M.F. Nongrum, C.W. Wan, *Tetrahedron*, 1998, 54, 8543
28. G.H. Mehl, I.M. Saez, *Appl. Organomet. Chem.*, 1999, 13, 261
29. S.A. Ponomarenko, E.A. Rebrov, N.I. Boiko, N.G. Vasilenko, A.M. Muzafarov, Y.S. Freidzon, V. Shibaev, *Polym. Sci. Ser. A*, 1994, 36, 896
30. R.Y. Kannan, H.J. Salacinski, P.E. Butler, A.M. Seifalian, *Acc. Chem. Res.*, 2005, 38, 879
31. B. Donnio, D. Guillon, *Adv. Polym. Sci.*, 2006, 201, 45
32. G.H. Mehl, J.W. Goodby, *Angew. Chem.*, 1996, 105, 2791
33. I.M. Saez, P. Styring, *Adv. Mater.*, 1996, 8, 1001
34. J.W. Goodby, G.H. Mehl, I.M. Saez, R.P. Tuffin, G. Mackenzie, R. Auzely-Velty, T. Benvegnu, D. Plusquellec, *Chem. Commun.*, 1998, 2057
35. P.A. Jaffres, R.E. Morris, *J. Chem. Soc., Dalton Trans.*, 1998, 2767
36. I.M. Saez, J.W. Goodby, *Liq. Cryst.*, 1999, 26 (7), 1101
37. G.W. Gray, J.W. Goodby, *Smectic Liq. Cryst.:Textures and Struct.*, 1984, 1
38. I.M. Saez, J.W. Goodby, R.M. Richardson, *Chem. Eur. J.*, 2001, 7 (13), 2758
39. M.W.P.L. Baars, M.C.W. van Boxtel, C.W.M. Bastiaansen, D.J. Broer, S.H.M. Sonjens, E.W. Meijer, *Adv. Mater.*, 2000, 12, 715
40. R. Elsässer, G.H. Mehl, J.W. Goodby, D.J. Photinos, *The Royal Society of Chemistry, Chemical Communications*, 2000, 851
41. V. Percec, C. Pugh, in: *Side Chain Liquid Crystal Polymers*, C.B. McArdle, Ed. Blackie, Glasgow, 1989, 1
42. K.E. Drexler, Wiley, New York, 1992; G.A. Baker, *Adv. Mater.*, 2005, 17, 639
43. A.P. DeSilva, H.Q.N. Gunaratne, C.P. McCoy, *Nature*, 1993, 364, 42
44. W. Gopel, *Biosensors and Bioelectronics*, 1998, 13, 723
45. L.C. Kennedy, L.R. Bickford, N.A. Lewinski, A.J. Coughlin, Y. Hu, E.S. Day, J.L. West, R.A. Drezek, *Small*, 2011, 7, 169
46. M.-C. Daniel, D. Astruc, *Chem Rev.*, 2004, 104, 293
47. M. Haase, H. Schafer, *Angew. Chem., Int. Ed.*, 2011, 50, 5808

48. D.V. Talapin, J.-S. Lee, M.V. Kovalenko, E.V. Shevchenko, *Chem. Rev.*, 2010, 110, 389
49. W.L. Barnes, A. Dereux, T.W. Ebbesen, *Nature*, 2003, 424, 824
50. R. Schlogl, S.B.A. Hamid, *Angew. Chem., Int. Ed.*, 2004, 43, 1628
51. C. Gautier, T. Burgi, *Chem. Phys. Chem.*, 2009, 10, 483
52. T. Yonezawa, S. Onoue, N. Kimizuka, *Langmuir*, 2000, 16, 5218
53. Z.W. Pan, Z.R. Dai, Z.L. Wang, *Science*, 2001, 291, 1947
54. S.A. Claridge, A.W. Castleman, S.N. Khanna, C.B. Murray, A. Sen, P.S. Weiss, *ACS Nano*, 2009, 3, 244
55. P. Reiss, E. Couderc, J. De Girolamo, A. Pron, *Nanoscale*, 2011, 3, 2, 446
56. J. Tian, J. Jin, F. Zheng, H. Zhao, *Langmuir*, 2010, 26, 11, 8762
57. H. Fan, K. Yang, D.M. Boye, T. Sigmon, K.J. Malloy, H. Xu, G.P. Lopez, C.J. Brinker, *Science*, 2004, 304, 567
58. D. Weller, A. Moser, *IEEE Trans. Magn.*, 1999, 35, 4423; S. Sun, D. Weller, *J. Magn. Soc. Jpn.*, 2001, 25, 1434
59. L.N. Lewis, *Chem. Rev.*, 1993, 93, 2693
60. A.N. Shipway, E. Katz, I. Willner, *Chem. Phys. Chem.*, 2000, 1, 18
61. M.J. Hostettler, J.E. Wingate, J. Zhong, *Langmuir*, 1998, 14, 17
62. M. Faraday, *Philos. Trans. R. Soc. London*, 1857, 147, 145
63. P.E. Libinis, R.G. Muzzo, G.M. Whitesides, *J. Phys. Chem.*, 1992, 96, 5097
64. C.J. Murphy, T.K. Sau, A.M. Gole, C.J. Orendorff, J. Gao, L. Gou, S.E. Hunyadi, T. Li, *J. Phys. Chem. B*, 2005, 109, 13857
65. G. Frens, *Nature, Phys. Sci.*, 1973, 241, 20
66. K.R. Brown, D.G. Walter, M.J. Natan, *J. Chem. Mater.*, 2000, 12, 306
67. S.T. Gentry, S.J. Fredericks, R. Krchnavek, *Langmuir*, 2009, 25, 2613
68. E. Gachard, H. Remita, J. Khatouri, B. Keita, L. Nadjo, J. Belloni, *New J. Chem.*, 1998, 22, 1257
69. J. Zhang, J. Du, B. Han, Z. Liu, T. Jiang, Z. Zhang, *Angew. Chem. Int. Ed.*, 2006, 45, 1116
70. D. Ray, V.K. Aswal, J. Kohlbrecher, *Langmuir*, 2011, 27, 4048
71. T. Sakai, P. Alexandridis, *Langmuir*, 2004, 20, 8426
72. A.E. Saunders, A. Ghezelbash, D.-M. Smilgies, M.B. Sigman, B.A. Korgel, *Nano Lett.*, 2006, 6, 2959
73. L.-s. Li, J. Wanda, L. Manna, A.P. Alivisatos, *Nano Lett.*, 2002, 2, 557

74. H. Qi, P. Wei, N. Sertova, T. Hegmann, *IEEE Conference on Nanotechnology*, 2005
75. A.-H. Lu, E.L. Salabas, F. Schüth, *Angew. Chem. Int. Ed.*, 2007, 46, 1222
76. B.K. Paul, S.P. Moulik, *Curr. Sci.*, 2001, 80, 990
77. J. Park, K. An, Y. Hwang, J.-G. Park, H.-J. Noh, J.-Y. Kim, J.-H. Park, N.-M. Hwang, T. Hyeon, *Nat. Mater.*, 2004, 3, 891
78. S. Sun, H. Zeng, D.B. Robinson, S. Raoux, P.M. Rice, S.X. Wang, G. Li, *J. Am. Chem. Soc.*, 2004, 126, 273
79. D. Farrell, S.A. Majetich, J.P. Wilcoxon, *J. Phys. Chem. B*, 2003, 107, 11022
80. C. Liu, X. Wu, T. Klemmer, N. Shukla, X. Yang, D. Weller, A.G. Roy, M. Tanase, D. Laughlin, *J. Phys. Chem. B*, 108, 20, 6121
81. V. Novotna, J. Vejpravova, V. Hamplova, J. Prokleska, E. Gorecka, D. Pocięcha, N. Podoliak, M. Glogarova, *RSC Adv.*, 2013, 3, 10919
82. G.D. Fasman, New York, USA: Plenum Publishing Corp, 1996
83. G.G. Hammes, New York, USA: John Wiley & Sons, Inc., 2005
84. N. Berova, K. Nakanishi, R.W. Woody, New York, USA: Wiley-VCH, 2000
85. L. Velluz, M. Legrand, M. Grosjean, New York, NY: Academic Press., 1965
86. A. Abu-Shumays, J.J. Duffield, *Anal Chem*, 1966, 38, 29
87. J.P. Hennessey, W.C. Johnson, *Biochemistry*, 1981, 20, 1085
88. S.M. Kelly, N.C. Price, *Biochim Biophys Acta*, 1997, 1338, 161
89. www.olympusmicro.com
90. www.microscopyu.com
91. www.experimentation-online.co.uk
92. M.C. Daniel, D. Astruc, *Chem. Rev*, 2004, 104, 293; M. Antonietti, G.O. Ozin, *Chem.-Eur. J.*, 2004, 10, 29; C. Burda, X. Chen, R. Narayanan, M.A. El-Sayed, *Chem. Rev.*, 2005, 115, 1025
93. B.I. Ipe, S. Mehima, K.G. Thomas, *J. Am. Chem. Soc.*, 2003, 125, 7174; F. Stellaci, C.A. Bauer, T. Meyer-Friedrichsen, W. Wenseleers, S.R. Marder, J.W. Perry, *J. Am. Chem. Soc.*, 2003, 125, 328
94. O. Buchnev, E. Ouskova, Y. Reznikov, H. Kresse, A. Grabar, *Mol. Cryst. Liq. Cryst.*, 2004, 422, 47; E.B. Barmatov, D.A. Pebalk, M.V. Barmakova, *Langmuir*, 2004, 20, 10868; H. Qi, T. Hegmann, *J. Mater. Chem.*, 2006, 16, 4197
95. J. Fukuda, M. Yoneva, H. Yokoyama, *Eur. Phys. J. E*, 2004, 13, 87; M.A. Bates, *Liq. Cryst.*, 2005, 32, 1525

96. J.C. Loudet, P. Barois, P. Auroy, H. Richard, P. Poulin, *Langmuir*, 2004, 20, 11336; I.I. Smalyukh, O.D. Lavrentovich, A.N. Kuzmin, A.V. Kachinski, P.N. Prasad, *Phys. Rev. Lett.*, 2005, 95, 157801
97. N. Kanayama, O. Tsutsumi, A. Kanazawa, T. Ikeda, *Chem. Commun.*, 2001, 2640; K. Kanie, T. Sugimoto, *J. Am. Chem. Soc.*, 2003, 125, 10518
98. L. Cseh, G.H. Mehl, *J. Am. Chem. Soc.*, 2006, 128, 13376
99. M. Marcos, R. Gimenez, J.L. Serrano, B. Donnio, B. Heinrich, D. Guillon, *Chem.-Eur. J.*, 2001, 7, 1006; T. Kato, N. Mizohita, K. Kishimoto, *Angew. Chem. Int. Ed.*, 2006, 45, 38
100. D.K. Christopolous, D.J. Photinos, L.M. Stimson, A.F. Terzis, A.G. Vanakaras, *J. Mater. Chem.*, 2003, 13, 2756; A.G. Vanakaras, D.J. Photinos, *J. Mater. Chem.*, 2005, 15, 2002
101. M. Brust, M. Walker, D. Bethel, D.J. Schiffrin, R. Whyman, *J. Chem. Soc., Chem. Commun.*, 1994, 801
102. M. Hasan, D. Bethell, M. Brust, *J. Am. Chem. Soc.*, 2002, 124, 1132; V. Chechik, *J. Am. Chem. Soc.*, 2004, 126, 7780
103. M.C.J. Ruiz, J.C. Blais, D. Astruc, *J. Am. Chem. Soc.*, 2003, 125, 2617
104. A.C. Tempeton, W.P. Wuelfing, R.W. Murray, *Acc. Chem. Res.*, 2000, 33, 27
105. L. Cseh, G.H. Mehl, *J. Mater. Chem.*, 2007, 17, 311
106. J.G. Hoggett, R.B. Moodie, J.R. Penton, K. Schofield, *Cambridge Univ. Press*, 1971
107. H. Leube, H. Finkelmann, *Pol. Bull.*, 1988, 20, 53
108. S. Diez, D.A. Dunmur, M.R. De la Fuente, P.K. Karahaliou, G.H. Mehl, T. Meyer, M.A.P. Jubindo, D.J. Photinos, *Liq. Cryst.*, 2003, 30, 1021
109. A. Tlili, N. Xia, F. Monnier, M. Taillefer, *Angew. Chem*, 2009, 48, 8725
110. Patent US 7045659 B2
111. H.C. Brown, R.B. Wetherill, *Tetrahedron*, 1987, 43, 18, 4071
112. D. Witt et al., *Current Org. Chem*, 2004, 8, 1
113. M.I. Bethencourt et al., *Langmuir*, 2009, 25, 1265
114. O.B. Wallace, D.M. Springer, *Tetrahedron Lett.*, 1998, 39, 2693
115. B. Hache, Y. Gareau, *Tetrahedron Lett.*, 1994, 35, 12, 1837
116. S. Kumar Pal, V.A. Raghunathan, S. Kumar, *Liq. Cryst.*, 2007, 34, 2, 135

117. T.N. Wheeler, S.G. Blanchard, R.C. Andrews, F. Fang, Y. Gray-Nunez, C.O. Harris, M.H. Lambert, M.M. Mehrotra, D.J. Parks, J.A. Ray, T.L. Smalley, *J. Med. Chem.*, 1994, 37, 4118
118. E.J. Corey, G. Schmidt, *Tetrahedron Lett.*, 1979, 5, 399
119. J. Turkevich, P.C. Stevenson, J. Hillier, *Discussions of the Faraday Society*, 1951, 11, 55
120. N. Katsonis, E. Lacaze, A. Ferrarini, *J. Mat. Chem.*, 2012, 22, 7088
121. D. Astruc *et al*, *J.Am.Chem.Soc.*, 2003, 125, 2617